The exercise-triggered release of extracellular vesicles into the circulation

Dissertation

zur Erlangung des Grades
Doktor der Naturwissenschaften

am Fachbereich Biologie
der Johannes Gutenberg-Universität Mainz

Alexandra Brahmer

geboren am 23.09.1988 in Freiburg i. Br.

Mainz, 2019

Inhalt

Zusammenfassung

Körperliche Aktivität löst eine akute Stressreaktion aus, welche starke Veränderungen von physiologischen Parameter mit sich bringt. Diese akuten Veränderungen verursachen systemische Anpassungen, die langfristig die körperliche und geistige Gesundheit fördern. Die zugrundeliegenden Mechanismen sind jedoch noch nicht völlig geklärt. Extrazelluläre Vesikel (EVs) sind von Zellen abgegebene membranumschlossene Einheiten, die bioaktives Material transportieren und als Vermittler der Zell-zu-Zell-Kommunikation zwischen verschiedenen Organen und Geweben fungieren. Die Menge an EVs in der Zirkulation nimmt in Folge verschiedener körperlicher Betätigungen zu und es wird spekuliert, dass EVs an physiologischen Anpassungsprozessen beteiligt sind, welche durch regelmäßige körperliche Bewegung ausgelöst werden. Das Wissen über die Dynamik, den Ursprung und die Zusammensetzung von EVs, die während und nach dem Sport im Blut zu finden sind (bezeichnet als „ExerVs“), ist jedoch begrenzt. Zudem stellt die erschwerte Isolation von EVs aus Blutplasma eine Hürde für die Charakterisierung von ExerVs dar.

Hier wurde eine detaillierte Analyse verschiedener ExerV-Subklassen mit dem Ziel einer genauen Beschreibung ihrer Freisetzungskinetik und ihrer zellulären Herkunft durchgeführt. Dafür wurden 21 gesunde männliche Athleten einem stufenweisen Ausbelastungstest auf dem Fahrradergometer unterzogen. Die EV-Isolierung mittels Größenausschlusschromatographie (englisch „size exclusion chromatography“ = SEC), Immunaffinitäts-Isolation sowie die Kombination von SEC mit Dichtegradientenzentrifugation führten zur Anreicherung von EVs aus Blutplasma. Semi-quantitative Analysen der ExerV-Dynamik in SEC-EVs und Immunaffinität-isolierten EVs ergaben Anstiege über den Verlauf der Belastung. Die Phänotypisierung von ExerVs mittels zweier Multiplex-Analysemethoden direkt im Blutplasma oder mit isolierten SEC-EVs, $CD9^+$EVs, $CD63^+$EVs und $CD81^+$EVs ergab eine Reihe an zellulären Markerproteinen, die auf ExerVs zu finden sind. Die Ergebnisse deuten darauf hin, dass ExerVs von Leukozyten, einschließlich Lymphozyten ($CD4^+$EVs, $CD8^+$EVs), Monozyten ($CD14^+$EVs) und antigenpräsentierenden Zellen ($MHCI^+$EVs, $MHCII^+$EVs), sowie Endothelzellen ($CD105^+$EVs, $CD146^+$EVs)

und Thrombozyten ($CD41b^+$EVs, $CD62P^+$EVs), freigesetzt werden. Die massive Beeinträchtigung der Analyse des Proteoms von verschieden isolierten ExerVs, sowie der Nanopartikel-Tracking-Analyse und der bildgebenden Durchflusszytometrie verdeutlicht die Notwendigkeit einer weiteren Verbesserung der EV-Reinheit, um tiefere Einblicke in die tatsächlichen Konzentrationen und die Zusammensetzung von ExerVs zu erhalten.

Schlussendlich kann festgehalten werden, dass verschiedene Zelltypen des Kreislaufsystems während physischer Belastung dazu beitragen, dass extrazelluläre Vesikel ins Blut abgegeben werden. Diese heterogenen ExerV Spezies könnten an Signalprozessen beteiligt sein, die in Zusammenhang mit Koagulation, Endothelfunktion und Inflammation stehen.

Summary

Physical exercise induces acute physiological changes leading to massively enhanced cross-talk between cells, organs, and tissues. These acute alterations cause systemic adaptations which promote physical and mental health on a long-term. Though, the molecular basis underlying these bodily adaptations remains elusive. Extracellular vesicles (EVs) are cell-derived membranous entities which transport bioactive material and function as mediators of cell-cell-communication between several organs and tissues. EVs in the circulation increase upon diverse exercise interventions and are speculated to be involved in the physiological adaptation processes induced by regular physical exercise. However, knowledge on the dynamics, the origin, and the composition of EVs present in blood during and after exercise (ExerVs) is poor. In addition, the difficulties in EV-isolation from blood plasma represents a hurdle for the characterization of ExerVs.

Here, a detailed analysis of different ExerV subclasses to define their release kinetics and their origin was performed in an incremental cycling exercise setting involving 21 healthy male athletes. EV isolation via size exclusion chromatography (SEC), immuno-affinity capture as well as combination of SEC with density gradient centrifugation lead to enrichment of EVs from human plasma samples. Semi-quantitative analyses of ExerV dynamics in SEC-EVs and immuno-affinity captured EVs revealed elevations in a load-response related fashion. Phenotyping of ExerVs using two multiplexed analysis approaches directly in blood plasma or isolated SEC-EVs, $CD9^+$EVs, $CD63^+$EVs, and $CD81^+$EVs revealed a panel of cellular marker proteins present on ExerVs. The results indicate that ExerVs originate from leukocytes, including lymphocytes ($CD4^+$EVs, $CD8^+$EVs), monocytes ($CD14^+$EVs) and antigen presenting cells (MHCI+EVs, $MHCII^+$EVs), as well as endothelial cells ($CD105^+$EVs, $CD146^+$EVs), and platelets ($CD41b^+$EVs, $CD62P^+$EVs). Impaired downstream analysis of proteomic content, nanoparticle tracking analysis, and imaging flow cytometry analysis of differentially isolated ExerVs demonstrated the need for further improvement of EV purity to gain deeper insights on actual concentrations and the composition of ExerVs.

Conclusively, various cell types of the circulatory system contribute to the exercise-triggered release of extracellular vesicles into the blood stream. This heterogeneous pool of ExerVs may be involved in signaling processes associated with coagulation, endothelial function and inflammation.

List of Figures

List of Tables

Abbreviations

Alix	apoptosis-linked gene-2-interacting protein
AP cell	antigen presenting cells
APC	allophycocyanin
ApoA1	apolipoprotein A1
APS	ammonium peroxodisulfate
ASGPR2	asialoglycoprotein receptor 2
BBB	blood-brain-barrier
BCSFB	blood-cerebrospinal fluid-barrier
CCS	cell culture supernatant
CD	cluster of differentiation
cfDNA	cell-free DNA
CO_2	carbon dioxide
CoC3	complement component 3
DC	dendritic cell
DNA	desoxyribonucleic acid
DTT	1,4-Dithiothreitol
ECL	enhanced chemiluminescence
EDTA	ethylenediaminetetraacetic acid
EM	electron microscopy
EMP	endothelial cell microparticle
eNOS	NO synthase
ESCRT	endosomal sorting complex required for transport
EV	extracellular vesicle
ExerVs	EVs released upon exercise
FBS	fetal bovine serum
Flot1	flotillin-1
HDL	high-density lipoprotein
HPA	hypothalamic pituitary adrenal axis

HRS	hepatocyte growth factor-regulated tyrosine kinase substrate
IA	immuno-affinity
IAT	individual anaerobic threshold
ICAM	intercellular adhesion molecule
IDG	iodixanol density gradient centrifugation
IDL	intermediate-dense lipoprotein
IF	imaging flow cytometry
IGK	immunoglobulin κ light chain
IL	interleukin
ILV	intraluminal vesicle
LAMP	lysosomal-associated membrane protein
LC-MS	Liquid-chromatography mass spectrometric
LDL	low-density lipoprotein
LOD	limit of detection
MFI	mean fluorescence intensity
MHC	major histocompatibility complex
miRNA/miR	microRNA
MMP	matrix metalloproteinase
MP	microparticles
MSC	mesenchymal stem cell
MV	microvesicles
MVB	multivesicular body
NK cell	natural killer cell
NO	nitric oxide
NTA	nanoparticle tracking analysis
PBS	phosphate buffered saline
pen/strep	penicillin/streptomycin
PES	polyethersulfone
PMN	polymorphnuclear neutrophils
PMP	platelet microparticle

PPM	parts per million
qPCR	quantitative polymerase chain reaction
RBC	red blood cell/erythrocyte
RHO	Ras homologue
RNA	ribonucleic acid
RNA-seq	RNA-sequencing
ROCK	RHO-associated protein kinase
ROS	reactive oxygen species
RQ	respiratory quotient
RT	room temperature
S	subject
SDS-PAGE	sodium dodecyl sulfate-polyacrylamide gel electrophoresis
SEC	size exclusion chromatography
SGCA	α-sarcoglycan
SNARE	soluble N-ethylmaleimide-sensitive-factor attachment receptor
SOD	superoxide dismutase
TEMED	N,N,N',N'-Tetramethylethylenediamin
TF	tissue factor
tPA	tissue plasminogen activator
TSG101	tumor susceptibility gene 101 protein
UC	ultracentrifugation
UF	ultrafiltration
VLDL	very low-density lipoprotein
VO_2max	maximal oxygen consumption
vWF	von Willebrand factor
WB	western blotting

1 Introduction

1.1 Physical exercise

Physical exercise induces an acute stress situation in the body which immediately persuades several organs and cell populations to maintain whole-body homeostasis. In order to supply the tissues with an increasing amount of nutrients and oxygen, the respiratory, the cardiovascular as well as the neuromuscular systems are activated. Consequently, enhanced shear forces, oxidative stress and inflammatory reactions can be observed. When physical activity is performed under controlled conditions these bodily alterations are beneficial for health and exercise has become an important instrument in disease prevention, diagnostics and rehabilitation (Zierath et al., 2015), (fig. 1.1).

1.1.1 Health benefits of physical exercise

Regular physical activity and exercise leads to the primary and secondary prevention of several chronic diseases and is linked to reduced risk of premature death. A graded linear relationship between the volume of physical activity and health status seems to exist. As reviewed by Warburton et al. (2006), increased levels of physical activity reduce the risk for cardiovascular diseases and mortality. Physically active people are less likely to develop type 2 diabetes and exercise interventions improve glucose homeostasis which is associated with an improved course of disease (Warburton et al., 2006). Likewise, the clinical risk factors of the metabolic syndrome are reduced, including abdominal obesity, hypertension, elevated serum triglycerides, low serum high-density lipoprotein (HDL) and insulin resistance (Pitsavos et al., 2006). Furthermore, the incidence of specific cancers, particularly colon and breast cancer, is reduced in persons that are routinely physically active. In the secondary prevention, regular physical exercise improves health status of cancer patients and reduces their relative risk for death. Additionally, physical exercise affects bone mineral density, reducing the incidence of osteoporosis. Subsequently, the risk of fractures is reduced, especially in elderly people (Warburton et al., 2006).

Next to the physiological effects, exercise is known to have cognitive benefits in the general population including neuroprotection. Exercise is associated with enhanced neurogenesis and synaptic plasticity (Lourenco et al., 2019; van Praag, 2008). In the aging process, this leads to a reduced decline in age-related impairments. Active persons are less prone to develop Alzheimer's as well as Parkinson's diseases and disease progression is reduced in exercising patients (Paillard et al., 2015). In addition, exercise reduces the cognitive decline (Sun et al., 2018) and improves quality of life in depressive patients (Blumenthal et al., 2007; Haller, Lorenz, et al., 2018). Similarly, overall resilience to stressors seems to be improved in trained persons (Tsatsoulis et al., 2006).

Thus, adaptive mechanisms induced by exercise seem to exhibit an overall positive effect on physical and neuronal health.

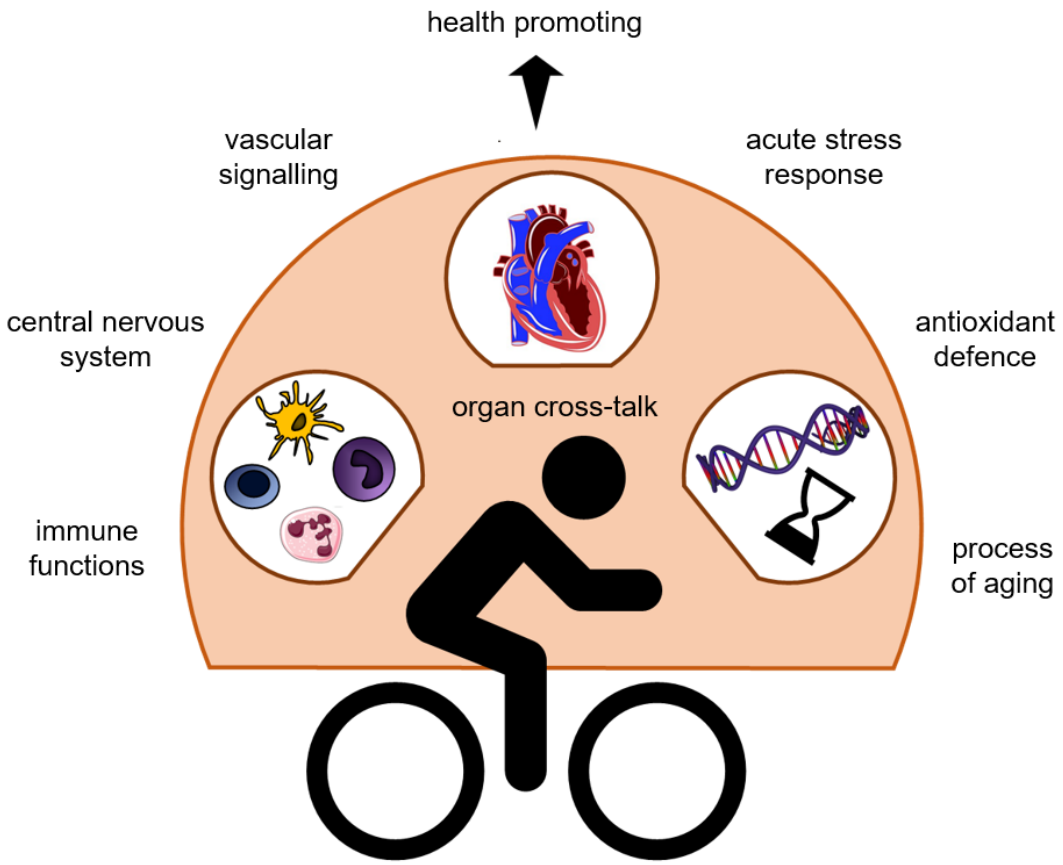

Figure 1.1: Systemic benefits of exercise. Exercise exhibits several physiologic changes which promote inter-organ cross-talk leading to beneficial systemic adaptations.

1.1.2 Physiological changes of the body in response to exercise

Catecholamines and glucocorticoids

Activation of the hypothalamic pituitary adrenal (HPA) axis, which is stimulated by neuronal and circulating homeostatic signals as well as inflammatory mediators, causes catecholamine and glucocorticoid release during exercise (Duclos et al., 2016). The catecholamines adrenaline and noradrenaline are released within seconds and the concentrations increase with power and duration of physical activity (Zouhal et al., 2008). The glucocorticoid cortisol can be found in the circulation after few minutes during acute exercise and remains elevated for up to two hours (Duclos et al., 2016). Signaling processes involving these circulating stress hormones trigger an increased mobilization of metabolic substrates (gluconeogenesis, lipolysis, proteolysis) and their rapid delivery to muscle cells by an enhanced cardiovascular tone (Sapolsky et al., 2000; Zouhal et al., 2008). Interestingly, trained subjects, in contrast to untrained persons, are capable of sequential HPA activation induced by exercise. Alterations of the glucocorticoid receptor representation in the brain may be a major adaptation related to the regulation of the circulating cortisol levels in active persons (Duclos et al., 2016). Also, catecholamine secretion seems to be promoted in trained versus sedentary humans and rats (Kjaer, 1998; Schmidt et al., 1992). Physiologic adaptations underlying these observations may involve increased adrenal medulla volume, adrenergic receptor density or sensitivity as well as genetic predisposition (Zouhal et al., 2008).

Shear stress

Increasing heart rate and blood pressure lead to highly elevated levels of shear stress under exercise conditions. As a result, endothelial cells release increasing levels of nitric oxide (NO) leading to flow-mediated dilatation (Vanhoutte et al., 2017). This is, among other processes, mediated by activation of the NO synthase (eNOS). Under physiological conditions, NO release is important for proper endothelial functions to prevent clot formation and abnormal vasoconstriction. Aggregated platelets release serotonin and adenosine diphosphate which persuade the endothelium to release NO. This leads to the constriction of vascular smooth muscle cells as well as inhibition

of coagulation and a subsequent clot formation process. Endothelial dysfunction due to disrupted vessel walls or decreased NO production leads to higher susceptibility to atherosclerosis, clot formation and ischemic insults (Vanhoutte et al., 2017). Chronic exposure to elevated levels of shear stress induced by regular training leads to an upregulation of eNOS in endothelial cells and, thus, higher levels of NO are released upon stimulation (Rizzo et al., 1998; Woodman et al., 2005). Finally, the increase of intraluminal shear forces is considered a major stimulus for the exercise-triggered enhancement of vascular function and reduction of the risk for cardiovascular diseases development.

Oxidative stress

Enhanced metabolic turnover during physical exercise results in incomplete oxidative phosphorylation. Thus, liberation of free radicals leads to a strong increase of reactive oxygen species (ROS) in blood. After prolonged or excessive exercise, the resulting oxidative stress exhibits harmful impact especially on muscle cells (Powers et al., 2011). However, in trained individuals elevated superoxide dismutase (SOD) concentrations as well as altered redox signaling mediated by the transcription factor nuclear factor erythroid 2-related factor or beneficial oxidation of involved proteins' cysteine residues can be observed (He et al., 2016). This indicates that, when performed under controlled conditions, exercise leads to adaptive responses of the antioxidant defense system.

Immune reactions

Exercise induces an inflammatory reaction of the body with each individual bout of exercise. This is reflected by increased levels of cytokines and leukocytes in the blood. Several lymphocyte subpopulations [cluster of differentiation (CD)4^+ T cells, $CD8^+$ T cells, $CD16^+$ natural killer (NK) cells $CD56^+$ NK cells, and $CD19^+$ B cells] are recruited to the circulation, while the ratio of $CD4^+$ to $CD8^+$ T cells declines due to a higher increase in $CD8^+$ T cells (Pedersen et al., 2000). Early during exercise interleukin (IL)-6 concentrations in the circulation rise up to 100-fold and decline to baseline thereafter (Walsh et al., 2011). With contradicting results, other cytokines like tumor necrosis

factor α and IL-1β, which strongly increase during inflammatory reactions in several diseases, were found either to increase or remain at baseline depending on exercise duration and intention (Pedersen et al., 2000). This possibly indicates that induction of a similar inflammatory reaction as in disease states is only found under intense exercise conditions like marathon running (Pedersen et al., 2008). After exercise, an anti-inflammatory reaction is mediated by an elevated level of IL-6 propagating IL-10 and IL-1 receptor antagonist release from peripheral blood mononuclear cells (Steensberg et al., 2003). Also, long-term anti-inflammatory effects may be attributed to IL-6, IL-15 and follistatin-related protein 1 release during exercise which mediates improvement of cardiovascular health (Pedersen et al., 2012). In line with this, a reduction of circulating inflammatory markers can be observed due to regular physical activity in combination with reduced energy intake (Petersen et al., 2005). In pathophysiological situations, like rheumatoid arthritis, systemic sclerosis, idiopathic inflammatory myopathies, and systemic lupus erythematosus, exercise also exhibits anti-inflammatory effects (Benatti et al., 2015). Taken together, the pro- and anti-inflammatory reactions observed during and after acute bouts of physical exercise may be responsible for beneficial log-term immune adaptations.

In conclusion, physical exercise induces broad systemic changes which on the long-term lead to a wide range of beneficial properties. Multiple complex adaptational processes occur in the circulation and the embedding tissues including muscle and brain. Still, the exact molecular mechanisms responsible for these positive effects remain incompletely understood.

1.1.3 Evaluation of physical exertion

In order to study the molecular basis including adaptations to regular physical exercise, the precise evaluation of exercise performance is crucial. The implication of various exercise settings enables induction of acute stress situations in healthy persons or disease patients and a subsequent analysis of the body's physiological response. To characterize physical fitness and acute physical exertion, several parameters like heart rate, blood lactate levels and oxygen consumption can be assessed. To this end, incremental exercise tests

with increasing exercise intensities are frequently applied e.g. at a treadmill or a cycling ergometer.

The heart rate can easily be determined and stated as percentage of maximum heart rate to evaluate individual exertion. Subjective estimation of perceived exertion of the participants can be determined with the Borg scale (6 = no exertion; 20 = very, very hard) (Borg, 1982). The maximal oxygen consumption (VO_{2max}) is an important determinant for the aerobic capacity of a person (Howley et al., 1995; Taylor et al., 1955). It is defined as the maximum amount of oxygen per minute that can be taken up, transported and metabolized by the exercising muscles. Oxygen consumption and ventilatory thresholds can be assessed by applying spiroergometric analysis (Svedahl et al., 2003). Also in spiroergometric analysis, the respiratory exchange ratio (RER) is estimated by the division of the produced carbon dioxide (CO_2) by the consumed O_2. The RER can be used as an approximation for the respiratory quotient (RQ). The RQ allows evaluation of the nutrients which are mainly used for energy production since different amounts of oxygen are needed for the final oxidation of carbohydrate (RQ = 1.0), fat (RQ = 0.7), and protein (RQ = 0.82). Consequently, an RQ of 0.9 indicates the approaching switch from fatty acid metabolism to glucose metabolism due to increasing exertion during exercise (Issekutz et al., 1961; Wasserman et al., 1973). Lactate, the end product of the anaerobic glycolysis, is formed in muscle tissue and accumulates in the blood which similarly reflects the increasing demands for energy during strenuous exercise. Measurement of the blood lactate concentration is used for the estimation of the individual anaerobic threshold (IAT) which can be defined by multiple threshold concepts (Dickhuth et al., 1999; Faude et al., 2009; Mader et al., 1986; Stegmann et al., 1981). As a novel molecular marker in exercise physiology, circulating cell-free DNA (cfDNA) has gained increasing attention in the last years. It was demonstrated that cfDNA concentrations are increasing in various exercise settings and might provide more detailed knowledge on the molecular mechanisms activated during physical exercise (Beiter et al., 2011; Breitbach et al., 2012). Development of highly sensitive detection methods (Breitbach, Sterzing, et al., 2014; Breitbach, Tug, et al., 2014) enables routine analysis of cfDNA in exercise studies (Breitbach, Sterzing, et al., 2014; Haller, Helmig, et al., 2018; Tug et al., 2017).

Conclusively, many different methods for the estimation of an athlete's fitness level and the characterization of an acute exercise intervention exist. However, controversial discussion is ongoing about different diagnostic concepts and new methods are developed for performance diagnostics also in pathophysiological settings. Controlled exercise settings are most reliable to study intercellular signaling and adaptational processes in response to physical activity.

1.2 Extracellular vesicles – mediators of cell-cell communication

In the last decades extracellular vesicles (EVs) have evolved as important players of cell-cell communication. Upon diverse stimuli EVs are released in a variety of body fluids including blood plasma, urine, lymph and cerebrospinal fluid (Yanez-Mo et al., 2015). They compose of a phospholipid bilayer membrane encapsulating proteins, lipids, and several nucleic acid species, which differ dependent on their parent cells, environmental factors and certain stimuli (Raposo et al., 2013). Furthermore, an increasing number of studies evolved which show the transport of bioactive material to recipient cells. This makes them versatile entities in various physiologic and pathophysiologic processes (Raposo et al., 2013; van Niel et al., 2018; Yanez-Mo et al., 2015).

1.2.1 EV biogenesis and fate

Initially, vesicles found in the extracellular space were assumed to be cellular waste products (Johnstone et al., 1987; Wolf, 1967). However, defined EV release mechanisms of different subcellular origins were discovered in the last years. Despite today a highly diverse nomenclature exists, three main types of EVs can be differentiated: a) small exosomes originating from the endosomal machinery, b) microvesicles (MVs) directly shedding from the plasma membrane and c) apoptotic bodies formed as large vesicles during the process of apoptosis, (Colombo et al., 2014; van Niel et al., 2018), (fig. 1.2). Exosomes, due to their endosomal origin, are around 50-150 nm in size, MVs and apoptotic bodies vary in diameter of 50-1000 nm with apoptotic bodies also found larger than 1 µm (Jeppesen et al., 2019; van Niel et al., 2018). While the process of apoptosis and subsequent formation of apoptotic bodies is known

for long time (Elmore, 2007), the active secretion of exosomes and MVs is recently under intense investigation.

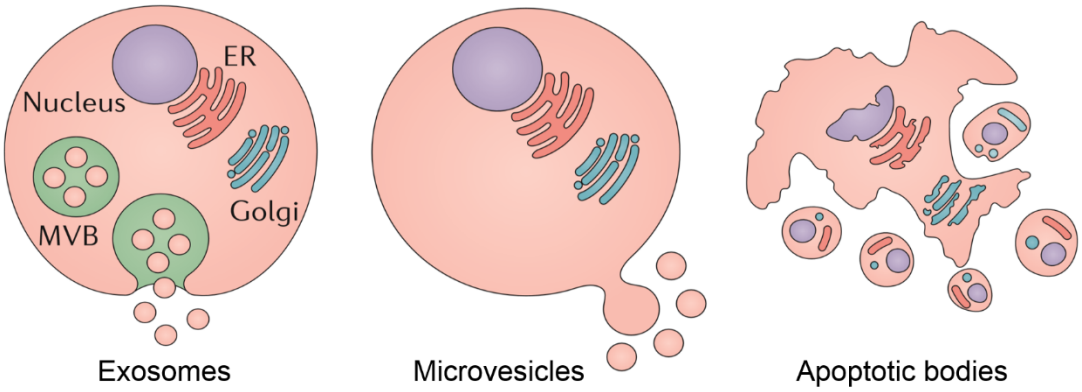

Figure 1.2: EV formation and release. EVs can be classified as exosomes released from multivesicular bodies (MVBs), microvesicles blebbing from the plasma membrane, and apoptotic bodies formed during apoptotic processes. Adapted from (Karpman et al., 2017).

Exosomes are formed as intraluminal vesicles (ILVs) within the endosomal machinery and actively released upon fusion of multivesicular bodies (MVBs) with the cellular membrane. ILV-formation by inward-budding of the early endosomal membrane is driven by different endosomal sorting mechanisms (Colombo et al., 2014; van Niel et al., 2018), (fig. 1.3 lower part). The endosomal sorting complex required for transport (ESCRT)-dependent machinery requires a complex interplay of around 30 proteins (Hanson et al., 2012). ESCRT-0 and ESCRT-I complexes are responsible for the assembly of ubiquitinated transmembrane cargoes on microdomains of the MVB membrane. HRS (hepatocyte growth factor-regulated tyrosine kinase substrate) of ESCRT-0 binds to tumor susceptibility gene 101 protein (TSG101) of ESCRT-I which further promotes the recruitment of ESCRT-III by ESCRT-II or apoptosis-linked gene-2-interacting protein (Alix). This finally leads to vesicle budding into the lumen of the MVBs. Moreover, Syndecan and Syntenin are important players of these ESCRT-mediated processes (Baietti et al., 2012). However, also ESCRT-independent ILV formation can be observed. Local enrichment of ceramide by hydrolysis of sphingomyelin on membrane subdomains can lead to membrane inward-budding (Goni et al., 2009; Trajkovic et al., 2008). Additionally, tetraspanins which consist of four transmembrane domains cluster in high concentrations on the MVB membrane

(Charrin et al., 2014). The tetraspanins CD9, CD63 and CD81 were shown to be involved in direct sorting of cargo to these so formed microdomains (Buschow et al., 2009). Inward budding and scission of the microdomains as ILVs are further triggered by the tetraspanin family members without the presence of the ESCRT complexes (Charrin et al., 2014; van Niel et al., 2011). MVB transport to the plasma membrane is mediated by Rab (ras-related in brain) GTPases like Rab11, Rab27, and Rab35 (Stenmark, 2009). Subsequently, fusion of the MVB membrane with the cellular membrane is driven by SNARE (soluble N-ethylmaleimide-sensitive-factor attachment receptor) proteins and synaptogamin family members resulting in exosome secretion to the extracellular space (Jahn et al., 2006).

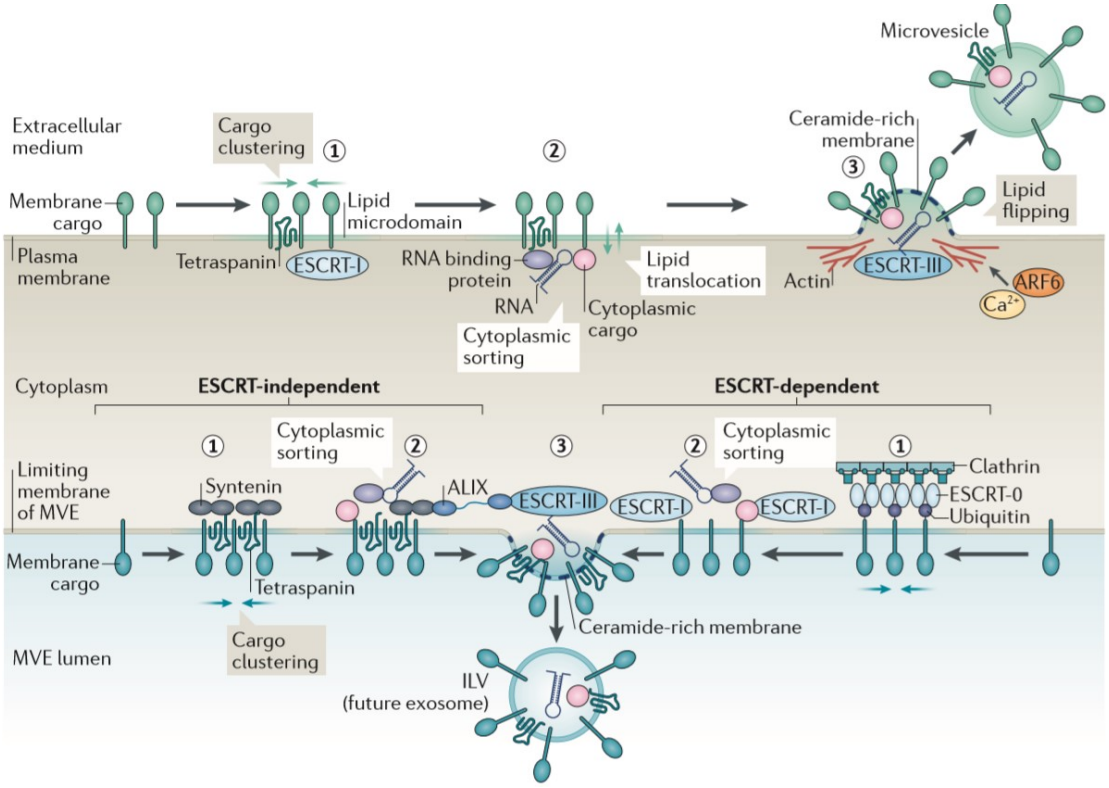

Figure 1.3: Distinct formation and release mechanisms of exosomes and MVs. Upper part: Cargo clustering in tetraspanin-rich domains is followed by cytoplasmic sorting and lipid translocation. Finally, lipid flipping initiates budding of the ceramide rich domain and shedding of MVs. Lower part: ESCRT-dependent (right) and -independent (left) cytoplasmic sorting of cargo in clusters is likewise followed by bending of the ceramide-rich domain and ILV scission into the MVB lumen. ILVs will be released to the extracellular space as exosomes after fusion of the MVB membrane with the cellular membrane. Adapted from (van Niel et al., 2018).

MV secretion directly from the cellular membrane shows certain similarities with exosome generation (van Niel et al., 2018), (fig. 1.3 upper part). Also prior

to MV release, membrane domains are formed involving tetraspanins for cargo clustering. Subsequently, restructuring of the cytoskeleton and membrane bending is required for MV blebbing. This is induced by Ca^{2+}-dependent pathways causing the exposition of phosphatidylserine to the cell surface where it generates a ceramide-rich membrane (Bianco et al., 2009; Piccin et al., 2007). Additionally, interaction of GTPases of the RHO (Ras homologue)-family and ROCK (RHO-associated protein kinase) with the cytoskeleton mediates MV release (McConnell et al., 2009). However, also proteins involved in exosome formation including TSG101, components of the ESCRT machinery, and Rab proteins were shown to act as mediators of MV shedding (Colombo et al., 2014).

After liberation to the extracellular space, EVs may target recipient cells and either function as signaling molecules themselves or deliver their cargo. Though EV targeting to recipient cells remains incompletely understood, it is likely dependent on specific adhesion molecules embedded in their membranes (Mathieu et al., 2019; van Niel et al., 2018). For instance, tetraspanins on EVs interact with intercellular adhesion molecules (ICAMs) at the membrane of acceptor cells (Morelli et al., 2004). But also integrins, lipids, lectins, heparan sulfate proteoglycans and extracellular matrix components are involved in EV-target cell recognition (van Niel et al., 2018). EV uptake can then be mediated by clathrin-dependent or -independent endocytosis as well as through endocytosis via caveolae and lipid rafts or by direct membrane fusion (Mathieu et al., 2019; van Niel et al., 2018). Once taken up by the cell, EVs are shuttled through the endosomal pathways and their cargo can be released into the cytoplasm where it may induce phenotypic changes. Though the actual mechanisms of EV cargo retrieval are poorly understood, numerous studies emerged (reviewed in Yanez-Mo et al., 2015) demonstrating the active release of EVs from one cell followed by uptake into a recipient cell and functional signaling of selected encapsulated cargo (Yanez-Mo et al., 2015).

1.2.2 EV-mediated intercellular signaling in the circulation

The capability of transporting bioactive material makes EVs interesting mediators of intercellular signaling and tissue homeostasis. EVs in blood

comprise a heterogeneous mixture of vesicles derived from platelets, red blood cells (RBCs; together > 50 %) (Arraud et al., 2014), and other blood cells including NK cells, dendritic cells (DC), monocytes and neutrophils as well as from cells of the surrounding tissues and organs (Yanez-Mo et al., 2015). Reports on blood EV numbers are diverse, ranging from 200 to 10^9/µl plasma highly depending on the method of examination (Dragovic et al., 2011; Shet et al., 2003), but more sophisticated analysis indicates an EV concentration of around 50,000/µl plasma (Arraud et al., 2014). Their presence in the circulation is restricted to few minutes or hours before they reach their targets (Rand et al., 2006; Takahashi et al., 2013; Willekens et al., 2005). Subsequently, EVs are taken up from their recipient cells and their cargo can be functionally retrieved.

EVs in blood homeostasis

Multiple EV subtypes in the circulation contribute to the maintenance of blood homeostasis via contribution to coagulative processes. Platelets release several EV subtypes triggered by diverse platelet activation routes (Heijnen et al., 1999; van der Pol et al., 2012). Large phosphatidylserine- or tissue factor (TF)-positive platelet-EVs induce thrombin generation (Biro et al., 2003; Tripisciano et al., 2017) but also small EVs or specifically exosomes may be responsible for pro-coagulative reactions (Berckmans et al., 2001; Thery et al., 2009; van der Pol et al., 2012). However, also EVs from other cellular sources bear pro-coagulative capacity. For example, EVs originating from polymorph nuclear neutrophils were demonstrated to trigger TF expression in endothelial cells (Mesri et al., 1999). Furthermore, EVs derived from monocytes were reported to be TF-positive and to promote coagulation upon binding to P-selectin-positive platelets (Del Conde et al., 2005). Interestingly, also anti-coagulant (Heijnen et al., 1999; Steppich et al., 2005) and fibrinolytic activity (Lacroix et al., 2012) can be attributed to EVs. This indicates that EVs may be part of a sensitive signaling machinery for precise homeostatic maintenance under physiologic conditions (Melki et al., 2017; Tans et al., 1991). Intriguingly, coagulation and thrombus formation are increased under several pathologic conditions like cancer, cardiovascular disease and rheumatoid diseases (Melki et al., 2017; Yanez-Mo et al., 2015). The described clinical conditions lead to elevated levels of circulating platelets and monocytes and increased pro-

coagulant activity of endothelial cells. These findings are accompanied by enhanced generation of pro-coagulant EVs, as well as increased risk for clot formation and thrombosis.

EVs in angiogenesis and vessel sprouting

EVs were reported to contribute to angiogenic signaling under healthy and pathologic conditions. Endothelial cell-derived EVs which contain matrix metalloproteinase proteins (MMP2 and MMP9) induced matrix degradation and therefore promoted blood vessel formation *in vitro* (Taraboletti et al., 2002). Moreover, platelet-derived EVs are described to promote proliferation and formation of vessel-like structures in endothelial cell culture as well as vessel-sprouting and revascularization of rat heart muscle after ischemia (Brill et al., 2005; Kim et al., 2004). Transport of growth factors like vascular endothelial growth factor, basic fibroblast growth factor and platelet derived growth factor seems to be involved in these pro-angiogenic signaling processes (Brill et al., 2005). Also, transfer of RNA species from mononuclear cells to endothelial cells via EVs with pro-angiogenic effects was demonstrated *in vivo* and *in vitro* (Deregibus et al., 2007). Furthermore, mesenchymal stem cell (MSC)-derived EVs induced vascular adaptations in endothelial cells under hypoxic conditions (Salomon et al., 2013). Accordingly, also tumor angiogenesis is supported by EVs originating from cancer and other cells via induction of growth factor or MMP expression (Janowska-Wieczorek et al., 2005; Skog et al., 2008). Next to pro-angiogenic signaling, also anti-angiogenic effects were reported for endothelial cell- and lymphocyte-derived EVs. These were reflected by enhanced ROS production and decreased NO release of endothelial cells upon stimulation with EVs (Mostefai et al., 2008; C. Yang et al., 2008). Conclusively, EVs exhibit modulating effects on angiogenic signaling, including induction and inhibition of vessel sprouting and tumor growth.

EVs as mediators of immune signaling

EVs play a versatile role in innate as well as acquired immunity by mediating inflammatory signaling. NK cells, monocytes/macrophages, and polymorphnuclear neutrophils (PMN), the first line of immune defense, release EVs under various conditions. Propagating pro- or anti-inflammatory reactions,

these EVs carry cytokines like IL-1β or IL-6, pattern recognition receptors like TLRs (toll-like receptors) as well as pro-inflammatory ligands like HMGB1 (high mobility group box 1), miRNAs, DNA, and PAMPs (pathogen-associated molecular patterns) (Yanez-Mo et al., 2015). For example, macrophage-derived EVs encapsulating miR-223 were potent to stimulate differentiation of monocytes to macrophages (Ismail et al., 2013). Also, EVs liberated by NK cells were Fas ligand- and perforin-positive and displayed cytotoxic activity against tumor cells as well as activated immune cells (Fais, 2013; Lugini et al., 2012). As part of the acquired immune response, EVs are involved in antigen processing and presentation. Antigen presenting (AP) cells can be affected by the capture of EVs carrying antigens from originating cells which experienced an inflammatory stimulus (van der Pol et al., 2012). This may lead to enhancement or reduction of subsequent T cell stimulation processes. Furthermore, AP cells were demonstrated to liberate EVs carrying major histocompatibility complex (MHC) I or MHCII and co-stimulatory molecules, thus, utilizing EVs for antigen presentation. For example, different subpopulations of dendritic cell-derived $MHCII^{+}$EVs stimulated the activation and proliferation of T cells (Tkach et al., 2017). Interestingly, DC-EV subclasses may induce divergent reactions in T cells (Th1- or Th2-associated), dependent on DC maturation state. Finally, the involvement of EVs in the described inflammatory processes is found under various pathologic conditions like infection, sepsis, rheumatoid arthritis, atherosclerosis, autoimmune diseases, and cancer (Yanez-Mo et al., 2015).

Organ cross-talk via EVs

Several lines of evidence demonstrate that EVs in the circulation reach tissues and organs to mediate organ-cross talk. For instance, accumulating data suggests that EVs are capable of crossing the blood-brain-barrier (BBB) and contribute to signaling processes between the periphery and neuronal tissue. Under physiologic conditions, the central nervous system is protected from insult from the circulation by the BBB as well as the blood-cerebrospinal fluid-barrier (BCSFB) which facilitate proper exchange of substances between blood and brain. Recently, it was demonstrated that EVs presumably originating from the hematopoietic lineage can cross the BBB and transfer bioactive cargo to recipient neuronal cells which seems to be enhanced under

inflammatory conditions (Chen et al., 2016; M. K. Qu et al., 2018; Ridder et al., 2014). Likewise, EV-mediated cell-cell communication at the BCSFB appears to be part of the immune reaction in neuronal tissue (Balusu et al., 2016). Additionally, the use of EVs to shuttle therapeutics from blood to brain (Kalani et al., 2014; M. Qu et al., 2018; T. Yang et al., 2015) as well as the ability of MSC-derived EVs to cross the BBB and their positive influence on several brain disease (Morales-Prieto et al., 2018) have gained increasing attention. However, while the capability of EVs to cross the BBB is widely accepted, the underlying molecular mechanisms are barely understood. Taken together, EVs can be regarded as important mediators of the exchange between tissues and organs, e.g. from periphery to brain, which makes them exciting targets for diagnostic and treatment of diseases.

1.3 Challenges in the isolation and characterization of plasma EVs

The heterogeneity of EV populations and other bioactive components found in the circulation faces the EV research with numerous challenges. Next to the different EV subclasses, also lipoprotein species in high concentrations, plasma proteins, including albumin, clotting factors, immunoglobulins, and further structures are present in blood (fig. 1.4).

The most frequently used EV isolation techniques from blood plasma or serum are differential ultracentrifugation (UC) and commercial precipitation-based methods (EV-Track knowledgebase; (Van Deun et al., 2017)). However, it was demonstrated that application of UC or EV precipitation results in low purity EVs with high amounts of co-isolated plasma proteins and lipoproteins (van der Pol et al., 2014) and may lead to the formation of aggregates (Linares et al., 2015). As a result, multiple different EV purification techniques emerged over the last couple of years trying to separate EVs from these main contaminants (Li et al., 2017; Monguio-Tortajada et al., 2019). Lipoproteins, which are found in concentrations of 10^{16}/ml in plasma, share either the size [chylomicrons, very low-density lipoprotein (VLDL)] or the density (HDL) with EVs (Simonsen, 2017), (fig. 1.4). Size exclusion chromatography (SEC) can be used to separate the majority of plasma proteins and lipoproteins (Boing et

al., 2014; Lobb et al., 2015; Welton et al., 2015) from EVs which can be subjected to various downstream analysis methods. However, the remaining contaminants still hamper the subsequent use of EV eluates for sensitive downstream analysis like RNA-sequencing (RNA-seq) or proteome analysis. It turned out that combination of different EV strategies, especially with density gradient centrifugation, leads to high-purity EVs (Jeppesen et al., 2019; Karimi et al., 2018; Onodi et al., 2018). Though, these approaches need an elevated sample input, are highly laborious, and show a low recovery, which hampers their usage in clinical settings. Immuno-affinity (IA) isolation including magnetic separation of captured EVs from plasma components offers a quick possibility to enrich for specific EV populations (Greening et al., 2015; Kowal et al., 2016; Nakai et al., 2016). However, applying IA isolation introduces a selection bias for the chosen EV-associated protein. Finally, more and more innovative isolation strategies appear with the aim to overcome the named disadvantages of the frequently used purification strategies (Bryl-Gorecka et al., 2018; Li et al., 2017; Sitar et al., 2015).

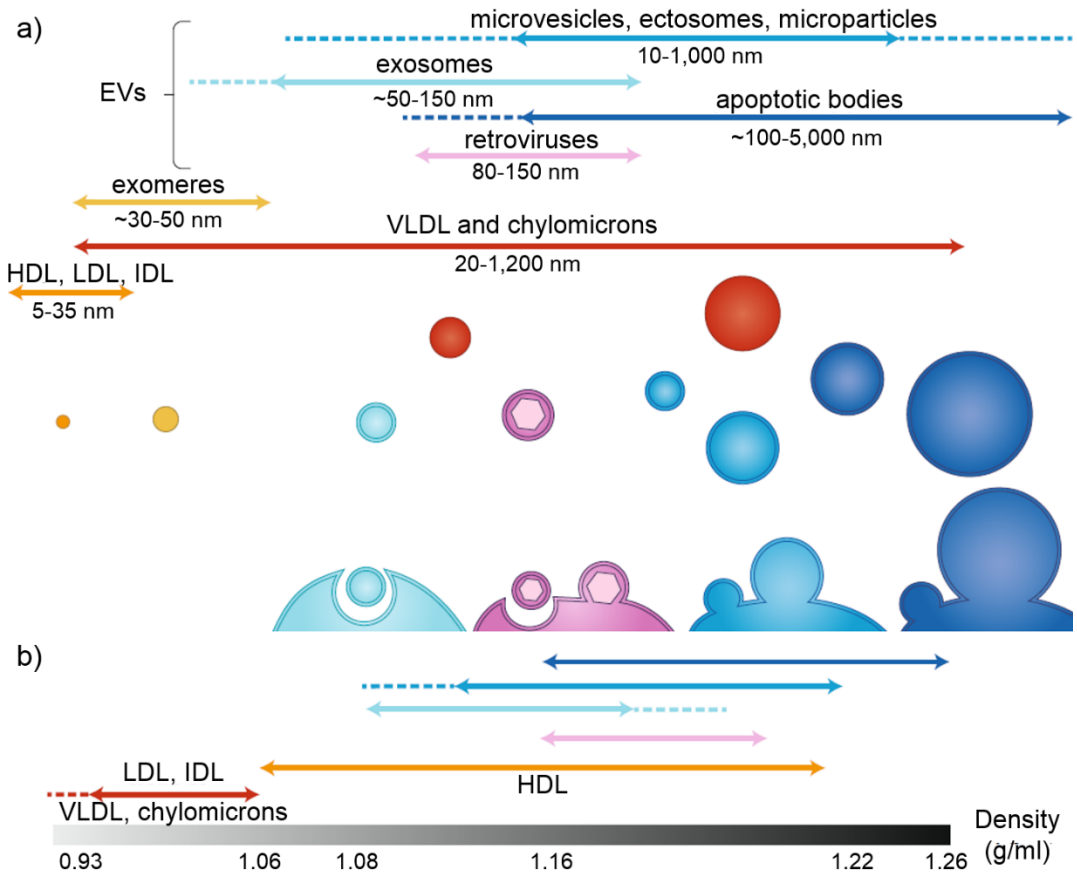

Figure 1.4: EVs and non-EVs in the circulation. Size (a) and density (b) of different EV-subsets and other circulating particles. HDL = high-density lipoprotein, LDL = low-density lipoprotein, IDL = intermediate-dense lipoprotein, VLDL = very-low-density lipoprotein. Adapted from (Mathieu et al., 2019).

Given the complex composition of the plasma EV-pool and the limitations in EV purification, EV characterization is similarly challenging as EV isolation. Western blotting (WB), single particle tracking, and electron microscopy (EM) are the most frequently used methods to characterize EV size and composition (Gardiner et al., 2016). Due to the lack of exclusive marker proteins and purification strategies for the EV subclasses (exosomes and MVs) the primary criteria to differentiate EVs in blood is size, preferably speaking of small and large EVs (Jeppesen et al., 2019; Kowal et al., 2016; Tkach et al., 2017). EM, specially coupled with immuno-gold labeling, is the gold standard of basic EV characterization (Thery et al., 2018; van der Pol et al., 2014). However, this technique is laborious and is only available in expertized facilities. Single particle tracking offers a fast possibility to estimate a size profile and concentration of an EV sample (Dragovic et al., 2011). Though, this technique does not cover the complete size spectrum of EVs and is highly susceptible to be biased by co-isolates (Jamaly et al., 2018; van der Pol et al., 2014). Further

information about the nature of the vesicles is provided by the presence of the tetraspanins CD9, CD63, and CD81, or other genuine EV markers such as TSG101, Syntenin or Alix (Jeppesen et al., 2019; Kowal et al., 2016; Tkach et al., 2017). Cell type specific markers which are embedded in the membranes of the vesicles enable examination of the cell types of origin. Therefore, next to straight-forward WB or highly sensitive mass spectrometry proteome analysis, microarray or flow cytometry techniques are frequently applied (Arraud et al., 2016; Jorgensen et al., 2013; van der Pol et al., 2014). For the latter, especially the resolution of conventional flow cytometric devices constitutes a main obstacle since particles smaller than 500 nm are hard to detect (Erdbrugger et al., 2016; Erdbrugger et al., 2014). Research on this topic is evolving fast and new approaches including bead-based assays (Koliha et al., 2016) or imaging flow cytometry (IF) (Görgens et al., 2019; Lannigan et al., 2017) are developing. Finally, the analysis of proteomic and nucleic acid content in plasma EVs by mass-spectrometric profiling or RNA-seq, respectively, may reveal functional properties. Here similarly, choice of isolation technique may confound analysis results (Simonsen, 2017; Van Deun et al., 2014).

In conclusion, plasma-EV isolation and characterization is highly challenging. One must carefully consider the combination of EV purification with subsequent characterization method in order to prevent contaminants to falsify the experimental outcomes. When precautions are taken, blood plasma samples offer the possibility to study EV signaling in a variety of physiologic or pathophysiologic settings.

1.4 Extracellular vesicles in physical exercise

The physiologic changes found during physical exercise are accompanied by the liberation of EVs into the circulation. Several studies monitored the release of EVs in response to different exercise interventions. Research in humans is focused on large platelet and endothelial EVs, also called platelet microparticles (PMPs) and endothelial microparticles (EMPs). PMPs are demonstrated to increase during physical activity, starting at an early phase of exercise and reaching baseline few hours after the exercise session (Wilhelm

et al., 2018). Their release can be attributed to the activation of coagulative processes (Ahmadizad et al., 2010) and shear stress (Wilhelm et al., 2016) during exercise. In contrast, EMPs are mainly found in elevated concentrations 24 h or longer after an exercise intervention. They are considered to result from apoptotic processes and exhibit harmful effects in functional analyses (Wilhelm et al., 2018).

Recently, small EVs have caught attention in the context of physical activity and a possible contribution to beneficial adaptations (Piccirillo, 2019; Safdar et al., 2018). An increasing number of divergent studies appeared, which addressed the release and their possible involvement in signaling pathways. In healthy persons, it was shown that physical exercise leads to an acute increase of EVs including CD41b-positive platelet-EVs in the human circulation while MV numbers remained unchanged immediately after physical activity (Frühbeis et al., 2015). In diabetic patients, EVs released in response to exercise might carry miRNAs that interfere with MMP9-signaling which leads to attenuated fibrosis and myocyte uncoupling (Chaturvedi et al., 2015). Furthermore, a 3-weeks swimming protocol compared to a sedentary lifestyle of mice enhanced the positive effect of isolated EVs against acute ischemia/reperfusion injury in recipient mice (Bei et al., 2017). A set of EV-associated miRNAs was differentially expressed in the blood of rats after acute aerobic exercise and could be involved in the MAPK (mitogen-activated protein kinase)-pathway (Oliveira et al., 2018). Addressing muscle-derived EVs, it was shown that 1-5 % of EVs released during exercise are α-sarcoglycan (SGCA) positive and contain muscle specific miRNAs and/or proteins which could indicate involvement in muscle regeneration processes following exercise (Guescini et al., 2015). Proteomic analysis of EVs isolated via low-speed centrifugation implied that EVs released into the blood after cycling exercise comprise muscle-derived EVs transporting myokines to the liver (Whitham et al., 2018). However, examination of miRNA changes in circulating small EVs after muscle damaging exercise did not reveal alterations in muscle specific miRNA species (Lovett et al., 2018). Summarized, these studies provide evidence that small EVs are actively released into the blood stream during physical exercise, might function as mediators of different key signaling

pathways and possibly be involved in adaptation processes triggered by exercise.

1.5 Aim of the study

Acute physiological chanegs during physical exercise seem to trigger the active release of EVs into the circulation which might be involved in homeostatic and adaptational tissue-cross-talk. However, detailed knowledge on small EV release kinetics, originating cell populations as well as their cargo during acute exercise is scarce and putative functions of the liberated EVs in target cells remain elusive. Here, a detailed phenotyping of extracellular vesicles released upon exhaustive exercise, designated as ExerVs, will be performed.

First, eligible EV purification from human blood plasma to study ExerVs will be established. To this end, isolation i) based on size by SEC and ii) based on EV-marker presence (CD9, CD63, or CD81) by IA capture will be implemented. To further improve purity of EVs, SEC will be combined with iodixanol density gradient purification (IDG). Secondly, a modified IA capture isolation protocol will be tested. Subsequently, a basic characterization of the differentially isolated EVs will be performed via estimation of protein content, WB, NTA or EM, where applicable.

In a second step, release kinetics and origin of ExerVs will be studied in a defined cycling exercise setting until exhaustion involving 21 subjects. Therefore, WB, NTA, and IF analyses will be implemented and evaluated concerning validity. For a detailed phenotyping analysis two multiplexed assays, the microarray-based EV Array and the commercial bead-based flow cytometric assay MACSPlex, will be applied.

Based on these examinations, originating cell populations of ExerVs will be defined and putative functions of ExerVs as well as their possible involvement in beneficial signaling in health and diseases can be postulated.

2 Materials and Methods

2.1 Equipment

2.1.1 Chemicals

Table 2.1: Chemicals

Name	Item	Source
1,4-Dithiothreitol (DTT)	#6908.2	Carl Roth
10 % ammonium peroxodisulfate (APS)	#9592.2	Carl Roth
10 x phosphate buffered saline (PBS)	#P5493-1L	Sigma Aldrich
20 x NuPAGE MES SDS running buffer	#NP0002	Life Technologies
30 % hydrogen peroxide	#8070.2	Carl Roth
Acrylamide mix 30% (Rotiphorese Gel 30)	#3029.1	Carl Roth
Color prestained protein standard, broad range (11–245 kDa)	#P7712L	NEB
DMEM, high glucose, no glutamine	#11960044	Life Technologies
Ethanol	#9065.4	Carl Roth
Fetal bovine serum (FBS)	#10270106	Life Technologies
H_2O ultrapure	#W4502	Sigma Aldrich
L-glutamine 200 mM 100 ml	#25030024	Life Technologies
Milk powder	#T145.2	Carl Roth
N,N,N',N'-tetramethylethylenediamin (TEMED)	#2367.1	Carl Roth
NuPAGE Novex 4-12% Bis-Tris protein gels	#NP0335BOX	Life Technologies
OptiPrep density gradient solution 60%	#D1556	Sigma Aldrich/ Axis-Shield PoC AS
Penicillin/streptomycin	#P0781-100ML	Sigma Aldrich
Ponceau S	#P7170	Sigma Aldrich
RPMI medium 1640	#21875034	Life Technologies
Sepharose CL-2B	#17014001	GE Healthcare
Silica microspheres, 0.1 µm	#24041	Polysciences
Tween 20	#9127.2	Carl Roth

2.1.2 Buffers, media and solutions

Table 2.2: Buffers, media and solutions

Buffer/medium/solution	Composition
Homemade enhanced chemiluminescence (ECL) solution	Solution A: 50 mg luminol in 200 ml 0.1 M Tris-HCl pH = 8.6
	Solution B: 11 mg para-hydroxy coumaric acid in 10 ml DMSO (dark)
	ECL solution: combine 1 ml solution A + 100 µl solution B + 0.3 µl H_2O_2
IDG homogenization solution	250 mM sucrose, 1 mM EDTA, 10 mM Tris-HCl
IDG working buffer	250 mM sucrose, 6 mM EDTA, 60 mM Tris-HCl
Lysis buffer LC-MS	20 mM Tris pH 8.0, 1 % SDS, sterile filtered
Lysis buffer P	50 mM Tris-HCl, pH 8, 120 mM NaCl, 5mM EDTA, 0.5 % NP-40, sterile filtered
4 % milk	4 % milk powder in PBS-T
PBS	150 mM NaCl, 8 mM Na_2HPO_4, 1.7 mM NaH2PO4, pH = 7.2
PBS-T	0.1 % Tween in PBS
8 %-polyacrylamide separation gel	For 10 ml (1 gel): 4.6 ml ddH_2O, 2.7 ml acrylamide mix 30 %, 2.5 ml Tris (1.5 M, pH 8.8), 0.1 ml 10 % SDS, 0.1 ml 10 % APS, 6 µl TEMED
10 %-polyacrylamide separation gel	For 10 ml (1 gel): 4 ml ddH_2O, 3.3 ml acrylamide mix 30 %, 2.5 ml Tris (1.5 M, pH 8.8), 0.1 ml 10 % SDS, 0.1 ml 10 % APS, 4 µl TEMED
12 %-polyacrylamide separation gel	For 10 ml (1 gel): 3.3 ml ddH_2O, 4 ml acrylamide mix 30 %, 2.5 ml Tris (1.5 M, pH 8.8), 0.1 ml 10 % SDS, 0.1 ml 10 % APS, 4 µl TEMED
5 %-polyacrylamide stacking gel	For 3 ml (1 gel): 2.1 ml ddH_2O, 0.5 ml acrylamide mix 30 %, 0.38 ml 1.0 M Tris pH 6.8, 0.03 ml 10 % SDS, 0.03 ml 10 % APS, 3 µl TEMED
5 x SDS running buffer for electrophoresis	125 mM Tris, 1.25 M glycine, 0.5 % SDS, pH = 8.3
WB transfer buffer	24 mM Tris, 192 mM glycine, 20 % ethanol in dH_2O
4 x WB sample buffer	200 mM Tris-HCl, pH = 6.8, 10 % SDS, 0.4 % bromophenol blue, 40 % glycerol, if reducing conditions desired: 400 mM DTT

2.1.3 Materials

Table 2.3: Materials

Material	Item	Manufacturer
µ columns with plungers	#130-042-701	Miltenyi Biotec
0.22 µm PES-filter membranes	#CX07.1	Merck Millipore
Amicon Ultra-4, regenerated cellulose membrane, 10 kDa pore size	#UFC801024	Merck Millipore
Amicon Ultra-15, regenerated cellulose membrane, 100 kDa pore size	#UFC910024	Merck Millipore
BCA Protein Assay Kit	#71285-3	Merck Millipore/Novagen
Clear-view Snap-Cap micro tubes, 1.5 ml, low retention	#T4816-250EA	Sigma Aldrich
Exosome Isolation Kit, human (CD63)	#130-110-918	Miltenyi Biotec
Exosome Isolation Kit, human (CD81)	#130-110-914	Miltenyi Biotec
Exosome Isolation Kit, human (CD9)	#130-110-913	Miltenyi Biotec
MACSPlex Exosome, Kit, human	#160-001-032	Miltenyi Biotec
Monovettes: S-Monovette 7.5 ml K3E S-Monovette 2.7 ml K3E S-Monovette 7.5 ml Z-Gel Microvette CB 300 K2E	 #01.1605.001 #05.1167 #01.1602 #16.444	Sarstedt
Plastic capillary 20 µl, sodium-heparinized	#7111-0011-20H	EKF Diagnostics
Polyallomer UC tubes, 14 ml	#331374	Beranek/Beckman Coulter
Protein LoBind Tubes 5.0 ml, PCR clean	#525-0792	Eppendorf
PVDF-membrane Immobilon-P, 0.45 µm pore size	#IPVH00010	Merck Millipore
Safety-lancet, normal, 21 G, 1.6 mm	#85.1016	Sarstedt
Safety-Multifly needle, 21 G 200 mm	#85.1638.235	Sarstedt
Syringe 10 ml	#613-3931	VWR
X-ray films Hyperfilm ECL	#28-9068-37	VWR/Amersham

2.1.4 Antibodies

Table 2.4: Primary antibodies used in western blotting

Antigen	Clone	Host species	Dilution	Manufacturer
Alix	49/AIP1	mouse	1:1000	BD
ApoA1	12C8	mouse	1:200	Santa Cruz
ASGPR2	C-4	mouse	1:200	Santa Cruz
CD9	MM2/57	mouse	1:2000	Merck Millipore
CD41b	SZ.22	mouse	1:1000	Santa Cruz
CD63	RFAC4	mouse	1:500	Merck Millipore
CD81	B-11	mouse	1:1000	Santa Cruz
Calnexin	polyclonal	rabbit	1:1000	Enzo
Flotillin-1	polyclonal	rabbit	1:1000	Sigma
HSP70	7/Hsp70	mouse	1:1000	BD
Na/K-ATPase	464.6	mouse	1:5000	Novus Biologicals
SGCA	D-7	mouse	1:500	Santa Cruz
Syntenin	polyclonal	rabbit	1:2000	Abcam
TSG101	4A10	mouse	1:1000	GeneTex

Table 2.5: Secondary antibodies used in western blotting

Host species	Target species	Conjugation	Dilution	Cat. No.	Manufacturer
goat	mouse	HRP	1:10,000	115-035-166	Dianova
mouse	rabbit	HRP	1:10,000	211-032-171	Dianova

Table 2.6: Primary antibodies included in EV Array analysis

Antigen	Clone	Manufacturer	Info
Alix	#3A9	Biolegend	EV marker
Annexin V	polyclonal	R&D Systems	Antibody against Annexin V, not phosphatidylserin
Apo E	#395004	R&D Systems	Lipoprotein marker
CAIX	#2D3	Abcam	Carbonic anhydrase
Cathepsin D	polyclonal	R&D Systems	Lysosome
CAXII	#315602	R&D Systems	Carbonic anhydrase
CD14	#M5E2	BD Biosciences	TLR4 co-receptor, monocytes
CD142	#323514	R&D Systems	Tissue factor, endothelial cells, leukocytes
CD146	#P1H1	Abcam	Cell surface glycoprotein 18, endothelial cells
CD151	#210127	R&D Systems	Tetraspanin
CD171	polyclonal	Sigma-Aldrich	L1 protein, cell adhesion
CD235a	#R10	R&D Systems	Glycophorin A, erythrocytes
CD31	polyclonal	R&D Systems	PE-CAM1, platelets, endothelial cells

CD4	#34930	R&D Systems	T cells(, monocytes)
CD42a	polyclonal	LS Bio, Seattle	Glycoprotein 9, von Willebrand factor (vWF)-receptor, platelets
CD42b	#486805	R&D Systems	Glycoprotein 1b, von vWF, platelets
CD45	#2D1	R&D Systems	Proteintyrosine phosphatase C, leukocyte common antigen, B cells, T cells
CD62E/P	#BBIG-E6	R&D Systems	E and P-selectin, endothelial cells, platelets (activated)
CD62E	#1.2B6	Thermo Scientific	E-selectin, endothelial cells
CD63	#MEM-259	Bio-RAD	Tetraspanin, EV marker
CD81	#1.3.3.22	Ancell	Tetraspanin, EV marker
CD82	#423524	R&D Systems	Tetraspanin, EV marker
CD8a	#37006	R&D Systems	T cell receptor co-receptor, cytotoxic T cells, NK cells, DCs
CD9	#SN4/C3-3A2	Ancell, Bayport	Tetraspanin, EV marker
EpCAM	#0.N.277	Santa Cruz	CD326, Epithelial cell adhesion molecule
Flotillin-1	polyclonal	Abcam	EV marker
GRP78	#N-20	Santa Cruz	Binding immunoglobulin protein, chaperone, ER
HLA-ABC	#W6/32	Biolegend	MHCIa
HLA-DR	#L243	Biolegend	MHCII
HLA-DRDPDQ	#HB-145	Loke Diagnostics	MHCII
Hsp70	polyclonal	Assay Design	Chaperone, EV marker
Hsp90	polyclonal	Abcam	Chaperone, EV marker
ICAM-1	#R6.5	eBioscience	CD54, endothelial cells and immune cells
LAMP-1	#508921	R&D Systems	Lysosomal membrane protein, late endosome and MVB marker
LFA1	#HI111	Ab Biotec	Lymphocyte function-associated antigen 1
TGFb1	#A75-2	BD Pharmingen	Transforming growth factor β, cytokine
TLR3	#TLR3.7	Santa Cruz	Anti-viral response, binds dsRNA
tPA	polyclonal	R&D Systems	Tissue plasminogen activator, conversion of plasminogen to plasmin, anti-coagulation, endothelial cells
TSG101	polyclonal	Abcam	EV marker
VE-Cadherin	polyclonal	R&D Systems	CD144, endothelial cells
VEGFR2	#7D4-6	Biolegend	Endothelial cells, angiogenesis

Table 2.7: Capture antibodies included in the MACSPlex analysis (MACSPlex exosome human kit, Milteny Biotec)

Antigen	Antibody isotype	Info
CD1c	mIgG2a	Glycoprotein, APC
CD2	mIgG2b	Cell adhesion molecule, T cells, NK cells
CD3	mIgG2a	T cell co-receptor
CD4	mIgG2a	Glycoprotein, T cells(, monocytes)
CD8	mIgG2a	Transmembrane glycoprotein, T cell receptor co-receptor, cytotoxic T cells
CD9	mIgG1	Tetraspanin, EV marker
CD11c	mIgG2b	Integrin αX, DCs, leukocytes
CD14	mIgG2a	TLR4 co-receptor, monocytes
CD19	mIgG1	B-lymphocyte antigen
CD20	mIgG1	B-lymphocyte antigen
CD24	mIgG1	Signal transducer 24, sialoglycoprotein, B cells
CD25	mIgG1	Interleukin-2 receptor α chain, lymphocytes
CD29	$mIgG1_K$	integrin β-1, cell surface receptor
CD31	mIgG1	PE-CAM1, platelets, endothelial cells
CD40	$mIgG1_K$	Protein receptor, AP cells
CD41b	REA	integrin αIIβ, platelets
CD42a	REA	Glycoprotein 9, vWF-receptor, platelets
CD44	mIgG1	AP cells, immune signaling
CD45	mIgG2a	Proteintyrosine phosphatase C, leukocyte common antigen, B cells, T cells
CD49e	mIgG2b	integrin α-5
CD56	REA	ICAM-1, endothelial cells and immune cells
CD62P	REA	P-selectin, platelets (activated)
CD63	$mIgG1_K$	Tetraspanin, EV marker
CD69	$mIgG1_K$	transmembrane C-type lectin protein, immune cells
CD81	REA	Tetraspanin, EV marker
CD86	mIgG1	AP cells, T cell activation
CD105	mIgG1	Endoglin, type I membrane glycoprotein, endothelial cells
CD133/1	$mIgG1_K$	Prominin-1, glycoprotein
CD142	$mIgG1_K$	Tissue factor, endothelial cells, leukocytes
CD146	mIgG1	Cell surface glycoprotein 18, endothelial cells
CD209	mIgG1	Dendritic Cell-Specific Intercellular adhesion molecule-3-Grabbing Non-integrin, C-type lectin
CD326	mIgG1	Epithelial cell adhesion molecule
HLA-ABC	REA	MHCI
HLA-DRDPDQ	REA	MHCII
MCSP	mIgG1	melanoma-associated chondroitin sulfate proteoglycan
ROR1	$mIgG1_K$	Tyrosine-protein kinase transmembrane receptor
SSEA-4	REA	Stem cells

2.1.5 Devices

Table 2.8: Devices

Type	Name	Manufacturer
Centrifuge	Centrifuge 5810R; rotor FA-45-24-11	Eppendorf
Centrifuge	Centrifuge 5424R; rotors FA-45-6-30, A-4-81, A-2-DWP	Eppendorf
Centrifuge	Hettich Universal 320 R	Andreas Hettich
Centrifuge	Tabletop Biofuge fresco	Heraeus
Centrifuge	Centrifuge ZK496	Hermle
Cycling ergometre	Ergoselect 200	Ergoline
Electronic pipette	Single channel electronic pipette E4 XLS	Rainin
Flow cytometer	MACSQuant Analyzer 10	Miltenyi Biotec
Lactate biosensor	Biosen 5140	EKF Diagnostics
Magnetic stand	µMACS Separator	Miltenyi Biotec
Nanoparticle tracking	Nanosight LM10 system, camera model Hamamatsu C11440-50B/A11893-02, 532 nm laser	Malvern
pH meter	pH meter Lab 850	Schott
Plate reader	Tecan Infinite M200 Pro	Life Science
Refractometre	Refractometer T; Refractometer 2T	Atago
SDS-PAGE system	Mini-PROTEAN TetraVertical electrophoresis cell	Bio-Rad
SDS-PAGE system	XCell SureLock Mini-Cell electrophoresis system	Invitrogen
Thermocycler	CFX384 Touch real-time PCR detection system	Bio-Rad
Ultracentrifuge	Optima L-90 K ultracentrifuge; SW40 Ti rotor	Beckman Coulter
WB system	Mini Trans-Blot cell	Bio-Rad
X-ray film processor	Optimax Typ TR x-ray film processor	MS Laborgeräte

2.1.6 Software

Table 2.9: Software

Software	Developer
Blue Cherry	Geratherm Respiratory
CorelDRAW X7	Corel Corporation
FiJi ImageJ 64 V5	Open source, NIH
GraphPad PRISM	Graphpad Software
JMP	SAS
MACSQuantify software	Miltenyi Biotec
Nanosight 2.3 software	Malvern
R Studio Version 3.5.0	RStudio Inc
Winlactat	Mesics GmbH, Münster

2.2 Study design

2.2.1 Study participants

Study participants were recruited by employees of the department of sports medicine, Mainz, in training hours of the university sports as well as during regular performance diagnostics. Healthy male persons aged between 20 and 40 years with regular exercise training were included. Participants should be non-smokers and absent from medication for at least two weeks. They were informed orally and in writing about the procedure as well as possible complications and signed a consent form for participating in the study.

2.2.2 Study procedure

Several criteria were implemented in favor of standardization of the study procedure. To exclude an influence of the circadian rhythm on study outcomes, all tests were performed between 8 and 10 am. An acute impact of the diet on results was avoided by at least eight hours of over-night fasting. Participants should not be exposed to exhaustion prior to the test to ensure proper estimation of resting values. To this end they abstained from exercise training for 24 h, chose a non-exhaustive way to arrive at the department of sports medicine and rested for a minimum of 30 min before the first blood drawl. Prior to the exercise tests a medical examination including anamnesis, estimation of lung function, electrocardiography and blood pressure at rest as well as bioelectrical impedance analysis was performed.

2.2.3 Exhaustive exercise setting

The athletes were subjected to an incremental cycling test until exhaustion which was indicated subjectively by the participant. The tests were conducted on a cycling ergometer *ergoselect 200*. The standard exercise protocol comprised a starting power of 40 W and increasing levels by 40 W every 3 minutes. In few cases during pilot experiments the exercise protocol was adapted to the athletes' physical fitness. Borg values were stated by the subject at the end of each 3 min-level. Heart rate, blood pressure and electrocardiography were recorded, which gave the supervisor the possibility

to abort exertion in case of anomalies that could expose the participant to health risk. Also, respiratory analysis was implemented to monitor ventilatory equivalents. Estimation of respiratory data was done using the *Blue Cherry* software.

2.2.4 Blood sampling

Venous blood collection was performed at three time points. Prior to the test, blood was drawn at resting conditions during the medical examination. During the test, when a respiratory quotient of 0.9 was reached, the second venous blood drawl was performed. The third venous blood drawl was performed within 2 min after exhaustion and completion of the test. In indicated experiments, additional venous blood was taken at a recovery time after exhaustion. In this case, participants were kept at resting conditions after the test. For venous blood collection 33 ml of blood were obtained from the median cubital vein with a Safety-Multifly needle (0.8 × 19 mm) and collected in tripotassium-EDTA covered Monovettes and serum-gel Monovettes.
Capillary blood sampling was performed for lactate and/or cfDNA estimation. For assessment of lactate levels 20 µl of capillary blood were collected from the earlobe in sodium-heparinized capillaries and for cfDNA measurement 30 µl of capillary blood were collected with a dipotassium-EDTA covered Microvette CB 300 from the fingertip. Time points were prior to the test (for lactate and cfDNA), at the end of each 3 min level (for lactate and cfDNA), immediately after exhaustion (for lactate and cfDNA), and 3 min (for cfDNA only), 10 min (for cfDNA only) as well as 20 min (for cfDNA only) after exhaustion.

2.2.5 Blood cell counts, physiologic and metabolic parameters

Venous blood in serum-tubes and EDTA-tubes were sent to routine diagnostics in order to receive metabolic parameters and blood cell counts of the participants at rest and exercising conditions.
Blood lactate levels were assessed with the lactate analyser Biosen 5130 and evaluated with winlactate software. The individual anaerobic threshold was

determined at a net increase of lactate concentration of 1.0 mmol/l above lactate concentration at lactate threshold (Roecker et al., 2003).

2.2.6 Cell-free DNA

For cell-free DNA (cfDNA) analysis capillary blood was centrifuged 2 min at 1,600 x g at 4 °C and plasma was stored at -80 °C until measurement. Nucleic acid concentration was measured by Dr. Elmo Neuberger (Sports Medicine, Mainz, Germany) applying direct quantitative polymerase chain reaction (qPCR) of the L1PA2-repeat as published in Breitbach et al. with few changes. 2 µl of diluted plasma (1:10 in H_2O) were mixed with 13 µl of qPCR-mastermix (final concentrations: Velocity polymerase 0.6 u, 1.2x Hifi buffer, 0.15x SYBR Green, 0.001x FITC, 0.3 mM dNTPs, 0.15 µM primer-mix) and analyzed in triplicates in a final volume of 5 µl. Amplification of the 90 bp L1PA2 fragment was performed using the CFX384 thermocycler with 2 min 98 °C, followed by 10 s 95 °C and 10 sec 64 °C for 35 cycles (Breitbach, Tug, et al., 2014).

2.2.7 Preparation of platelet free plasma

To prevent platelet degranulation, venous blood in EDTA-tubes was kept vertically on room temperature (RT) avoiding agitation. To obtain platelet free plasma two consecutive centrifugation steps of 15 min at 2,500 x g at RT were performed. First centrifugation was started within 15 min after blood collection. Plasma was collected leaving 1 ml of plasma in the tube to avoid contamination with cells from the buffy coat. Then the collected plasma was subjected to a second centrifugation. The supernatant was collected and again, 0.5 ml were left in the tube to avoid carry-over of remaining blood cells. The prepared platelet-free plasma was kept on ice until EV preparation or frozen at -80°C.

2.3 Cell culture and primary cell isolation

2.3.1 K562 cells

The cell line K562 originates from a 53-year-old female patient suffering from acute myelogenous leukaemia (Lozzio et al., 1979). K562 cells display

erythroleukaemia type and cultivation enables differentiation to cells with monocyte, granulocyte, and erythrocyte characteristics (Lozzio et al., 1981).
Cultivation of K562 cells was performed in DMEM medium supplemented with 10 % fetal bovine serum (FBS), 1 % L-glutamine and 1% penicillin/streptomycin in concentrations from 2-10 x 10^5/ml. Cells were grown at 37 °C and 5 % CO_2. For passaging of cells, cell-containing medium was centrifuged for 5 min at 300 x g at RT. The supernatant was discarded and the cell pellet was diluted in fresh medium to the desired cellular concentration.
For the preparation of conditioned cell culture supernatant (CCS), cells were washed twice in PBS (resuspended and centrifuged for 5 min 300 x g RT) and subsequently seeded in a concentration of 5 x 10^5 cells/ml in medium supplemented with L-glutamine only. After 24 h conditioned CCS was collected by centrifugation for 5 min at 300 x g at RT and pre-cleared either by centrifugation for 15 min at 2,500 x g (protocol P1) or 30 min at 10,000 x g with filtering at 0.22 µm (P2). The cell pellets were washed in ice cold PBS, centrifuged at 300 x g for 5 min and used for cell lysate preparation (see chapter 2.3.4).

2.3.2 THP1 cells

The THP1 cell line is derived from immortalized cells isolated from the peripheral blood of a one year old boy suffering from acute monocytic leukaemia (Tsuchiya et al., 1980). THP1 cells exhibit characteristics of monocytic progenitor cells and can be differentiated to adherent macrophage-like cells induced by the stimulation with phorbol 12-myristate 13-acetate (Tsuchiya et al., 1982; Tsuchiya et al., 1980).
THP1 cells were cultured in RPMI1640 medium supplemented with 10 % FBS, 1 % L-glutamine and 1 % pen/strep in concentrations from 1-10 x 10^5cells/ml. Cells were incubated at 37 °C and 5 % CO_2. For passage of cells, cell-containing medium was subjected to a centrifugation of 5 min at 300 x g at RT. The supernatant was discarded, and the cell pellet was diluted in fresh medium to the desired cellular concentration.
To obtain cell lysates, cell pellets were washed in ice cold PBS, centrifuged again for 5 min at 300 x g and used for subsequent lysate preparation (see chapter 2.3.4).

2.3.3 *Ex vivo* platelet preparation

Platelet-preparation from fresh venous blood was performed by polysucrose density gradient centrifugation. The gradient was prepared by layering 3.5 ml 1.119 g/ml sucrose (Histopaque-1119) with 3 ml 1.077 g/ml sucrose (Histopaque-1077) in a 15 ml tube (fig. 2.1). After blood withdrawal (see chapter 2.2.4) 6 ml were carefully layered on top of the gradient and centrifuged for 30 min at 700 x g and 19 °C without brake. Then, the upper phase (= blood plasma) was discarded and the second phase, which contained mononuclear cells and platelets, was transferred into a fresh 15 ml tube. After a washing step in PBS by centrifugation at 300 x g for 10 min, the platelet-containing supernatant was transferred into a fresh 15 ml tube. Finally, platelets were pelleted at 3,000 x g for 5 min.

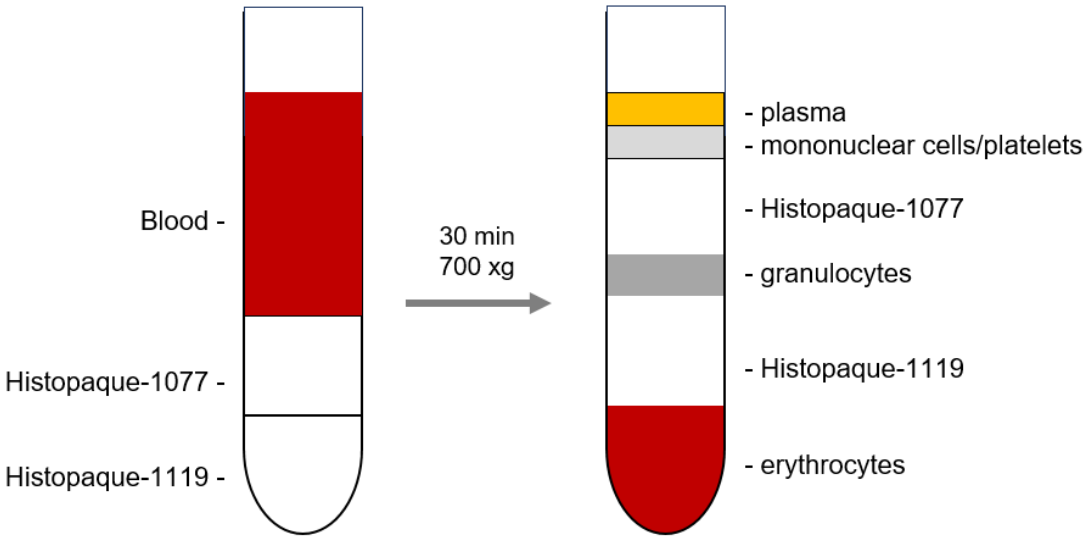

Figure 2.1: Principle of cell separation by density gradient centrifugation. Blood is layered on top of a gradient consisting of 1.119 g/ml sucrose (Histopaque-1119) and 1.077 g/ml sucrose (Histopaque-1077). After centrifugation, cellular phases are separated by the sucrose solutions due to their density.

2.3.4 Cell lysate preparation

For cell lysate preparation, cell pellets from cell culture or *ex vivo* platelet preparation were resuspended in 100 µl lysis buffer P (see tbl. 2.2) and incubated for 15 min on ice. After centrifugation for 15 min at 13,000 x g and 4 °C, the supernatant was stored at -20 °C for further analysis, the pellet was discarded.

2.4 Methods for EV isolation

The preparation of EVs from human blood plasma or cell culture supernatant was performed by applying different methods of EV enrichment, which are described in the following.

To reduce loss of whole vesicles or vesicle associated markers and cargo during the isolation process, several points were considered. In general, EV-containing sample material or isolated EVs were placed on ice or 4 °C to inhibit enzymatic processes. Furthermore, elution volume was kept at a minimum, and low-binding tubes were used to prevent EVs from sticking to the plastic surface of the tubes. In addition, excessive vortexing of samples was avoided and centrifugal speed was kept at a minimum whenever possible to hold EVs as intact as possible. Finally, isolated EVs which were not applied to downstream analysis were immediately stored at -80 °C.

2.4.1 Ultrafiltration

EV enrichment by ultrafiltration (UF) was performed in 10 kDa (0.5 ml and 4 ml loading capacity) or 100 kDa (15 ml loading capacity) Amicon filter devices. Depending on the starting volume of a sample and the volume of the final concentrate, Amicon filter devices with loading capacities of 0.5 ml, 4 ml, 15 ml or a gradual use of the named were applied. Prior to the use, filters were washed with PBS. Then, CCS or pooled SEC fractions (see chapter 2.4.2) were loaded onto the filter and centrifugation was performed at 5,000 x g until the desired volume was reached. After discarding the flow-through, filters were re-loaded with sample material to further elevate concentration. In addition, PBS was added to wash the concentrate in two washing steps. Depending on the used filter device, EV concentrate was eluted by reverse-spin of the Amicon for 2 min at 5,000 x g (0.5 ml-Amicon) or pipetting of the eluate directly from the filter cone (4 ml- and 15 ml-Amicon). In case of EV enrichment from plasma, filters were discarded after use. In case of EV enrichment from CCS, filters were incubated in 0.1 % SDS overnight, washed twice and stored in particle free dH_2O until re-use.

2.4.2 Size exclusion chromatography

EV isolation by SEC was implemented using self-made SEC columns based on the protocol published by Boing et al. (2014) with modifications (illustrated in fig. 2.2) (Boing et al., 2014).

SEC columns were packed in a 10 ml-syringe tube placing a 0.22 µm polyethersulfone (PES)-filter membrane at the bottom of the syringe. For one column 15 ml of Sepharose CL-2B suspension (in 20 % ethanol) was mixed with 5 ml of particle free PBS and gradually filled into the tube to receive a column volume of 10 ml of sepharose. Sepharose was then washed by applying 10 ml of PBS onto the surface while discarding the flow-through. Prepared SEC columns were either used immediately or stored overnight at 4 °C in an appropriate volume of PBS and covered with parafilm to prevent draining.

A sample volume of 2 ml was applied to the column, which was either platelet free plasma, UF-EVs from CCS (pre-enriched in 15 ml-Amicons, 100 kDA, see chapter 2.4.1) or fractions recovered from a density gradient (see chapter 2.4.3). 1 ml-fractions were collected to define EV-rich fractions by analysis of particle count using nanoparticle tracking analysis, protein content applying BCA assay, and presence of vesicular and non-vesicular markers by western blotting. Depending on the volume needed for each downstream analysis method, SEC fractions were further concentrated applying ultrafiltration (0.5 or 4 ml-Amicons, 10 kDa, see chapter 2.4.1).

Analyzing plasma EVs, fractions 4 to 6 were considered EV-rich while plasma-protein and lipoprotein poor, as specified in the results section. To reduce the complexity of the methodical set-up, in subsequent sample preparation the first 3 ml (#1-3) of SEC flow-through were discarded and the second 3 ml (#4-6) were collected as “SEC-EVs”. Subsequently, pooled fractions 4 to 6 were 30-fold concentrated to receive a final volume of 100 µl of SEC-EVs.

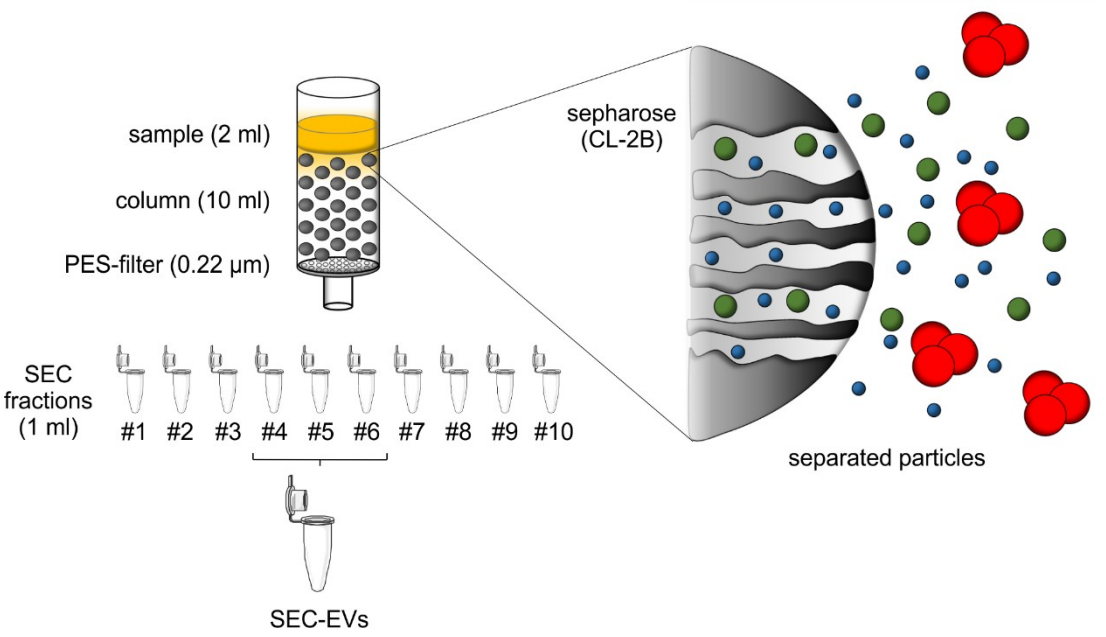

Figure 2.2: Principle of EV isolation by size exclusion chromatography. EVs are separated due to their size and interaction characteristics with the column matrix consisting of agarose spheres. Big particles elute first, small vesicles follow, smaller lipoproteins and plasma proteins elute in the later fractions. 2 ml of EV-containing sample are loaded on a column and 1 ml-fractions are collected for further analysis. The pool of fractions 4 to 6 is defined as SEC-EVs.

2.4.3 Iodixanol density gradient centrifugation

EVs were enriched using SEC in combination with discontinuous iodixanol gradient centrifugation (adapted from Vergauwen et al., unpublished data; IDG-step illustrated in fig. 2.3). The gradient was prepared by carefully layering different solutions of iodixanol (3 ml of 40 %, 3 ml of 20 %, 3 ml of 10 % and 2.5 ml of 5 % OptiPrep) in 14 ml-UC tubes. These were prepared by dilution of the 60 % OptiPrep stock solution with IDG working solution buffer and homogenization medium as specified by the manufacturer (Axis-Shield PoC AS, also see tbl. 2.2). Subsequently, 0.5 ml of the concentrated SEC eluate was loaded on top of the gradient. The samples were then centrifuged for 18 h at ~100,000 x g and 4 °C (Optima L-90K Ultracentrifuge, rotor SW40 Ti, average of 106,154 x g, maximum of 149,576 x g, *k*-factor 260). After centrifugation 1 ml-fractions were collected from the top of the gradient and density was determined using a refractometer. Iodixanol was removed from the fractions by SEC. As described in Vergauwen et al. (2017), SEC fractions 4-7 are considered iodixanol-free and were used for vesicle enumeration using

NTA. Enrichment of EVs after removal of iodixanol was performed using ultracentrifugation (Vergauwen et al., 2017).

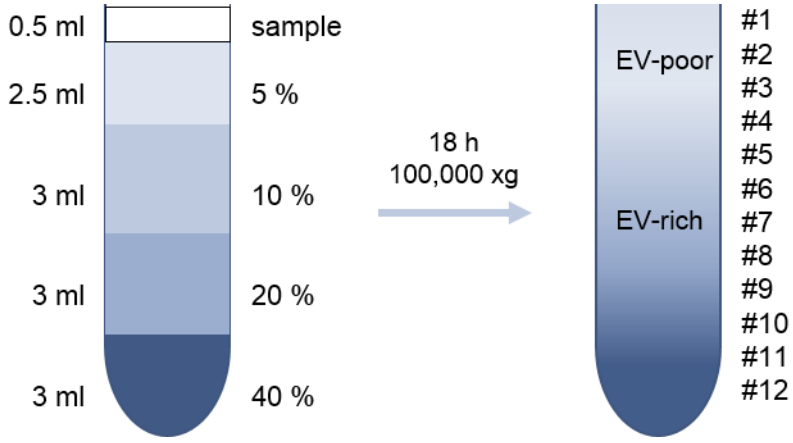

Figure 2.3: Principle of iodixanol gradient centrifugation. Different concentrations (%) of iodixanol are layered with the pre-enriched EV sample. After centrifugation 1 ml-IDG fractions containing EV-poor phase and EV-rich phase can be collected and further analyzed.

2.4.4 Ultracentrifugation

Pre-processed plasma EV samples were enriched by ultracentrifugation implementing a spin at ~100,000 x g (Optima L-90K Ultracentrifuge, rotor SW40 Ti, average of 106,154 x g, maximum of 149,576 x g, *k*-factor 260) and 4 °C for 2 h. Prior to centrifugation, samples were diluted to 13 ml in PBS in UC tubes. For further analysis, pelleted EVs were resuspended in PBS or WB sample buffer by pipetting 50 times up and down using an automatic pipette.

2.4.5 Immuno-affinity capture

EV preparation by IA capture was performed using the CD9-, CD63- or the CD81-Exosome Isolation Kit (Miltenyi Biotec, principle illustrated in fig. 2.4 a). 2 ml of undiluted platelet-free plasma were mixed with 50 µl of CD9-, CD63-, or CD81-antibody-coupled magnetic beads and incubated for 1 h at RT with constant shaking and absent from light. µ-columns were set-up on a magnetic stand and washed as specified in the kit instructions. The mix of plasma and isolation-beads was added to the µ-column and the flow-through was discarded. After washing, the µ-column was removed from the magnetic stand and elution was performed applying 100 µl isolation buffer and pushing the

plunger into the column (standard elution). Alternatively, EV elution was performed directly at the magnetic stand in lysis buffer LC-MS (see tbl. 2.2) in order to retain the magnetic beads in the µ-column (modified elution, illustrated in fig. 2.4 b). The final elution volume was 130 µl of $CD9^+$EVs, $CD63^+$ EVs or $CD81^+$EVs.

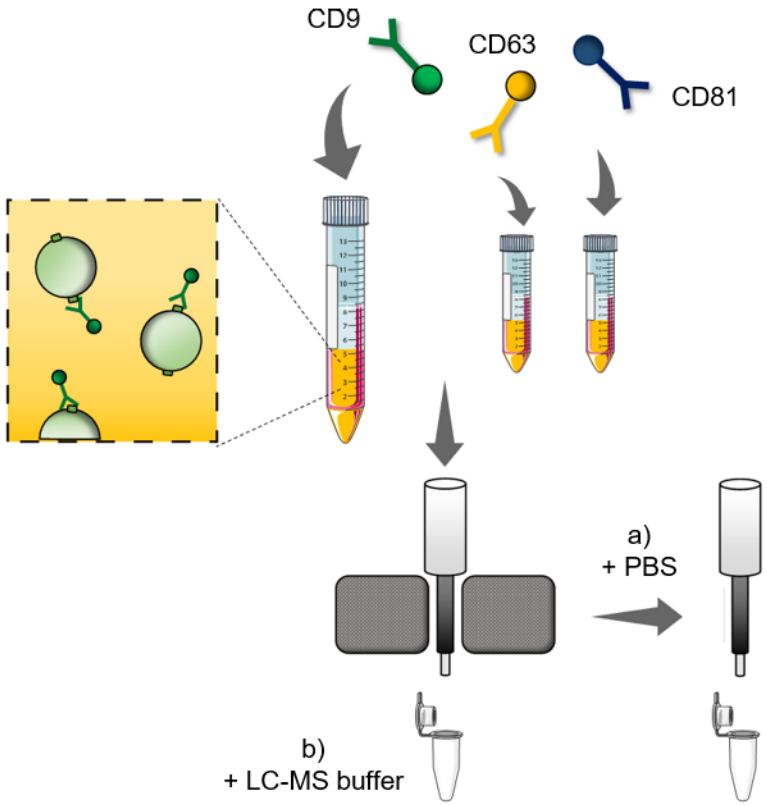

Figure 2.4: Principle of EV isolation by immuno-affinity capture. After magnetic labeling of EVs with beads conjugated to CD9, CD63 or CD81 antibodies, EVs are separated from plasma by magnetic separation. Elution of EVs is performed (a) detached from the magnet by applying isolation buffer/PBS or (b) directly at the magnet by applying LC-MS buffer.

2.5 Methods for EV characterization

2.5.1 Electron microscopy

Electron microscopy imaging was performed by Wiebke Möbius (Max Planck Institute of Experimental Medicine, Göttingen, Germany). SEC-EVs were fixed with 4 % paraformaldehyde and adhered to 100 mesh copper-grids for 5 min. Analysis was performed by transmission electron microscopy after 10 washing

steps with H_2O and embedding in 2 % methylcellulose with 0.4 % uranyl acetate.

2.5.2 Nanoparticle tracking analysis

EVs were subjected to NTA using the Nanosight LM10 system (camera model Hamamatsu C11440-50B/A11893-02) equipped with a 532 nm laser as well as the Nanosight 2.3 software. The temperature was controlled and constantly kept at 23 °C. A syringe pump was implemented in combination with the script control *"Repeatstart, Syringeload 500, Delay 5, Syringestop, Delay 15, Capture 30 and Repeat 4"*. Particle tracking was performed with camera control standard settings at camera level 14. Five videos of 30 s were recorded, particles were tracked, and detection was performed at detection threshold 8 and minimum expected particle size "auto". Average values from these five measurements were formed for particle concentration as well as mode and mean particle size. EV samples were diluted in particle-free PBS to obtain a particle concentration of 3-10 $x10^8$ particles/ml. Measurements were verified utilizing silica microspheres with a size of 100 nm as described in Gardiner et al. 2013 (Gardiner et al., 2013).

2.5.3 Imaging flow cytometry

The enumeration of EVs using imaging flow cytometry was performed by Rita Ferrer Tur and Andre Görgens at the Institute for Transfusion Medicine, University Hospital Essen on an Amnis ImagestreamX MkII. To this end EVs in plasma and SEC-EVs (each diluted 1:10 in PBS) were fluorescently labelled with BODIPY in 10 µM final concentration. After further dilution in PBS total EVs and EV subclasses were measured with the Amnis as described in Görgens et al., 2019 (Görgens et al., 2019).

2.5.4 Total protein content

Protein content of EV preparations was estimated using the Novagen BCA Protein Assay Kit according to the manufacturer's instructions implementing the enhanced assay protocol. The Tecan Infinite M200 Pro was used for the

measurement (Nunclon 96 flat bottom plates, absorbance at 562 nm, 5 flashes per well).

2.5.5 Western blotting

Differentially obtained EV-containing samples and cell lysates as antibody positive controls (K562-, THP1-cells and *ex vivo* platelets) were mixed with WB sample buffer (tbl. 2.2) and subjected to SDS-PAGE (sodium dodecyl sulfate–polyacrylamide gel electrophoresis) on self-made 8 %, 10 % and 12 % gels (buffer: 1x SDS running buffer for electrophoresis, tbl. 2.2) or pre-cast 4-12 % NuPAGE Novex 4-12 % Bis-Tris gels (buffer: NuPAGE MES SDS running buffer, tbl. 2.2). Proteins from the gel were transferred on a PVDF-membrane using Bio-Rad western blotting system (buffer: Western blotting transfer buffer, tbl. 2.2). To verify proper transfer of proteins, ponceau staining was performed by incubation with ponceau solution for 5 min followed by two washing steps of 1 min in H_2O. Membranes were then blocked with 4 % milk for 30 min. Incubation of primary antibodies (tbl. 2.4) in 4 % milk in PBS-T was performed for 2-3 h at RT or overnight at 4 °C. After three washing steps in PBS-T for 10 min, secondary antibody (tbl. 2.5) in 4 % milk in PBS-T was incubated for 30 min at RT. Subsequently, chemiluminescent detection was implemented by 2 min incubation of the membrane in ECL (tbl. 2.2) and visualization with x-ray films on an x-ray film processor. If applicable, the membrane was re-stained with a primary antibody for a different marker protein after a washing step in 4 % milk. For semi-quantitative evaluation, signals were normalized to sample volume (plasma-EVs) or NTA particle amount (K562-EVs) and analyzed in ImageJ software. Immuno-stainings showing high background noise were excluded from semi-quantitative analysis (e.g. presented $CD9^+$EVs Syntenin staining, fig. 3.17).

2.5.6 EV Array

EV Array experiments were performed by Dr. Malene Jorgensen and Rikke Baek (Department of Clinical Immunology, Aalborg University Hospital, Denmark) as described in Baek and Jorgensen, 2017 (Baek et al., 2017; Jorgensen et al., 2013). Shortly, EV containing plasma samples are applied to

epoxy-silane-coated microarray slides and EVs are captured by the coated antibodies depending on their specific surface marker proteins. Subsequently, a cocktail of biotinlabeled detection antibodies against the exosomal markers CD9, CD63, and CD81 is applied. Finally, fluorescently labeled streptavidin is added and detection of the captured EVs is performed. 10 µl of platelet free plasma were used to analyze the presence of 41 marker proteins (see tbl. 2.6). Analysis of EV Array data was modified from the original procedure as follows. First, the mean fluorescence intensities of a marker for the included controls (first: washing buffer on coated microarray spots; second: plasma on uncoated microarray spots) were calculated. The limit of detection (LOD) for a marker in a sample was then set to the fluorescence intensity at 3-times the standard deviation above the mean of each of the control samples. Further statistical analysis (see chapter 2.6) was restricted to those candidates that reached a mean fluorescence intensity above this LOD.

2.5.7 MACSPlex assay

MACSPlex analysis was performed using the MACSPlex Exosome, human, Kit (Miltenyi Biotec) according to the kit specifications (fig. 2.5). 120 µl of SEC-EVs and 50 µl of immuno-captured beads were used for MACSPlex-analysis. Accordingly, comparison between time points of analysis (pre, RQ, post) was based on sample volume. PBS was included as a background control sample. Samples were incubated overnight with 15 µl of the capture antibody mix (list of included capture antibodies in tbl. 2.7) in a total volume of 135 µl at RT with constant shaking and absent from light. After removal of excessive capture antibodies by a washing step, 15 µl of a mix of CD9-, CD63, and CD81-APC detection antibodies was added and incubated likewise in a total volume of 150 µl. After another washing step, flow cytometric analysis was carried out in round-bottom 96-well plates on the MACSQuant Analyzer 10 (Miltenyi Biotec) with the corresponding software, implementing the MACSPlex exosome application. Bead counts were monitored and values with counts below 10 were excluded from further analysis. For the evaluation of mean fluorescence intensities, background values of the control sample of each run was subtracted from the sample values. Surface marker values below the corresponding control antibody, considered as measurement threshold, were

regarded as negative. For the capture antibodies CD4 and CD14, data series in which the RQ 0.9 and/or post exercise values were clearly above the threshold, pre-values were included despite being under the threshold.

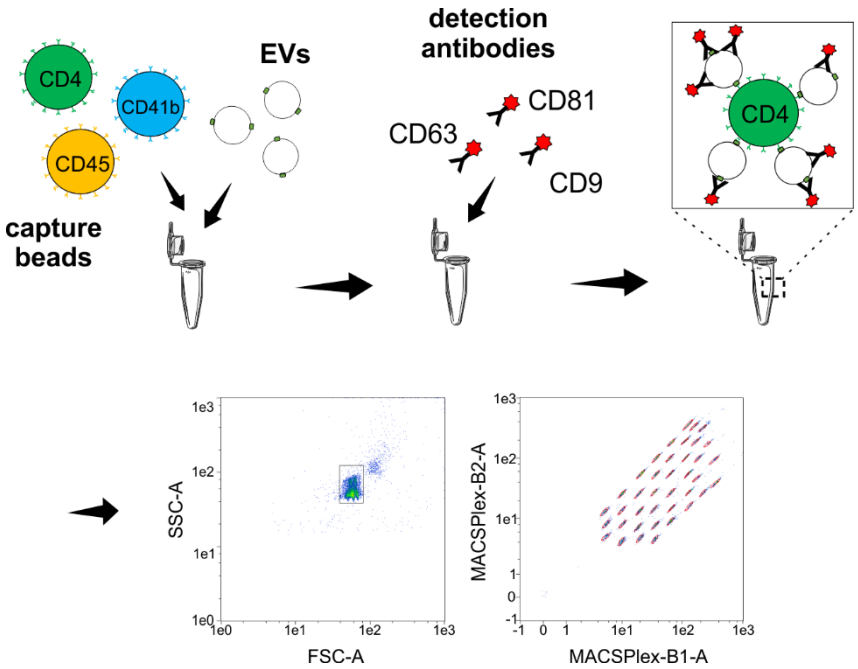

Figure 2.5: Principle of the MACSPlex assay. Isolated EVs are captured by color-coded beads carrying specific antibodies for cell surface markers (e.g. CD4, CD41b, CD45). Subsequently, detection antibodies for the EV markers CD9, CD63 and CD81 conjugated to the fluorophore APC bind to the EVs. Using flow cytometry, the surface marker profile of the sample is visualized.

2.5.8 Liquid-chromatography mass spectrometry

Liquid-chromatography mass spectrometric (LC-MS) analysis of proteomic EV-content was performed by Ruben Spohrer and Prof. Dr. Stefan Tenzer at the Core Facility for Mass Spectrometry, University Medical Centre, Mainz, as previously described (Distler et al., 2014; Sielaff et al., 2017). For the purity analysis of differentially prepared EV samples, the mean scores (parts per million of total proteins) of ApoA1, complement component 3 (CoC3), immunoglobulin κ light chain (IGK) and albumin were compared to EV associated markers CD81 and Syntenin.

2.6 Statistical analysis

Marker fold-changes obtained from EV Array, WB and MACSPlex analysis were statistically analyzed in JMP. Log base-2 normalized values were compared by ANOVA across the three time points in the exercise setting (pre exercise, RQ 0.9 and post exercise). A significant global F-test ($p<0.05$) was followed by a post-hoc test using each pair's student's t-test. Post hoc p-values were Bonferroni-Holm-corrected for the comparison 'pre to RQ 0.9' and 'pre to post' and a value of < 0.05 was considered significant (*=$p<0.05$, **=$p<0.01$, ***=$p<0.001$). Marker fold changes were transformed back and are presented in diagrams as geometric means with individual subject results for WB analysis and 95 % confidence intervals for EV Array and MACSPlex analysis. Full list including geometric mean fold changes, 95 % confidence interval and Bonferroni-Holm corrected post hoc p-values in tbl. S2 to S4.

The heatmaps of MACSPlex marker fold-changes were generated in R (version 3.5.0) with the ComplexHeatmap package (version 1.18.1), clustering was done with Pearson correlation (Gu et al., 2016).

3 Results

3.1 Evaluation of EV-isolation from human blood plasma

3.1.1 EV isolation based on size exclusion chromatography

Identification of EV-rich SEC fractions

Isolation of EVs from blood plasma can be performed based on different EV characteristics. Using size exclusion chromatography, EV enrichment is dependent on their size and interaction with a column matrix which is different for other plasma components. Here, plasma was subjected to SEC on self-made sepharose columns (see chapter 2.4.2) and EV-rich SEC fractions were defined using NTA, protein measurement and WB. Comparison of particle numbers and protein concentration indicates that fractions 4 to 6 are particle-rich while protein-poor (a representative result is shown in fig. 3.1 a). An increasing amount of protein was detected in fractions 7 to 10 which was also visible in NTA measurement by increasing light scattering due to the sample's background (see fig. S1). Particle-rich fractions 4 to 6 revealed a characteristic size distribution for small EVs with mean particle sizes of 107.9 nm (#4), 102.7 nm (#5) and 98.8 nm (#6) (fig. 3.1 b). WB analysis indicated presence of the vesicular marker proteins CD9, CD81 and CD63 and the platelet-EV marker CD41b in fractions 4 to 7 (fig. 3.2 a). ApoA1 protein was slightly detectable in fraction 6 and strongly increasing in fractions 7 to 10, indicating co-isolation of HDL. Additionally, unspecific binding in WB was increasing in comparable extend to the protein amount detected by BCA (fig. 3.1 a) and ponceau staining (fig. 3.2 b), most probably induced by the massive presence of albumin (65-70 kDa) and other plasma proteins in the later fractions. Finally, in favor of EV purity, fractions 4 to 6 were considered EV-rich while protein-poor and used for further analysis of EVs.

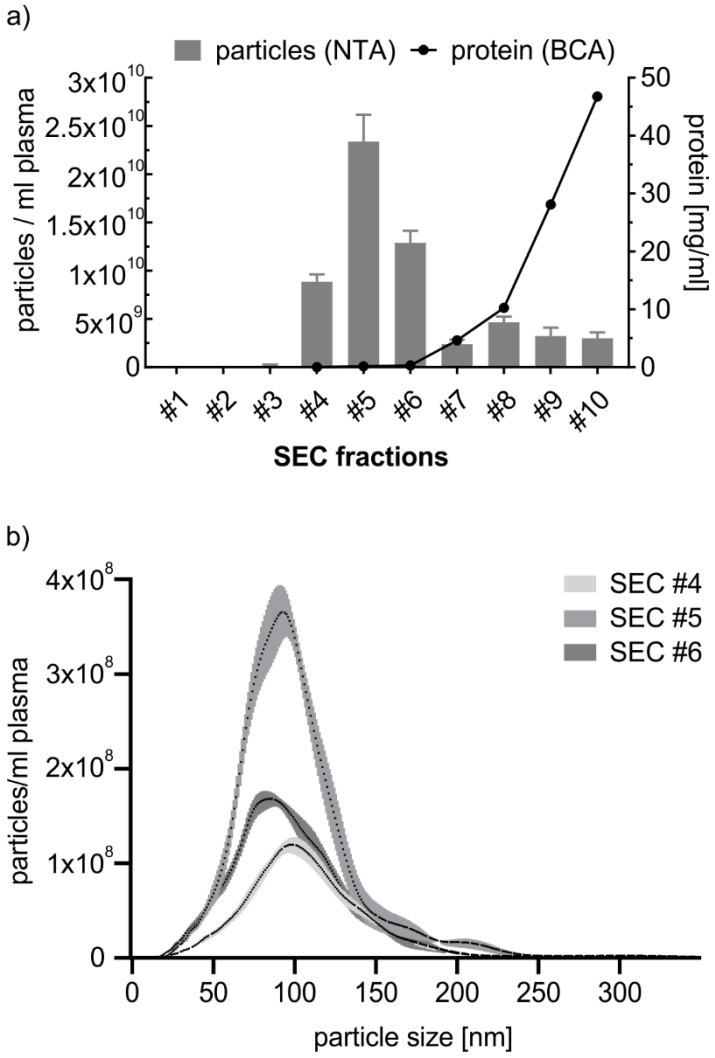

Figure 3.1: Identification of EV-rich SEC fractions I. (a) NTA (bars) and protein content (line) of SEC fractions. Bar graphs indicate mean particle number from one experiment, error bars indicate technical variation of NTA measurement. (b) Size distribution of particle-rich SEC fractions.

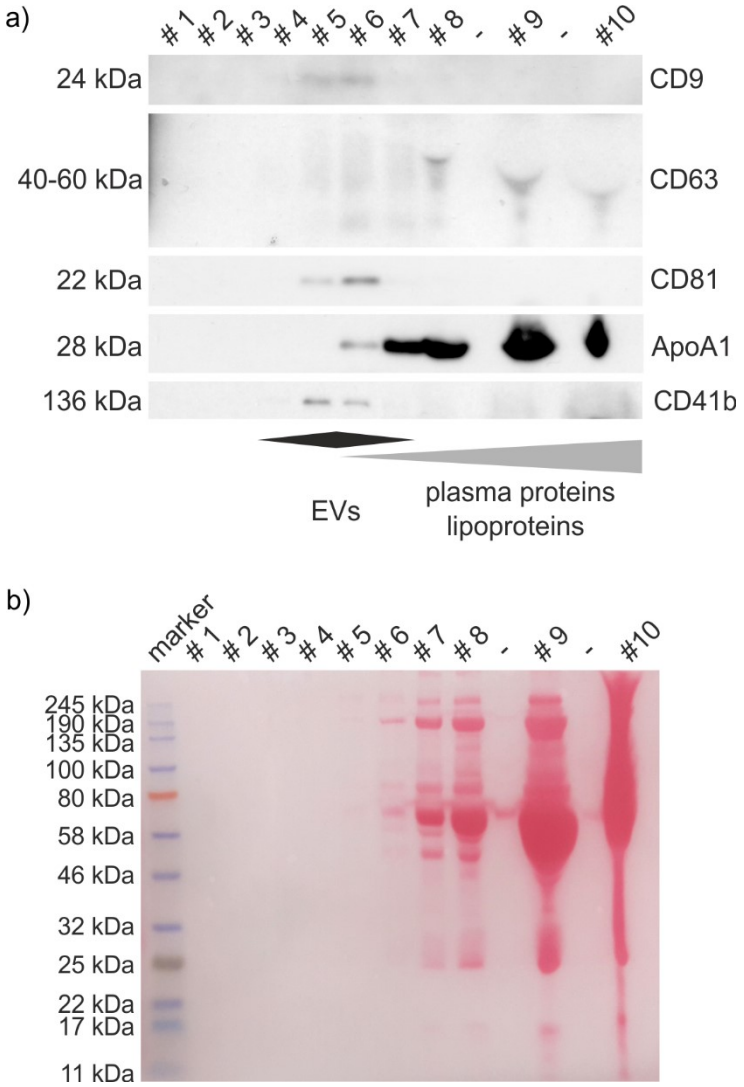

Figure 3.2: Identification of EV-rich SEC fractions II. (a) WB analysis of SEC fractions using EV associated markers (CD9, CD63, CD81), a platelet specific marker (CD41b) and apolipoprotein A1 (ApoA1) as lipoprotein marker. Fractions 4 to 6 (=SEC-EVs) are considered EV-rich while plasma protein- and lipoprotein-poor. (b) Ponceau staining of single SEC fractions subjected to SDS-PAGE.

Characterization of "SEC-EVs"

To characterize EVs purified by SEC in further analyses, pooled SEC fractions 4 to 6 were concentrated 30-fold by UF, defined as SEC-EVs and subjected to EM, NTA and WB. EM imaging revealed enrichment of vesicular structures in the size range of small EVs (fig. 3.3 a). Though, smaller non-EV structures were also detected, possibly indicating co-isolation of lipoprotein subclasses. Additionally, aggregation of EVs was visible which could be due to the isolation process or caused during sample storage or preparation for EM analysis. In NTA of SEC-EVs, a characteristic size profile of small EVs was observed (fig. 3.3 b). Mean particle size was 106.3 nm and particle concentration was

measured as 7.3 x10^{10} particles/ml plasma. These characteristics were reproducible and not influenced by the exercise intervention (see chapter 3.3.1). Importantly, estimation of particle size and concentration may not reflect actual EV size and concentration which will be addressed later (see chapter 3.3.1).

Marker analysis by WB of SEC-EVs confirmed marker presence of vesicular markers CD9, CD63 and CD81 and the platelet-EV marker CD41b (fig. 3.4 a). Additionally, vesicular markers TSG101 and Syntenin could be detected in the enriched SEC-EVs. Furthermore, staining for the membrane protein Na/K-ATPase was positive. As expected, lipoprotein co-isolation was not completely abolished which is reflected by presence of ApoA1 bands. Also, plasma proteins like albumin are still contained in the EV sample indicated by strong signals in ponceau staining (fig. 3.4 b). Interestingly, Alix, heat shock protein (HSP)70, and flotillin-1 (Flot1) which were previously shown to be present in plasma ExerV isolations (Frühbeis et al., 2015) were not detectable in SEC-EVs (data not shown). Though WB signals, except from ApoA1, are generally lower in plasma EV samples at rest, no markers appeared only after exercise intervention (see chapter 3.3.2). Next, SEC-EVs were analyzed with LC-MS in a pilot experiment which revealed strong co-isolation of non-EV components (fig. 3.4 c). CD81 and Syntenin were only marginally detected and markers such as CD63, Alix and TSG101 were absent. Apolipoproteins (e.g. ApoA1), proteins of the complement system (e.g. CoC3), immunoglobulins (e.g. immunoglobulin κ light chain) and albumin were found in roughly 50- to 5,000-fold higher proportion than the EV-associated markers. Therefore, SEC-EV samples need to be further purified for LC-MS assessment of markers incorporated within the membranes or the lumen of ExerVs. Taken together, the implemented SEC strategy leads to enrichment of EVs from blood plasma exhibiting characteristics of small EVs. SEC-EVs can successfully be used in EM and WB analysis, while further purification is necessary to implement sensitive proteomic analysis.

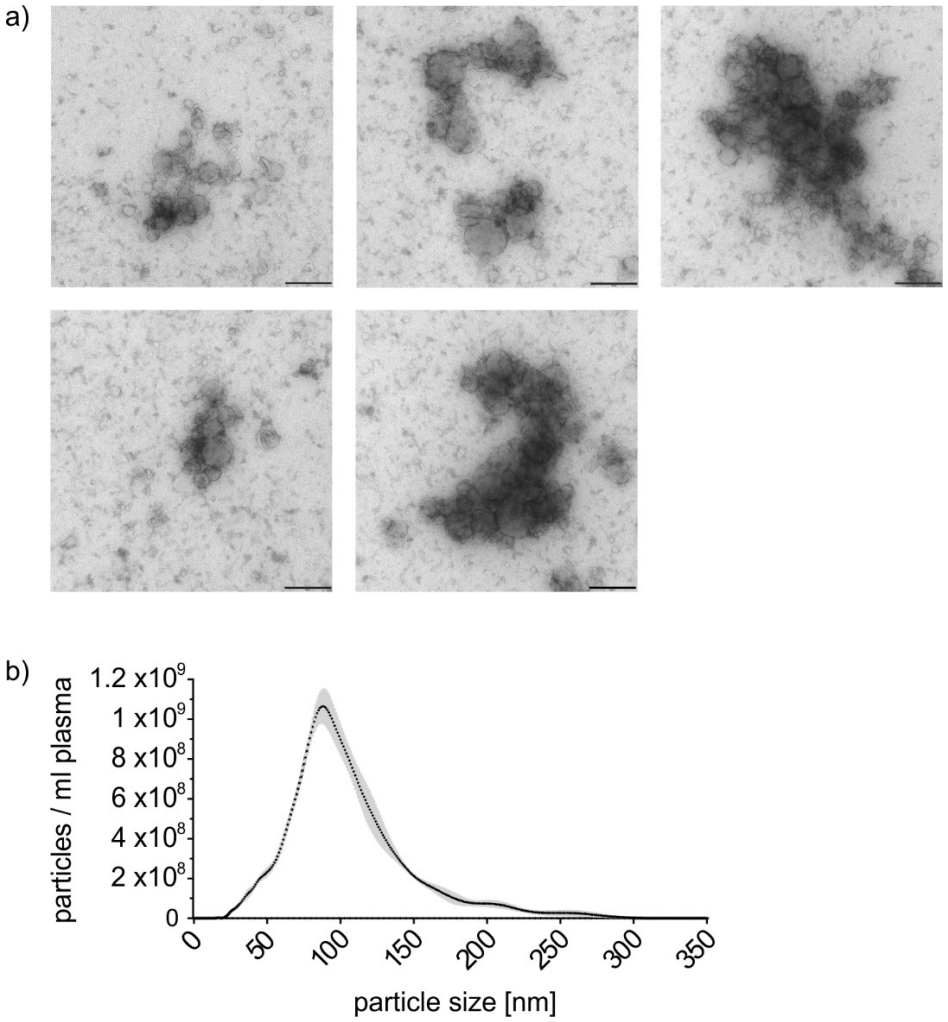

Figure 3.3: EM and NTA characterization of plasma-derived SEC-EVs. (a) Transmission electron microscopy image of SEC-EVs. Scale bar refers to 200 nm. (b) Representative NTA size distribution profile of SEC-EVs.

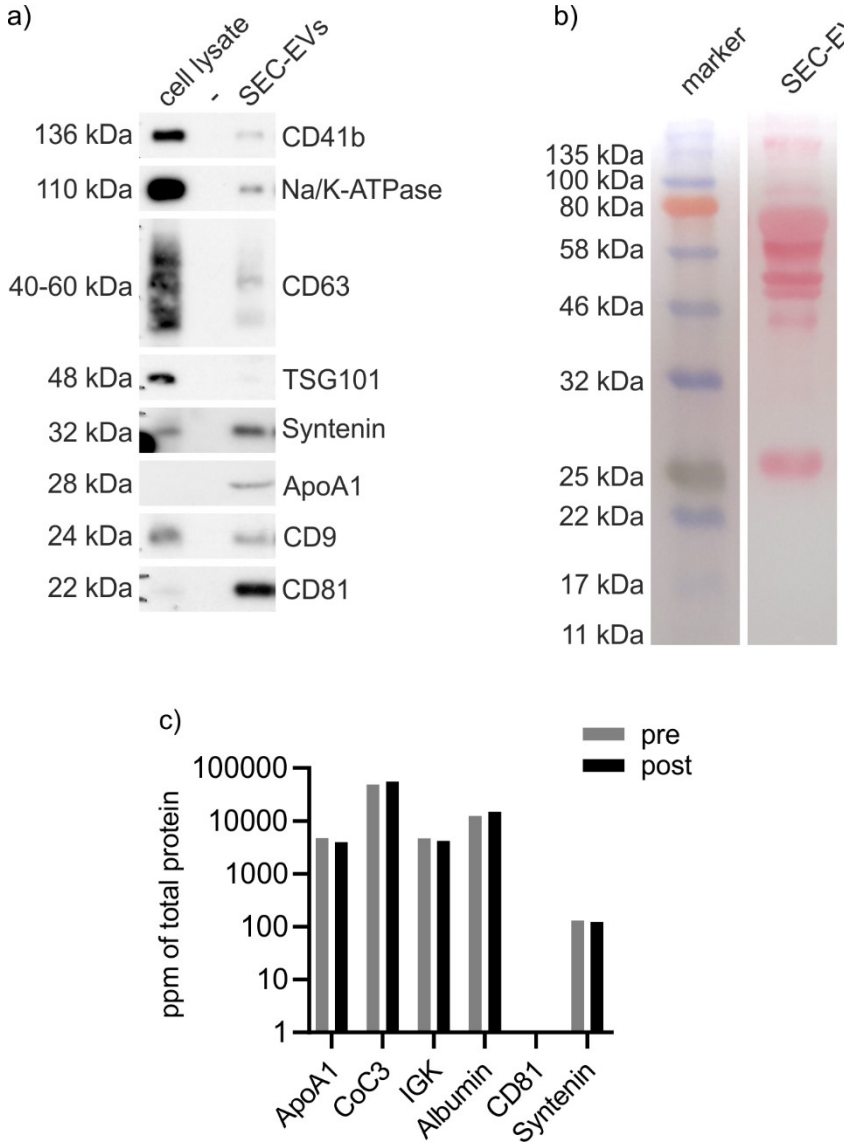

Figure 3.4: Proteomic characterization of plasma-derived SEC-EVs. (a) WB characterization of SEC-EVs using genuine EV-markers, CD41b and ApoA1. (b) Ponceau staining of SEC-EVs separated in SDS-PAGE. (c) LC-MS purity analysis of SEC-EVs by evaluating ApoA1, complement component 3 (CoC3), immunoglobulin κ light chain (IGK), Albumin and EV-associated marker proportion. ppm = parts per million.

SEC isolation from K562 cell culture supernatant

To improve knowledge on the method of SEC using less complex sample material, EVs were purified from the cell culture supernatant of the myelogenous leukemia cell line K562. EVs were pre-enriched using UF of conditioned CCS (protocol P1 or P2, see chapter 2.3.1) and further isolated by SEC of the UF-concentrated CCS (P1). For the experiment depicted in fig. 3.5 and 3.6, EVs derived from 3.15 x10^7 K562 cells within 24 h were loaded on the SEC column. The ultrafiltrate as well as pooled SEC fractions 3+4, 5+6 and

7+8 were analyzed in NTA and WB. UF-enriched EVs as well as SEC #5+6 revealed characteristic particle size distributions with mean particle sizes of 181.4 nm and 175.6, respectively (fig. 3.5 a). Concentration of UF-EVs was 6.5 $x10^8$ particles/ml CCS while SEC #5+6 had a reduced particle concentration of 2.1 $x10^8$/ml CCS (fig. 3.5 b). The pooled fractions 3+4 and 7+8 showed even lower particle concentrations around 0.5 $x10^8$/ml CCS. This overall course of SEC fractions in NTA was reproducible (see chapter 3.1.3, fig. 3.9). In WB analysis, SEC fractions #5+6 and #7+8 revealed markers of small EVs with positive staining for CD9, CD81, CD63, and Syntenin (fig. 3.6).

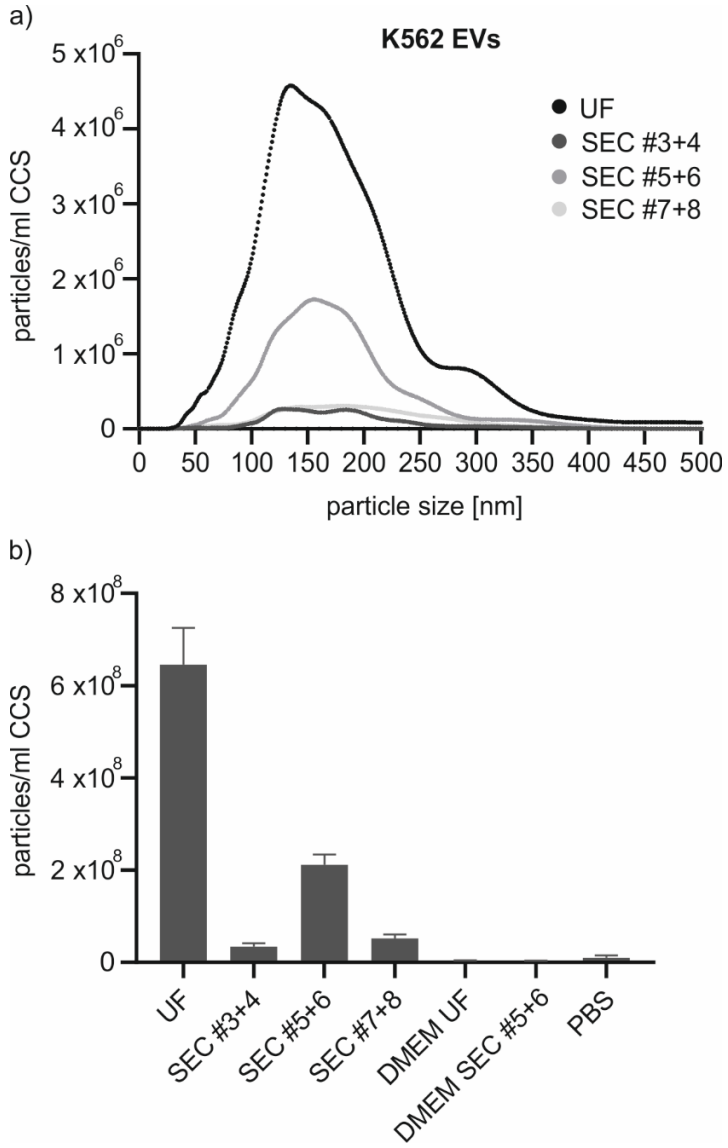

Figure 3.5: NTA of EVs isolated from K562 CCS. (a) Size distribution and (b) concentrations in cell culture supernatant (CCS) of UF-EVs and combined SEC fractions measured in NTA. Error bars indicate technical variation (SEM) of NTA measurement of one sample.

Additionally, HSP70, which was not detectable in plasma SEC-EVs, was visible in #7+8 possibly indicating that elution of free or vesicle-bound HSP70 is restricted to later SEC fractions. All analyzed markers were also detectable in UF-EVs though a clear enrichment in CD63 and CD81 became obvious in SEC #5+6 in comparison to UF-EVs. Furthermore, the EV-associated markers TSG101 and Flot1 are rarely detectable in UF-EVs while not detectable in SEC-EVs, which might be due to low marker concentrations on the EVs. The endoplasmic reticulum-associated protein Calnexin is also only visible in UF-EVs indicating efficient removal of remaining cell debris by SEC. These findings indicate that SEC is an efficient method to further enrich EVs from UF-EVs, though sample purity might be accompanied by loss of EVs resulting in less detectable markers in WB analysis and a lower particle concentration in NTA. Still, the implementation of SEC for K562-derived EVs confirmed the observations made for SEC of blood plasma EVs.

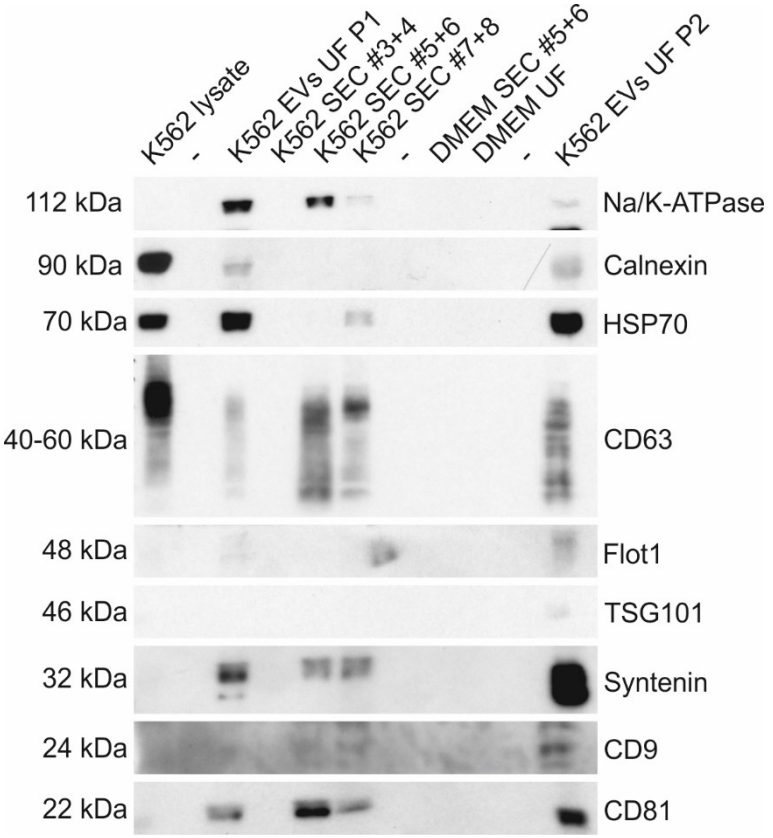

Figure 3.6: WB analysis of EVs isolated from K562 CCS. WB characterization of combined SEC fractions using genuine EV-markers and non-EV markers. UF-EVs and SEC #5+6 EVs were loaded in the same particle amount (NTA) of 3 x10^9/lane. The other samples were adjusted for volume.

3.1.2 Enrichment of EV subpopulations using immuno-affinity capture

Characterization of immuno-affinity captured EVs

An alternative method to purify EVs from blood plasma, is the isolation of EV subpopulations using magnetic beads coupled to antibodies specific for EV-associated marker proteins. Here, a commercial kit with antibodies against the tetraspanins CD9, CD63 or CD81 was utilized (see chapter 2.4.5).

WB analysis revealed that the EV markers CD9, CD63, CD81, Syntenin, and CD41b are detectable in $CD9^+$-, $CD63^+$-, and $CD81^+$EVs (fig. 3.7 a). Several of the markers were previously detected in SEC-EVs. No signals were observed for TSG101 in each of the three subpopulations. Consistently, CD9, CD63, and CD81 showed the strongest signals in the isolation with the respective antibody (example on fig. 3.7 a: same blot, same sample amount, same exposure time). This might indicate that the isolations are specifically enriching EV subpopulations. Furthermore, $CD9^+$EVs displayed the strongest signals for CD41b. Membrane marker Na/K-ATPase was not detectable in plasma samples taken at rest but were found in samples taken after exercise, while Calnexin was undetectable (not shown). Taken together, the use of immuno-affinity capture enables efficient isolation of $CD9^+$-, $CD63^+$-, and $CD81^+$ EV subpopulations from human blood plasma.

WB analysis further demonstrated that also non-EV components are eluted in the $CD9^+$-, $CD63^+$-, and $CD81^+$EV samples. Ponceau staining (fig. 3.7 b) revealed a prominent band at ~70 kDa most probably caused by co-isolated albumin, but overall co-isolation of plasma proteins seems to be reduced compared to SEC-EVs. Importantly, no HDL was co-isolated which is indicated by negative ApoA1 staining, except from very few samples (not shown). However, the secondary anti mouse antibody lead to staining of the light chain (~25 kDa) and the heavy chain (~50 kDa) of the isolation antibody in $CD9^+$- and $CD63^+$EVs. Additionally, unspecific bands at ~75 kDa ($CD9^+$EVs) and ~100 kDa ($CD9^+$- and $CD63^+$EVs) were visible which could be reduced via heating of the sample prior to SDS-PAGE (not shown). These might result from still linked antibody heavy and light chains or their dimers. Additionally, the magnetic beads which are used for separation of EVs from plasma remain in the EV samples (visible in SDS-PAGE as brown sediments remaining in the

gel pockets). This excludes subsequent size and concentration analysis of bead-isolated EVs by NTA. Conclusively, though lipoprotein and plasma protein co-isolation seems to be reduced in immuno-affinity isolated EVs compared to SEC-EVs, also non-EV components are eluted in the $CD9^+$-, $CD63^+$-, and $CD81^+$EV samples which affect certain downstream analyses.

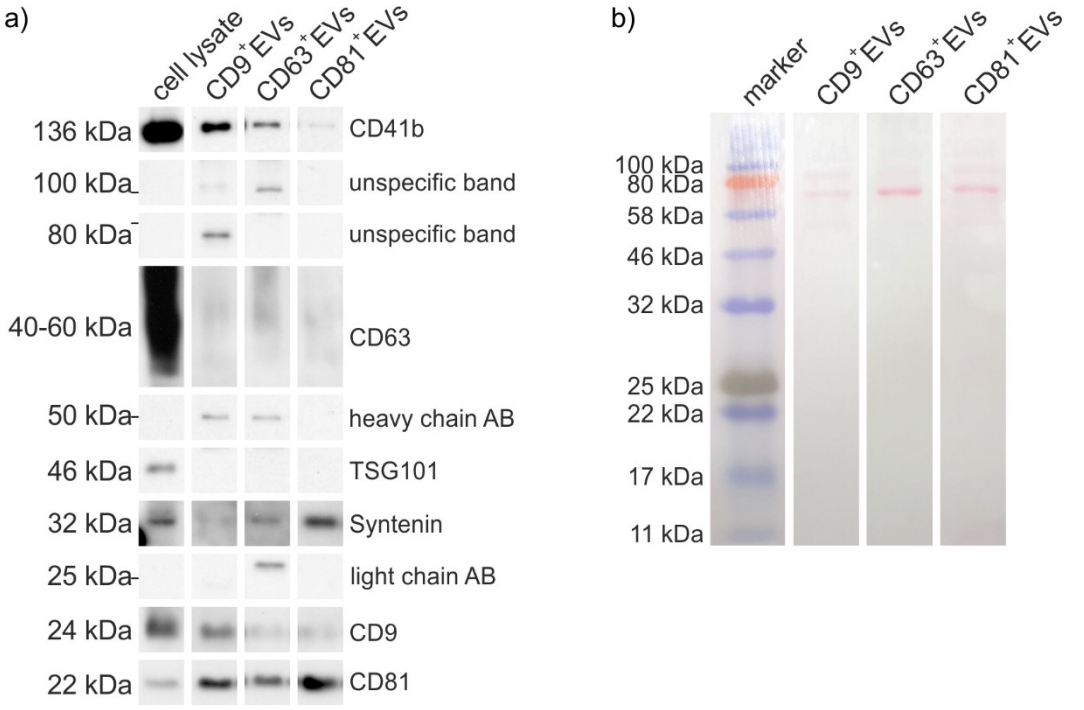

Figure 3.7: Characterization of immuno-affinity captured plasma EVs. (a) WB characterization of $CD9^+$EVs, $CD63^+$EVs and $CD81^+$EVs using genuine EV-markers and CD41b. (b) Ponceau staining of $CD9^+$EVs, $CD63^+$EVs and $CD81^+$EVs separated in SDS-PAGE.

Modification of immuno-affinity capture

To further increase the purity of immuno-affinity captured EVs, removal of the magnetic beads from the isolated EVs is necessary. To this end, $CD63^+$EVs were lysed directly on the column and recovered in the applied lysis buffer, instead of eluting EVs from the column detached from the magnetic device with PBS. In this case, beads remained at the magnetic device reflected by a colorless eluate and absence in SDS-PAGE gel pockets. Using WB analysis, the different protocols were compared, using plasma samples from a non-exercise setting (n=3). Interestingly, direct lysis at the magnet lead to increased band intensity of CD9, CD63, CD81, Syntenin, as well as CD41b (fig. 3.8 a). Proportion of the marker intensities between the individual samples

(1 to 3) remained similar indicating proper EV isolation. However, also Calnexin was detectable though being absent in the EV samples isolated according to the standard protocol. To increase EV concentration, it was tested weather the first drop of the eluate can be discarded since EV elution was expected to occur later. However, there were considerable marker intensities in WB analysis of the collected first drop of lysed EVs.

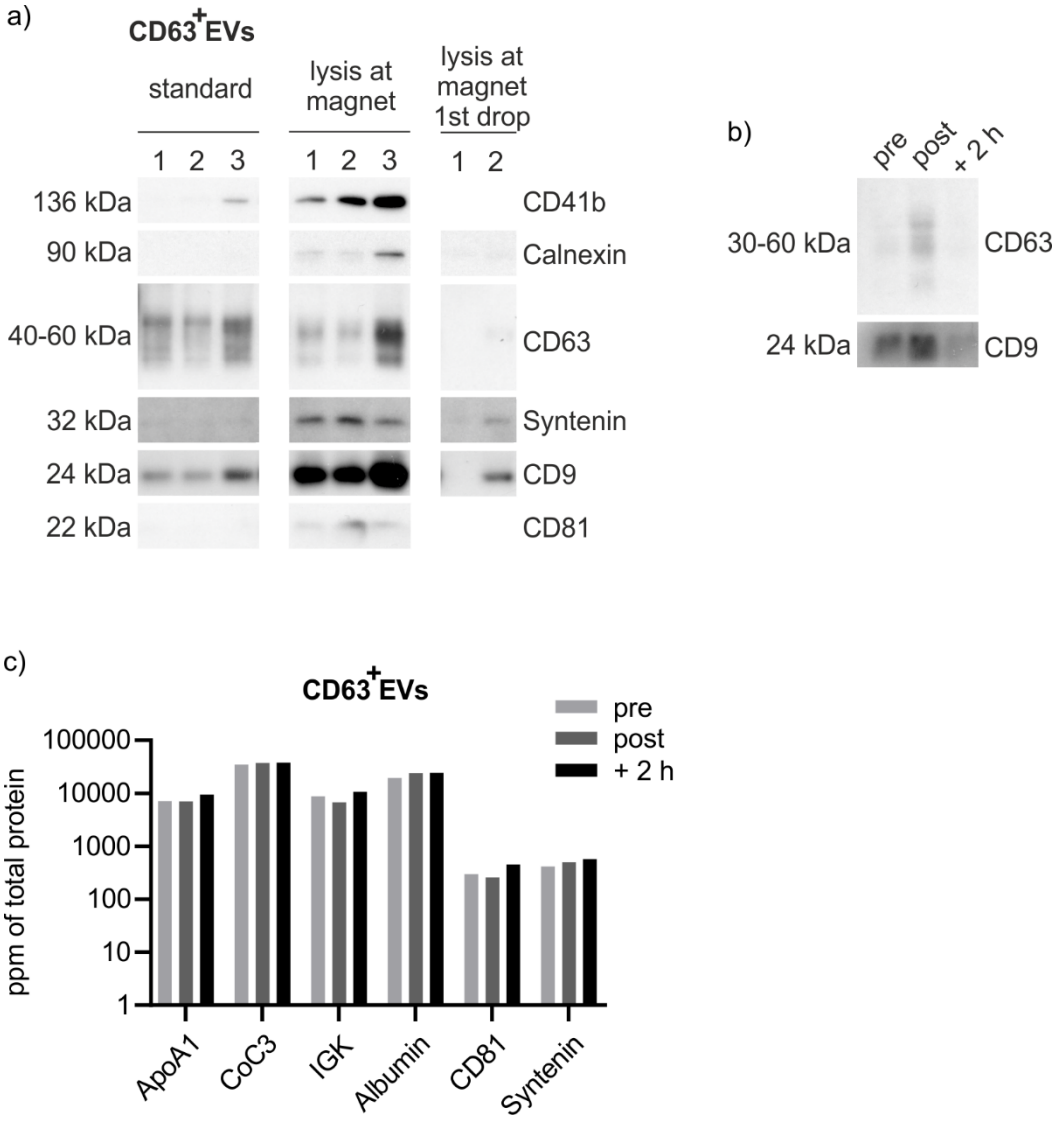

Figure 3.8: Modification of immuno-affinity capture of plasma EVs. (a) WB analysis of CD63$^+$EVs, derived from 3 different samples from a non-exercise setting (samples 1 to 3), captured following the manufacturer's instructions (standard) or by direct lysis at a magnetic device. (b) CD63 and CD9 staining in WB of lysed CD63$^+$ExerVs (same sample volume loaded). (c) Purity analysis of lysed CD63$^+$ExerVs by LC-MS. ppm = parts per million.

LC-MS analysis was further applied to estimate the purity of CD63$^+$EV samples. These were derived from an exercising subject at rest, immediately

after exhaustion and 2 h after completion of the test, which was performed as described above (see chapter 2.2). Though immuno-affinity capture possibly was impaired due to aggregation of magnetic beads, which was visible as brown precipitation in the tube, WB analysis revealed proper detection of the tested markers CD9 and CD63 (fig. 3.8 b). However, co-isolation of non-vesicular components was comparable as in SEC-EVs with high plasma protein contamination (LC-MS analysis, fig. 3.8 c). Thus, further improvements of the isolation process need to be implemented to prepare immuno-bead isolated EVs for proteomic analysis. Taken together, immuno-affinity capture is an efficient method to enrich $CD9^+$-, $CD63^+$-, and $CD81^+$EVs from human blood plasma. Magnetic beads can be detached from the EVs by direct lysis of the EVs at the magnetic device. This approach may further increase EV concentration. Additional improvements of the isolation protocol will further increase EV-purity to perform more sensitive downstream characterization like proteomic analysis.

3.1.3 Highly pure recovery of blood plasma EVs

In order to increase the purity of isolated plasma EVs, multiple consecutive steps of EV enrichment including SEC, UF, iodixanol density gradient (IDG) centrifugation and UC were implemented. The established experimental setting by Vergauwen et al. (unpublished) was transferred to our laboratory (fig. 3.9 a) to validate the isolation procedure. SEC-EVs of 12 ml plasma derived from a healthy volunteer who performed an incremental exercise test until exhaustion on a treadmill were recovered as described above. Subsequently, SEC-EVs were concentrated to a final volume of 0.5 ml and loaded onto the top of the IDG. After centrifugation, 2 ml of pooled IDG fractions were purified by SEC to remove iodixanol. NTA of pooled IDG fractions after SEC revealed characteristic size distributions for each of the analyzed fractions except from #10+11 (fig. 3.9 b) with mean particle sizes of 127.1 nm (#1-3), 129.1 nm (#4+5), 123.2 nm (#6+7), and 123.2 nm (#8+9). Highest particle concentrations (fig. 3.9 c) were measured in IDG #6+7 (1.7×10^{10} particles/ml plasma) and #8+9 (2.9×10^{10} particles/ml plasma). Also, IDG #1-3 exhibited a considerable particle concentration of 1.3×10^{10} particles/ml plasma supposedly attributed to the presence of lipoprotein

subclasses which was supported by the appearance of a yellow ring in the gradient after centrifugation (not shown). WB analysis of IDG fractions confirmed vesicle presence in particle-rich fractions by the presence of CD9, CD63, CD81, and CD41b (fig. 3.9 d). Interestingly, while stronger bands for CD9 and CD81 were visible in #6+7, CD41b was only detectable in #8+9. However, a band which might be attributed to Calnexin staining was visible in #8+9 though not at the exact molecular size. ApoA1 staining was negative for each of the samples (not shown). However, impaired functionality of the antibody cannot be excluded in this case since #1-3 were expected to be positive for the HDL marker ApoA1. Summarized, this isolation approach resulted in the identification of possibly four EV-rich fractions which might be separated from the lipoprotein-rich fractions.

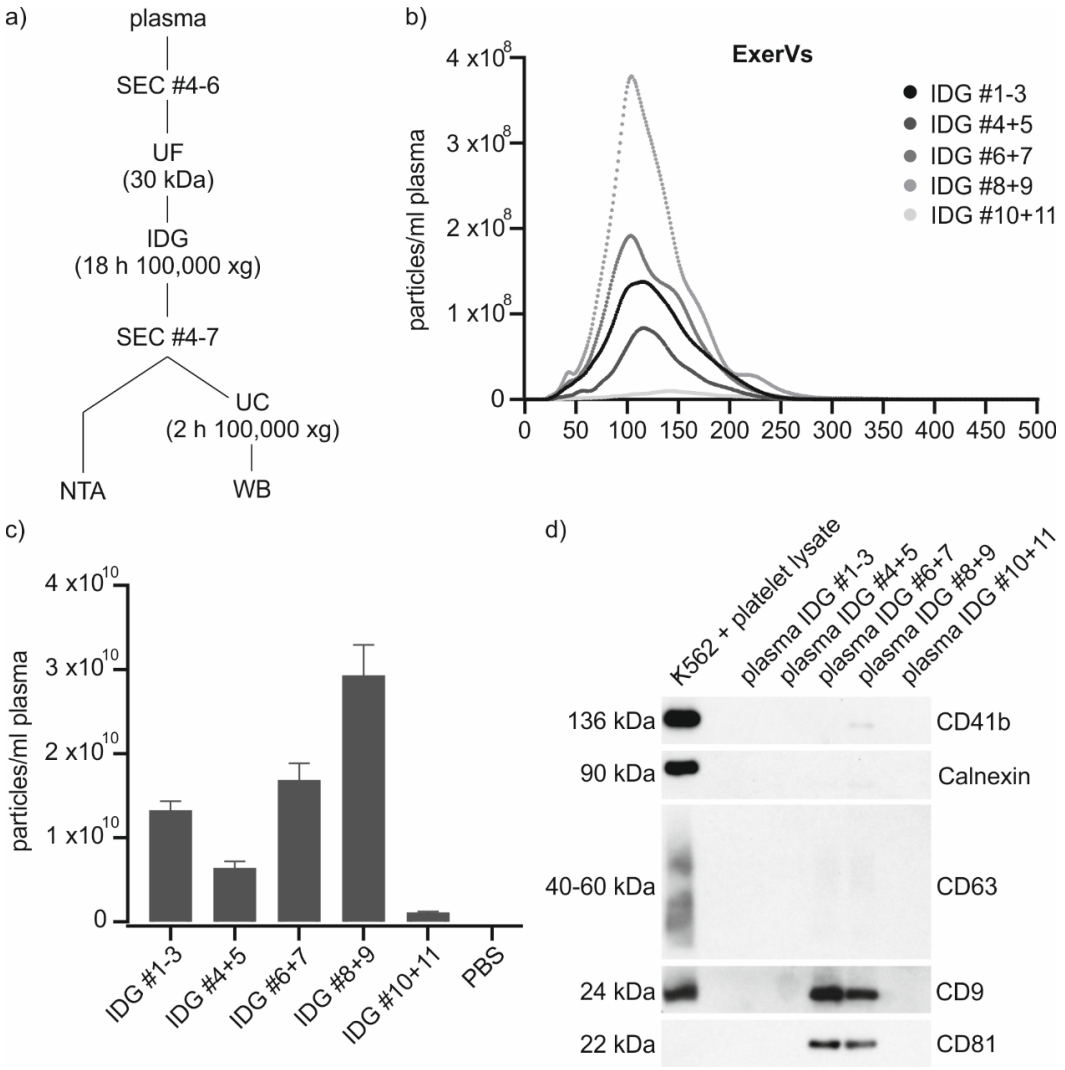

Figure 3.9: Combination of EV isolation strategies: plasma EVs. (a) Overview of the combined isolation strategy. (b, c) NTA size profiles and particle concentrations of SEC-purified IDG fractions. Bar graphs indicate mean particle number from one

experiment, error bars indicate technical variation of NTA measurement. (d) WB analysis of SEC-purified and pelleted IDG fractions.

In a next step, vesicular content of IDG fractions 6 to 9 were analyzed in more detail. To this end, the purification strategy described above was repeated with pre and post exercise SEC-EVs isolated from the plasma of a subject who had accomplished the standard incremental cycling test until exhaustion (see chapter 2.2). Vesicular markers CD81, Syntenin and CD41b exhibited the strongest intensities in WB analysis in IDG fractions 8 and 9 (fig. 3.10 a).

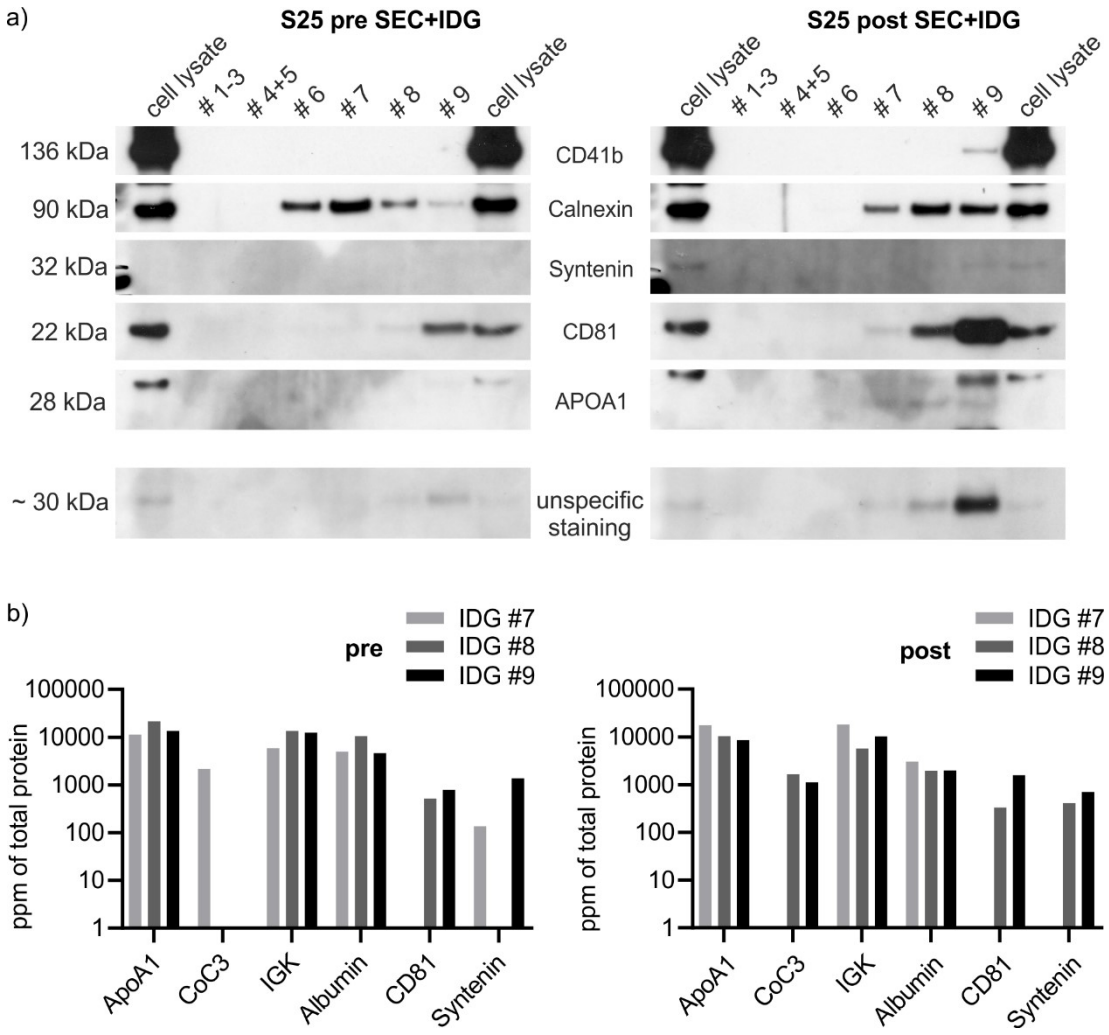

Figure 3.10: Proteomic content of EVs isolated with combined isolation approach. (a) WB analysis of SEC-purified and pelleted IDG fractions derived from pre (left) and post (right) exercise plasma. (b) LC-MS purity analysis of SEC-purified and pelleted IDG fractions by estimation of ApoA1, CoC3, IGK and Albumin co-isolation with EV-associated markers CD81 and Syntenin. ppm = parts per million.

However, marker distribution seems different from the previously described distribution (fig. 3.9 d) with a shift of vesicular content to later fractions. Also,

ApoA1 and Calnexin were found in the fractions enriched in EV markers while fractions 1-3, again, were free of ApoA1. Additionally, a strong unspecific band appeared in the fractions positive for EV-associated markers. LC-MS analysis of fractions 7 to 9 was performed to assess the purity of the EVs. An elevation of Syntenin and CD81 was confirmed in fractions 8 and 9 compared to fraction 7. Though, the presence of ApoA1 and other plasma components indicated poor purity of EV samples (LC-MS analysis, fig. 3.10 b). Conclusively, a relevant enhancement of ExerV purity could not be achieved. However, the approach needs to be repeated to exclude technical reasons like improper gradient preparation or sample recovery from the gradient after overnight centrifugation.

EVs from K562 CCS were analyzed in parallel to confirm purification of EVs via the depicted strategy. To this end, EVs derived from 4 $x10^7$ cells within 24 h were enriched by SEC. Fractions 5 to 7 were concentrated to 0.5 ml, loaded on the IDG and processed as described above. Though particle concentration of UF-EVs and SEC-EVs was comparable to previous isolations (fig. 3.11 a, b), NTA of IDG fractions did not result in measurable particle concentrations. However, WB revealed a weak presence of CD63 in IDG fractions #6+7 (fig. 3.11 c). Conclusively, WB analysis is in line with the first results for plasma EVs, although K562 EV sample material has to be increased for further observations.

Taken together, after further modification of the isolation protocol, combination of SEC and IDG might offer the possibility to increase the purity of EVs. These may be used in sensitive downstream analysis like RNA-seq or proteome analysis.

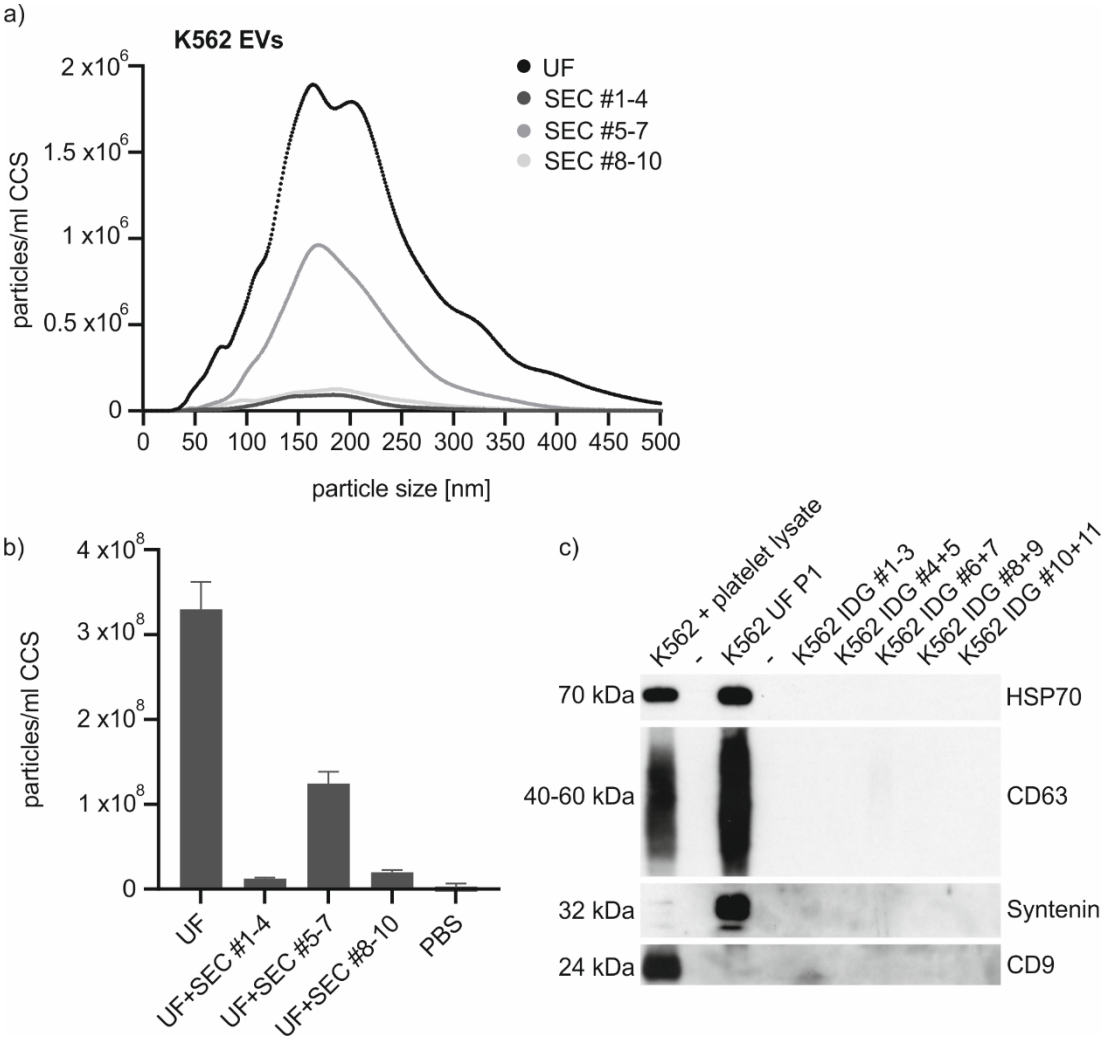

Figure 3.11: Combination of EV isolation strategies: K562 CCS. (a, b) Size distribution as well as concentrations of UF-EVs and combined SEC fractions. Bar graphs indicate mean particle number from one experiment, error bars indicate technical variation of NTA measurement. (c) WB characterization of UF-EVs and EVs enriched using the combined isolation approach.

3.2 Exercise study design for the analysis of ExerV

To study the release kinetics and the origin of EVs under exercise conditions, 21 healthy male athletes were subjected to an incremental cycling test until exhaustion. The study participants had an average age of 28.7 ±4.2 years and a BMI of 22.8 ± 2.0. Analysis of blood parameters did not show aberrations from the normal range. Several performance diagnostic parameters like O_2-consumption, lactate levels, cfDNA concentration and heart rate were monitored during the test and displayed stepwise elevation until exhaustion (tbl. 3.1). Lactate and cfDNA levels remained constant at reduced workloads

and increased strongly after the individual anaerobic threshold (exemplified for one study participant in fig. 3.12). Time points for EV analysis were prior to the exercise (pre), during the test at a respiratory quotient (RQ) of 0.9 and immediately at the end of the exercise (post). The average time until an RQ of 0.9 was 14 ±3.7 min and the mean load was 201 ±52.9 Watt. The average time until the end of the test was 23.6 ±2.8 min and the participants reached a mean of 324.3 ±49.5 Watt at exhaustion. ExerV kinetics (see chapter 3.3) and origin (see chapter 3.4) were examined based on data obtained from EV analysis in blood plasma or differentially isolated EVs. To this end, a comparative experimental set-up was implemented as illustrated in fig. 3.13 and included EV isolation by SEC and immuno-affinity capture and EV analysis via EV Array, MACSPlex, WB, NTA, and IF. Due to the restriction in the sample volume taken at each point of analysis (see chapter 2.2.4), EV characterization was not performed with each of the analysis strategies at all time points in parallel. However, the accumulation of EV data from multiple subjects, EV subclasses and examination methods (see tbl. S1) allows a detailed characterization of ExerVs.

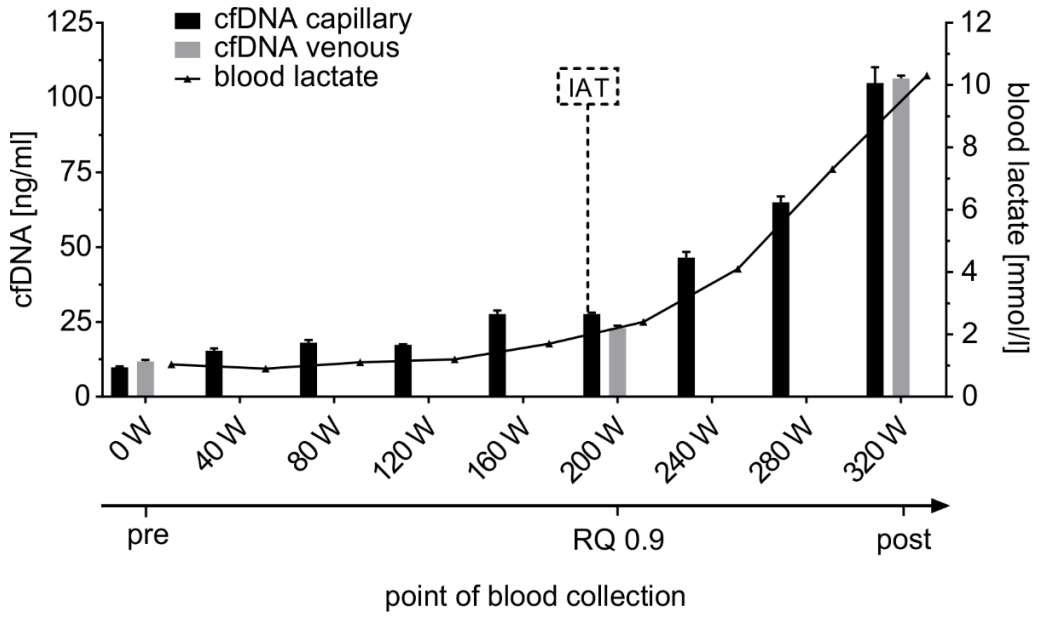

Figure 3.12: Characterization of the implemented cycling exercise setting. Illustration of a representative incremental cycling exercise test and the time points of EV analysis. Blood lactate (line) and cell-free DNA levels (cfDNA; bars) were measured every three minutes at increasing workloads. The individual anaerobic threshold (IAT) is indicated by a dashed vertical line. Venous blood was drawn prior

to the test (pre), during the exercise at a RQ of 0.9 and at the end of the test (post). Error bars indicate technical variation of cfDNA measurement.

Table 3.1: Test parameters of the cycling exercise study subjects

	time (min)	load (Watt)	load/ weight (Watt/kg)	Borg	lactate (mmol/l)	cfDNA (ng/ml)	heart rate (1/min)	VO_2 (ml/min /kg)	IAT (Watt)
pre	-	-	-	-	0.9 (0.2)	25 (11.9)	80.2 (14.4)	5 (1.1)	
RQ 0.9	14 (3.7)	201 (52.9)	2.7 (0.7)	14.6 (2.0)	2.3 (1.1)	45.2 (25.0)	145.4 (16.6)	33.7 (6.5)	197.8 (49.4)
post	23.6 (2.8)	324.3 (49.5)	4.4 (0.8)	19.6 (0.6)	9.4 (2.8)	163.5 (90.2)	184.7 (8.5)	48.8 (6.5)	

Values are given in mean ±SD, n=21

RQ respiratory quotient, *cfDNA* cell-free DNA, *VO_2* oxygen consumption (VO_2 at post = maximal oxygen consumption), *IAT* individual anaerobic threshold based on lactate accumulations according to Roecker et al., 2003 (Roecker et al., 2003).

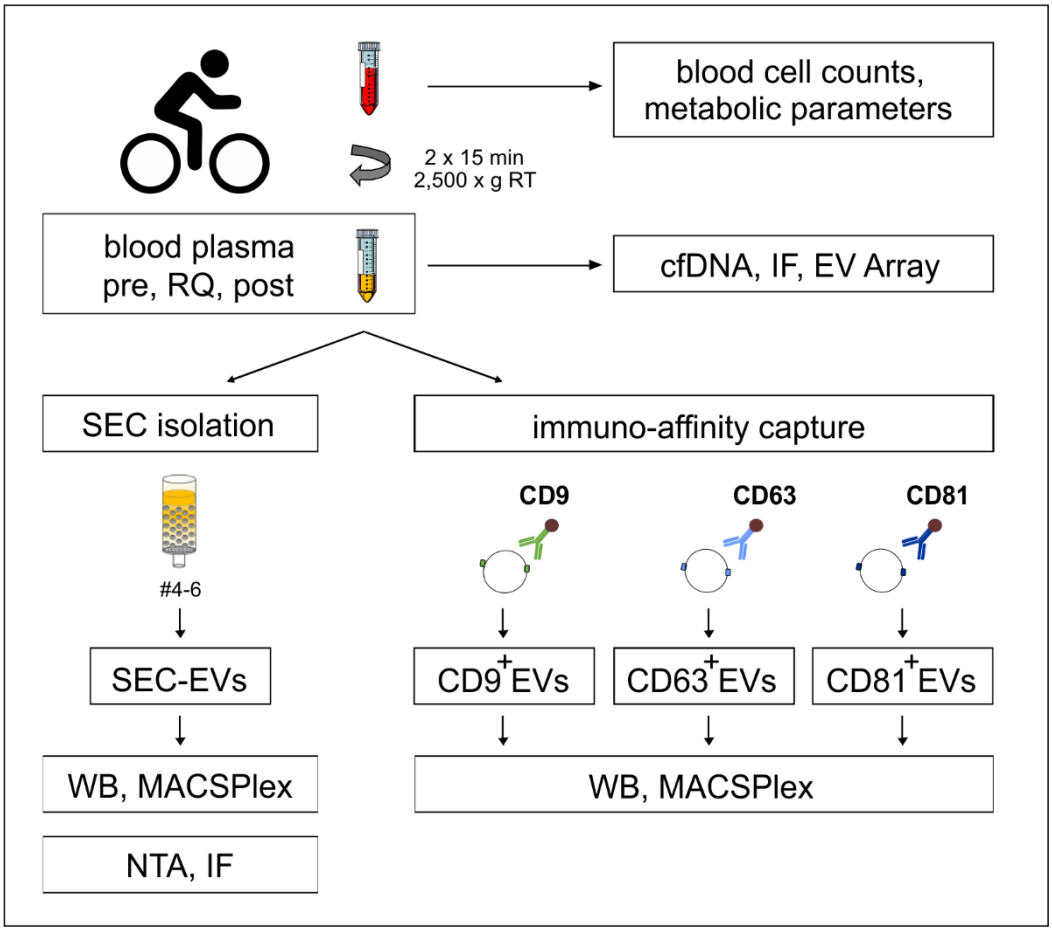

Figure 3.13: Experimental strategy to characterize ExerVs. Blood cell counts and metabolic parameters were evaluated in venous blood which was sampled pre exercise, at RQ 0.9 and post exercise. Unprocessed plasma was used for EV analysis in imaging flow cytometry (IF) and the EV Array as well as for cfDNA estimation. For WB and MACSPlex analysis, EVs were purified from plasma by SEC or immuno-

affinity capture using CD9-, CD63-, or CD81-magnetic beads. SEC-EVs were additionally analysed in nanoparticle tracking analysis (NTA) and IF.

3.3 EV kinetics during incremental cycling

3.3.1 Absolute quantification of ExerVs

To estimate EV concentrations and evaluate ExerV kinetics, EVs were analyzed by imaging flow cytometry (IF) and nanoparticle tracking analysis. For IF, EVs in plasma were stained with the membrane dye BODYPI and total EVs as well as the defined EV subpopulations “exosomes” and “MVs” were measured (see chapter 2.5.3). The total EV gate as well as the exosome gate in stained plasma samples showed fluorescent events while unstained plasma and PBS buffer control were free of fluorescent events (fig. 3.14 a). As expected due their small size, some vesicles in the exosome gate were only detectable in fluorescent mode but not in SSC mode (fig. 3.14 b, lower part). Measurement of ExerV kinetics in the plasma of two subjects indicated exosome numbers starting at 1.9 and 1.5 $x10^8$/ml plasma both increasing to a concentration of 2.2 $x10^8$/ml plasma at RQ 0.9 and decreasing to concentrations of 1.8 and 1.3 $x10^8$/ml plasma post exercise (fig. 3.14 c). MV kinetics followed the same trend starting at 1 and 0.7 $x10^8$/ml plasma evenly increasing to a concentration of 1.3 $x10^8$/ml plasma at RQ 0.9 and decreasing to concentrations of 1 and 0.7 $x10^8$/ml plasma post exercise. This summed up in total EV kinetics starting at 2.9 and 2.2 $x10^8$/ml plasma increasing to concentrations of 3.6 and 3.5 $x10^8$/ml plasma at RQ 0.9 and decreasing to concentrations of 2.9 and 2 $x10^8$/ml plasma post exercise. To further evaluate EV concentration changes in isolated ExerVs, SEC-EVs of seven subjects were analyzed in NTA. Particle size distribution of EVs was as described above (fig. 3.15 a, also see 3.1.1). Particle concentrations at rest varied between 8.1 $x10^9$ and 1.3 $x10^{11}$/ml plasma, at RQ 0.9 between 9.9 $x10^9$ and 1.9 $x10^{11}$/ml plasma and post exercise between 5.9 $x10^9$ and 3.4 $x10^{11}$/ml plasma (fig. 3.15 b). Interestingly, measured EV numbers were 2 to 3 orders of magnitude higher than in IF analysis. Calculation of mean fold changes at RQ 0.9 (0.97-fold) and post exercise (1.03-fold) compared to pre exercise revealed no difference in particle concentration (fig. 3.15 c). These observations

suggest no (NTA) or only a very short (IF) increase in EV numbers during exercise and a reduction to baseline at exhaustion. This is in contradiction to the results of earlier studies of the release kinetics of EVs during exercise in our group (Frühbeis et al., 2015).

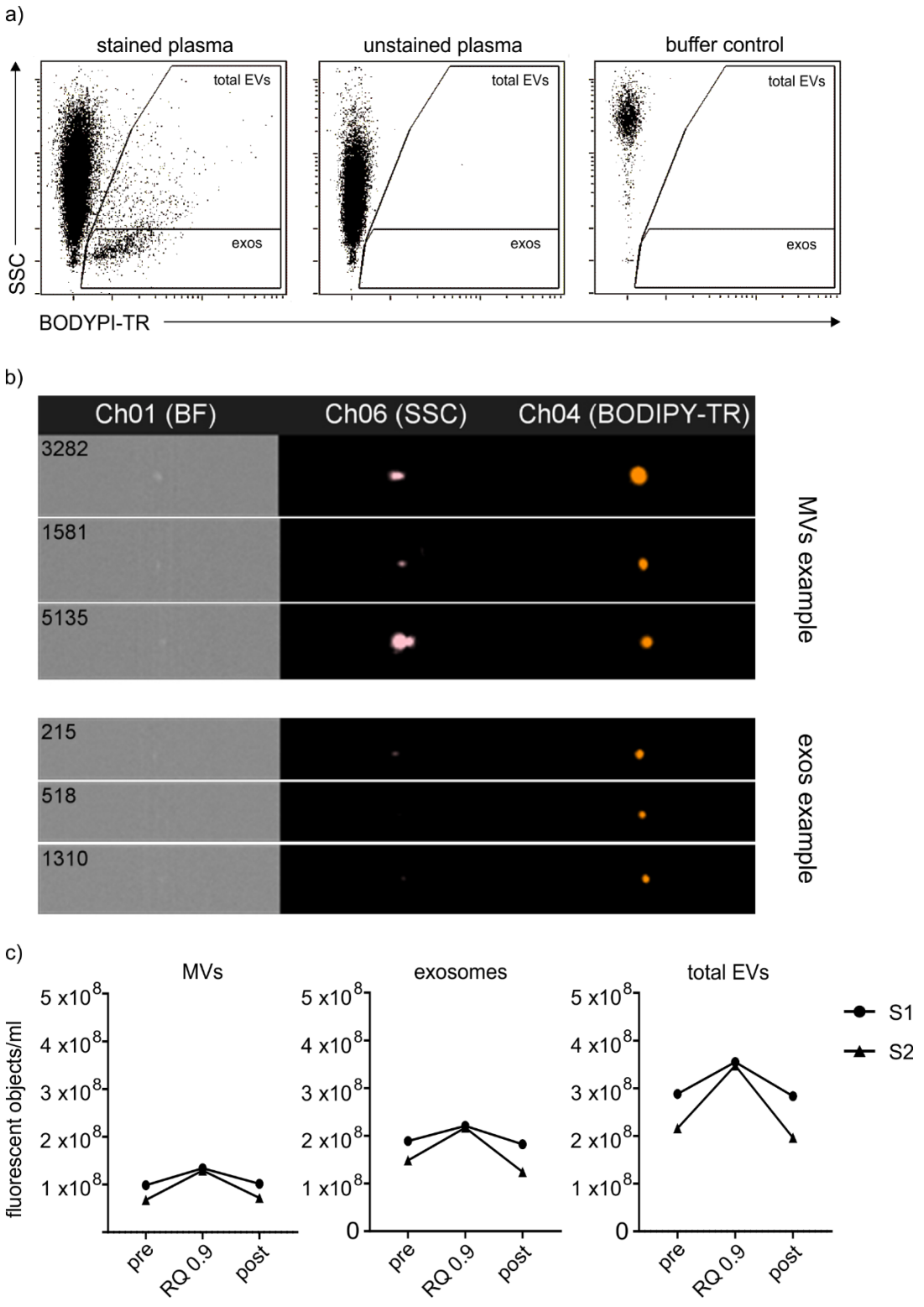

Figure 3.14: ExerV concentrations and kinetics - imaging flow cytometry. (a, b) Gating strategy and exemplified events of EVs in imaging flow cytometry. Exos =

exosomes/small EVs, MVs = total EVs minus small EVs. (c) Concentration and dynamics of BODYPI-stained plasma EVs and their subclasses of two study subjects pre, at RQ 0.9 and post exercise (S1, S2).

However, recent publications demonstrated that flow cytometry as well as nanoparticle tracking analysis is confounded by the strong presence of lipoproteins in plasma as well as isolated EVs (Jamaly et al., 2018; Sodar et al., 2016).

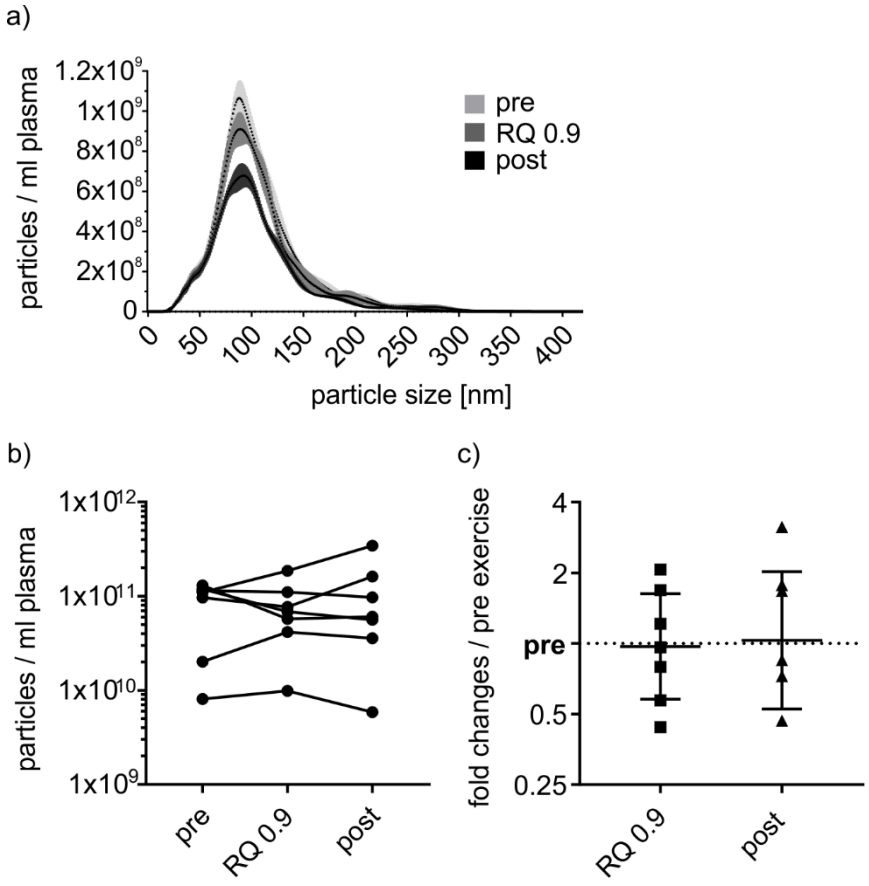

Figure 3.15: ExerV concentrations and kinetics - nanoparticle tracking analysis. (a) Exemplified NTA size profiles of SEC-EVs collected pre, at RQ 0.9 and post exercise. (b, c) Total NTA particle counts and fold changes in SEC-EVs during the exercise setting (geometric mean, SEM, n=7).

To further reveal details of the characteristics of NTA and IF of plasma EVs, single SEC fractions retrieved from the plasma samples of one study subject were either measured in NTA or stained with BODYPI and measured in IF. No change in EV numbers was detected in IF or NTA of the SEC-fractions during exercise and, again, EV numbers in NTA analysis were several orders of magnitude higher than in IF analysis (fig. 3.16). Furthermore, the EV-rich

fractions 4 to 6 identified by WB and NTA of single SEC-fractions before (see fig. 3.1) seem particle-low in IF analysis compared to fractions 7 and 10, which in turn showed reduced (#7) or no presence (#10) of EV markers in WB analysis. This was observed for each of the subpopulations analyzed in IF and was reproduced in analysis of SEC-fractions recovered from the subject's plasma after one freeze-thaw cycle (not shown). In light of the current literature (Jamaly et al., 2018; Sodar et al., 2016), these findings might indicate that different factors including different lipoprotein subclasses are confounding NTA and IF analysis which leads to misinterpretations of the study data. Hence, it can be concluded that neither NTA nor IF analysis performed under the presented conditions are suitable techniques to depict EV concentrations or kinetics during exercise.

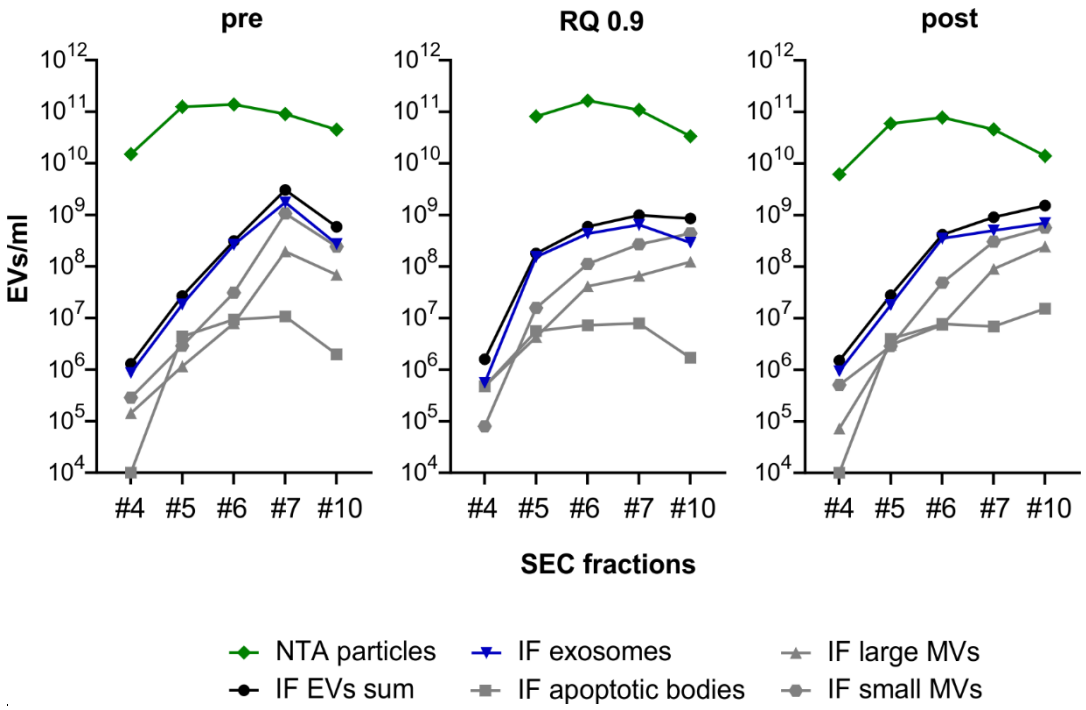

Figure 3.16: Comparison of NTA and IF to estimate EV concentration in SEC-fractions. Total NTA particle counts (green) and fluorescent (BODYPI) events (total EVs and EV-subclasses) in single SEC fractions.

3.3.2 Semi-quantitative analysis of ExerV release

In an alternative approach to visualize ExerV kinetics, exercise-induced changes of EV amount was further analyzed by semi-quantitative assessment in WB analysis. EV-associated markers were observed to increase in ExerV subclasses, normalized to plasma volume, from pre to RQ 0.9 and post

exercise (fig. 3.17 and 3.18). In SEC-EVs, significant increases of roughly 2-fold were observed for the tetraspanins CD9, CD63 and CD81 post exercise, which was already evident as slight elevation at increasing exercise intensity at RQ 0.9 (fig. 3.18), suggesting a load-responsiveness. For the immuno-affinity isolated ExerVs this was observed for CD9 and CD63 likewise. However, CD81 levels were less intensely increased. The markers TSG101 and Syntenin, associated with late endosome-derived small EVs, showed a trend to rise in response to exercise, though fold changes were not significant. On the contrary, ApoA1, which reflects lipoprotein co-isolation, remained unaffected in SEC-EVs during exercise**.** Taken together, WB analysis of ExerV subclasses suggests an elevation of the EV amount of roughly 2-fold in response to the applied exercise setting. This finding was validated for CD9-, CD63- and CD81-carrying EVs, possibly including MVs, while quantification of exercise-mediated effects on late endosome-derived small EVs need to be analyzed in more detail.

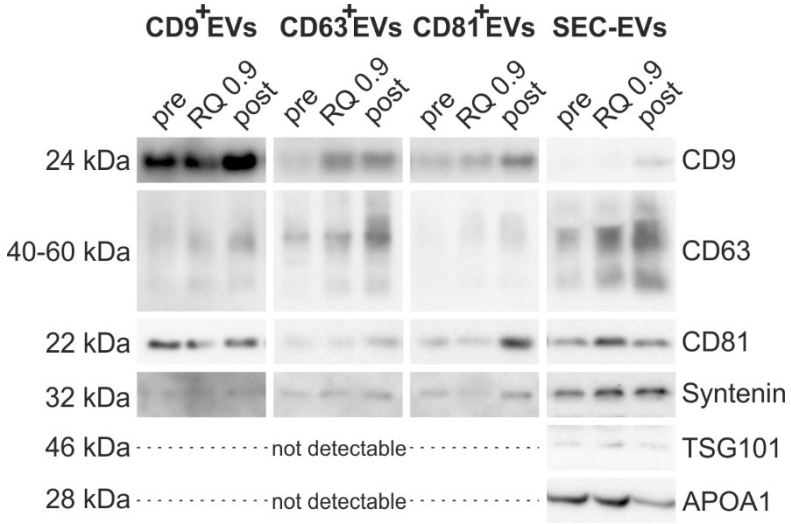

Figure 3.17: EV marker analysis of ExerVs. WB characterization of SEC-EVs, CD9$^+$EVs, CD63$^+$EVs and CD81$^+$EVs derived from exercising subjects using genuine EV-markers CD9, CD63, CD81, Syntenin and TSG101 as well as HDL marker ApoA1.

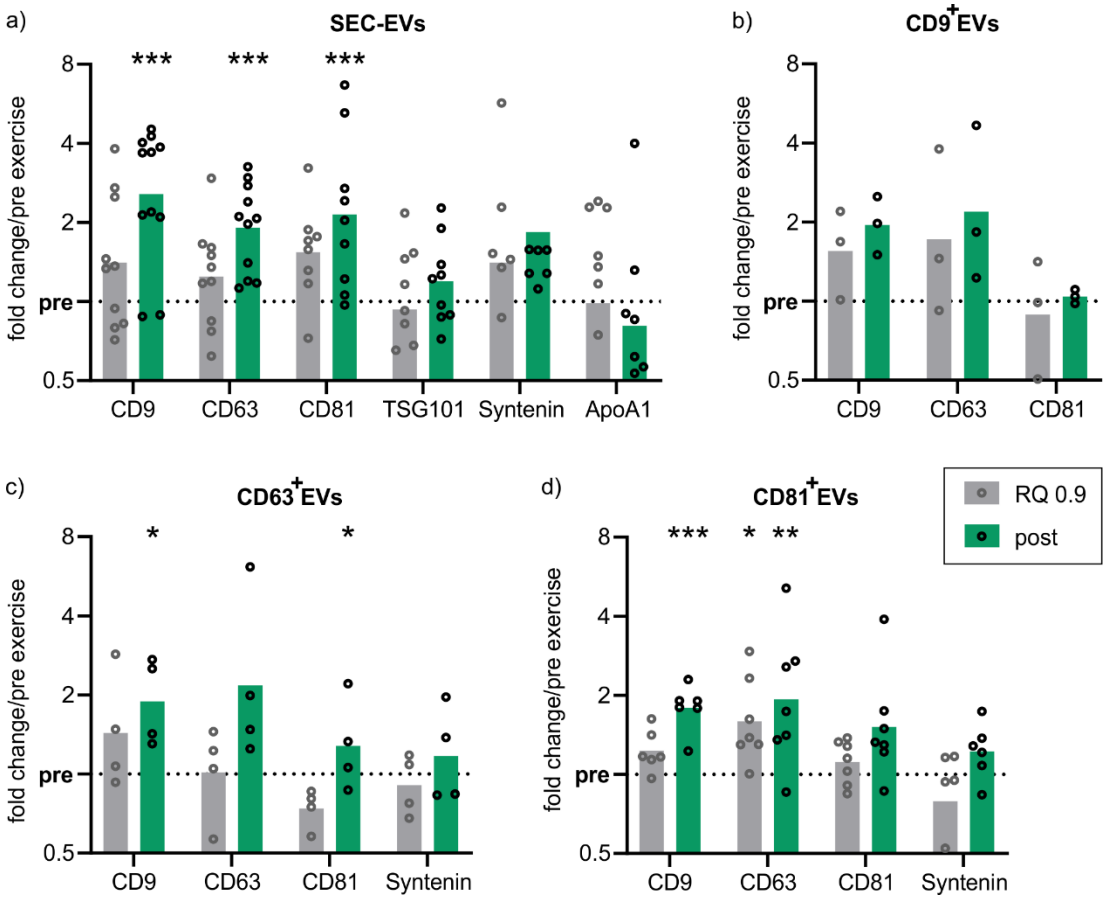

Figure 3.18: Semi-quantitative analysis of ExerV kinetics. Densitometric quantification of signals derived from WB analysis of the exercising subjects. Individual (circle) and mean (bar) fold changes of WB markers. RQ 0.9 and post expressed in relation to pre exercise (dashed line). Bonferroni-corrected students t-test, n=3-11, *=p<0.05, **=p<0.01, ***=p<0.001.

3.4 Origin of ExerVs

3.4.1 Multiplexed marker analysis of ExerVs – EV Array

To determine the cellular sources of EVs, liberated in response to the applied exercise setting, first, EV Array technology was implemented. This multiplex assay enables examination of the presence of several markers, including EV markers and cell surface markers, via an antibody-mediated detection approach (Jorgensen et al., 2013). Plasma samples of ten subjects were analyzed in the EV Array and intensity changes in response to exercise were observed for a variety of markers (fig. 3.19 a). Alix, CD14, CD142, HLA-ABC (MHCI), ICAM-1, LAMP-1 (lysosomal-associated membrane protein 1), and tPA (tissue plasminogen activator) displayed a significant elevation from pre exercise over RQ 0.9 to post exercise (fig. 3.19 b). Increases of these markers

indicated endosomal characteristics and a possible origin of ExerVs from endothelial cells and leukocytes. Strikingly, the tetraspanins CD9, CD63, and CD81 which were demonstrated to increase in WB analysis (see chapter 3.3.2), were below the detection threshold of the assay. This was also observed for Flot1, HSP70, and CD41b previously described to be released within EVs during exercise (Frühbeis et al., 2015). These findings suggest that the analysis of EV marker changes in the implemented exercise setting with EV Array methodology may be limited. Separation of EVs from the complex sample material blood plasma may be crucial to identify further phenotyping markers of ExerVs.

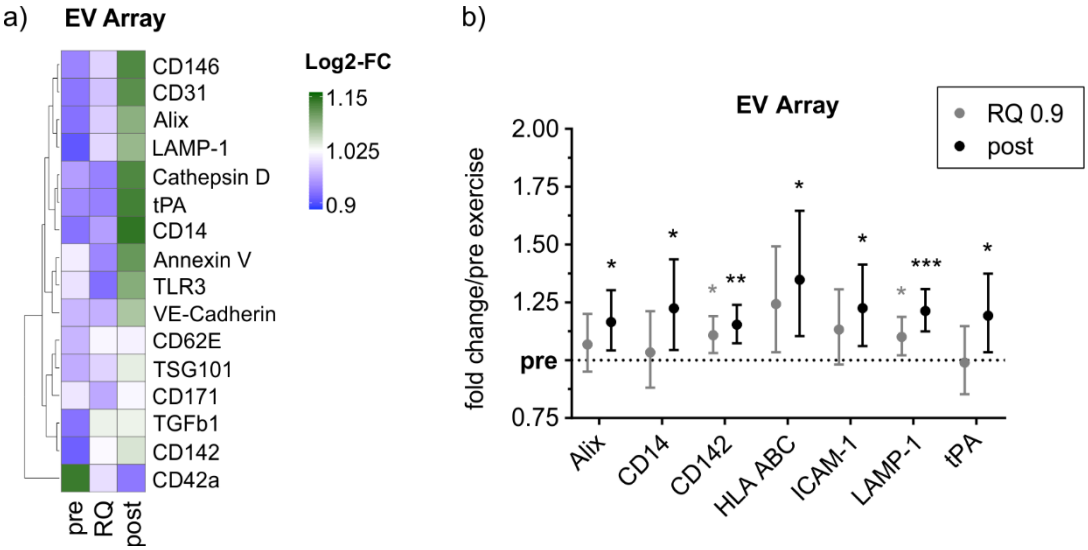

Figure 3.19: Marker profile of plasma-EVs analyzed in EV Array. (a) Heatmap visualization of marker changes during exercise. Markers depicted were higher than the LOD in more than 50 % of cases. (b) Mean fold changes of significantly increasing markers. 95 %-confidence intervals (CI) depicted. Individual values of biological replicates in fig. S2 and S3. Bonferroni-corrected students t-test, *=p<0.05, **=p<0.01, ***=p<0.001, n=10.

3.4.2 Cell type specific WB analysis of ExerVs

Origin of ExerVs from the cellular sources platelets, muscle, and liver, was investigated in WB analysis of isolated SEC-EVs, $CD9^+$EVs, $CD63^+$EVs, and $CD81^+$EVs.

CD41b, which is representative for platelet-derived EVs, was found to be increased during exercise in all four ExerV subclasses (fig. 3.20 a). Mean fold changes were ranging from 1.4- to 3.9-fold at RQ 0.9 and from 2.4- to 8.7-fold

post exercise (fig. 3.20 b). While at RQ 0.9 level this increase was only significant in CD81⁺EVs (2.9-fold, $p<0.05$), significant fold changes post exercise were found in CD81⁺EVs and SEC-EVs (8.7-fold and 2.4-fold, $p<0.01$). These findings strongly indicate a contribution of platelet-derived EVs to the pool of ExerVs in the applied exercise setting.

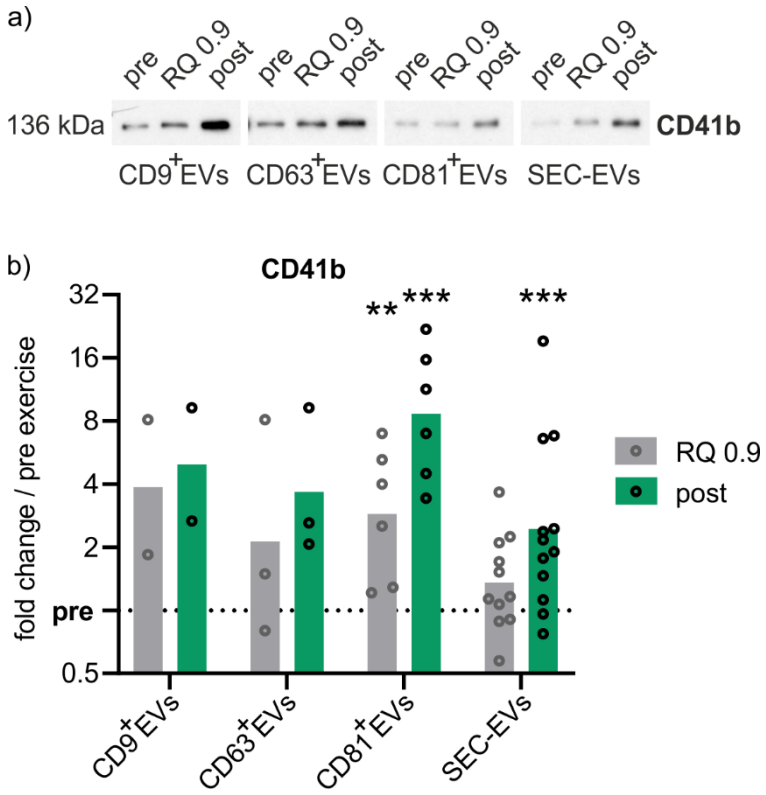

Figure 3.20: Platelet-specific WB analysis of ExerVs. (a) WB of CD41b in SEC-EVs, CD9⁺EVs, CD63⁺EVs and CD81⁺EVs derived from exercising subjects. (b) Densitometric quantification of CD41b signals. Individual (circle) and mean (bar) fold changes of WB markers. RQ 0.9 and post levels are displayed in relation to pre exercise (dashed line). Bonferroni-corrected students t-test, n=2-12, *=$p<0.05$, **=$p<0.01$, ***=$p<0.001$.

Further WB analysis of isolated ExerVs did not reveal presence of α-sarcoglycan (SGCA, fig. 3.21 a, b), which was described to be found in muscle-derived EVs (Guescini et al., 2015). Likewise, asialoglycoprotein receptor 2 (ASGPR2, fig. 3.21 c) an indicator for EV release from liver (Conde-Vancells et al., 2008), could not be detected.

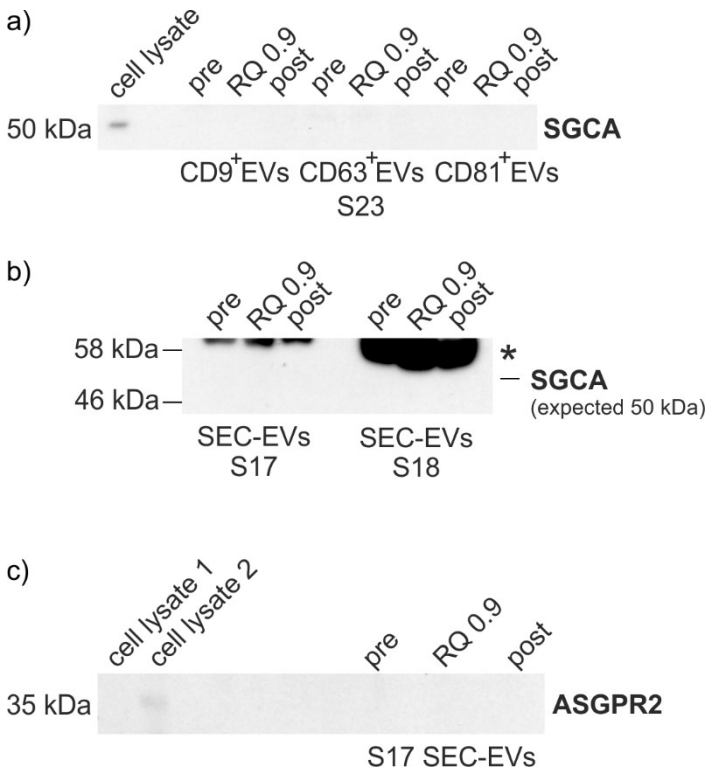

Figure 3.21: Muscle- and liver-specific WB analysis of ExerVs. WB of muscle-EV marker α-sarcoglycan (SGCA) in CD9$^+$EVs, CD63$^+$EVs and CD81$^+$EVs (a) and SEC-EVs (b) derived from exercising subjects. *=unspecific albumin binding. (c) WB staining of liver-EV marker asialoglycoprotein receptor 2 (ASGPR2) in SEC-EVs.

Summarized, the previously described exercise-induced release of EVs by platelets (Chaar et al., 2011; Frühbeis et al., 2015; Rakobowchuk et al., 2017; Wilhelm et al., 2016) was confirmed for SEC-ExerVs and immuno-affinity captured ExerVs, but there was no evidence for the release of ExerVs from muscle or liver.

3.4.3 Multiplex bead-based cell surface marker analysis of ExerVs - MACSPlex

To reveal further information about the cellular origin of ExerVs, the commercial multiplex bead-based analysis MACSPlex was implemented. The platform enables the examination of 37 cell surface markers in an EV-sample in parallel. The analysis is based on EV-capture by beads carrying antibodies for cell surface markers and subsequent detection with antibodies for the EV-associated markers CD9, CD63 and CD81, conjugated to APC using flow cytometry.

Surface marker profiles of ExerVs

Surface marker profiles of the differentially isolated EVs displayed high signals for platelet-associated markers (e.g. CD42a and CD62P), for leukocyte markers such as CD8 and HLA-DRDPDQ (MHCII), and endothelial markers (CD105), next to the genuine EV-markers CD9, CD63 and CD81 (fig. 3.22). Compared to SEC-EVs, a higher number of markers with strong mean fluorescence intensities (MFI) are found in the profiles of immuno-captured EVs (e.g. CD29 and CD49e). CD9, CD63, and CD81 signals were nearly completely reduced in the respective immuno-capture, while detection of e.g. CD63 in $CD81^{+}$EVs was successful. This finding may be explained by increasing competition for the respective antibody epitopes used for sequential isolation, capturing and detection, and was already described by others (Koliha et al., 2016; Wiklander et al., 2018). Interestingly, the overall surface marker profiles of $CD63^{+}$EVs and $CD81^{+}$EVs were observed as markedly similar while $CD9^{+}$EVs exhibited similarities with SEC-EVs (e.g. higher signals for CD62P and HLA-DRDPDQ compared to other markers).

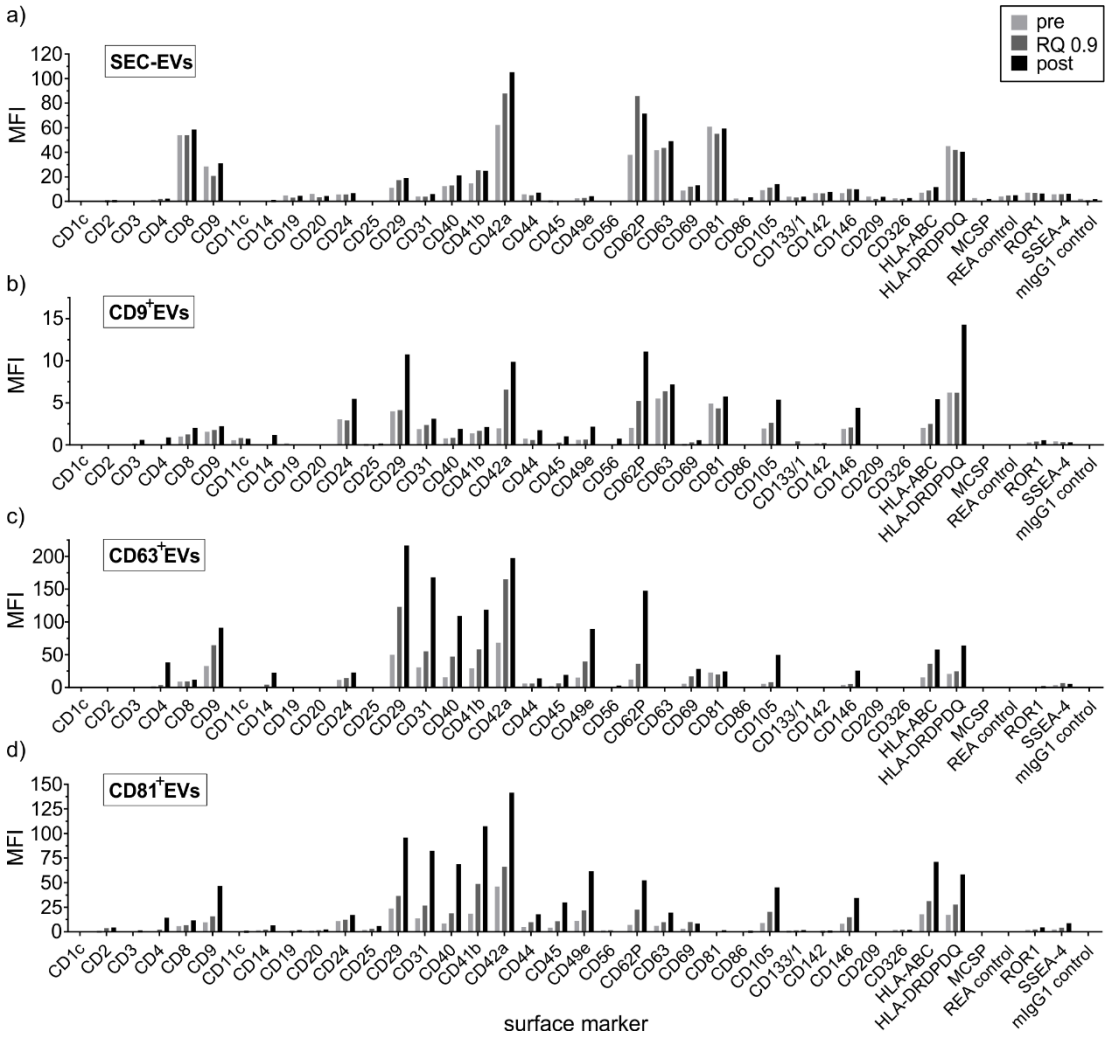

Figure 3.22: Cell surface marker profiles of ExerV subclasses. Representative mean fluorescence intensities (MFI) of markers determined in MACSPlex analysis of SEC-EVs (a) as well as immuno-affinity captured CD9$^+$EVs (b), CD63$^+$EVs (c), and CD81$^+$EVs (d).

Comparison of MACSPlex and WB analysis of ExerVs

To evaluate the capability of the MACSPlex system to resolve ExerV dynamics, tetraspanin and CD41b mean fold increases (fig. 3.23) were specifically compared with fold changes in WB (see chapters 3.3.2 and 3.4.2). Likewise, incremental increases in response to the exercise setting were observed for CD9, CD63, CD81, and CD41b in all four ExerV subclasses. However, while tetraspanin changes in CD9$^+$ExerVs, CD63$^+$ExerVs, and CD81$^+$ExerVs were comparable in the two semi-quantitative approaches, reduced values in MACSPlex analysis (1.3-1.6-fold) compared to WB (1.9-2.6-fold) were detected in SEC-ExerVs. In contrast, CD41b fold changes of immuno-affinity captured ExerVs were strongly decreased in the MACSPlex

assay. Conclusively, though exhibiting differing extends of marker changes, MACSPlex analysis confirms overall EV-kinetics during exercise.

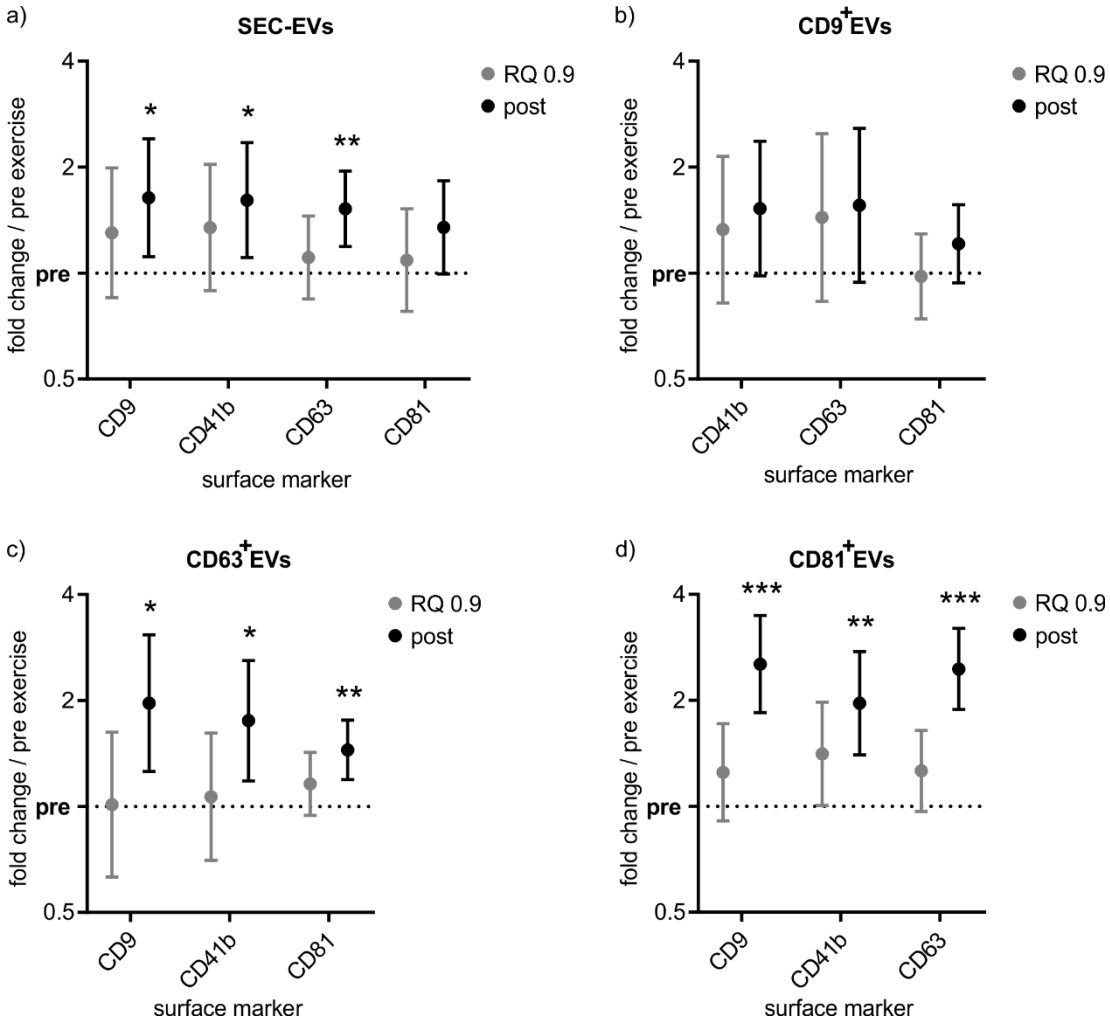

Figure 3.23: Tetraspanin and platelet marker kinetics in ExerV subclasses estimated by multiplex bead-based analysis. Mean tetraspanin and CD41b elevations with 95%-CI in (a) SEC-EVs (n=9), (b) $CD9^+$EVs (n=5), (c) $CD63^+$EVs (n=7) and (d) $CD81^+$EVs (n=9). Bonferroni-corrected students t-test, *=p<0.05, **=p<0.01, ***=p<0.001, n=9.

Identification of the cellular sources of ExerVs

Next, further analysis of changes in the surface marker intensities in response to the applied exercise setting was used for estimation of cellular sources of ExerVs. Incremental increases of several cellular markers were observed in the individual marker profiles from pre to RQ 0.9 and post exercise (fig. 3.24). Also, in heatmap clustering analysis, RQ samples are placed left to the respective post samples in almost all cases, though it does not perfectly separate RQ 0.9 samples from post samples. Furthermore, ExerVs specifically carry markers of lymphocytes (CD4 and CD8), endothelial cells (CD31, CD105

and CD146), AP cells (MHCII and CD40), and platelets (CD41b, CD42a, and CD62P). While the exposed marker fold-changes in SEC-EVs again remained moderate (fig. 3.24 a), higher fold changes were detected in immuno-captured EVs (fig. 3.24 b-d). Consistently, the ExerV-subclasses carrying CD4 (lymphocytes) and CD14 (monocytes) were at a detection minimum at rest, but exhibited robust signals after exercise, which is reflected by high fold changes for these two markers. In addition to the identification of ExerV-sources in the individual study participants, low-responders (e.g. S3 and S5) and high-responders (e.g. S19 and S23) may be defined.

Significant mean marker increases were strikingly similar between SEC-, $CD9^+$-, $CD63^+$- and $CD81^+$ExerVs (fig. 3.25). The surface markers showed a trend to increase at RQ 0.9 as well as significant mean fold increases post exercise, which is in in line with the statistics for the release kinetics observed in WB (see chapter 3.3.2). Overall, mean fold changes were ranging from 1.2- to 5.5-fold (SEC-EVs), 1.2- to 7.5-fold ($CD9^+$EVs), 1.4- to 10.4-fold ($CD63^+$EVs), and 1.5- to 9.6-fold ($CD81^+$EVs) post exercise. In SEC-ExerVs, $CD63^+$ExerVs and $CD81^+$ExerVs significantly elevated markers specific for platelets (CD41b, CD42a, CD62P, from 1.6- to 2.9-fold in mean), lymphocytes (CD4, 4.4- to 10.4-fold and CD8, 1.3 to 1.8-fold), and AP cells (MHCII, from 1.7- to 3.4-fold), as well as MHCI (1.6-to 2.9-fold) were observed. Furthermore, the markers CD105 (2.3- to 4.3-fold) and CD146 (2.0- to 3.5-fold), which are associated with endothelial cells, increased significantly upon exercise. In $CD63^+$ExerVs and $CD81^+$ExerVs also endothelial CD31 (2.5- and 3.7-fold) was significantly elevated. In $CD9^+$ExerVs, statistical significance was detected for similar but fewer cellular markers, which might be explained by a smaller sample size (n=5). Significant marker elevations were likewise detected for lymphocyte (CD4, 7.5-fold and CD8, 1.7-fold), endothelial (CD105, 3.7-fold, and CD146, 2.4-fold), AP cells (MHCII, 2.3-fold, and CD40, 2.6-fold), and platelet markers (CD62P, 2.6-fold). CD41b and CD42a increases, on the other hand, were not statistically significant. Interestingly, in SEC-EVs and $CD9^+$EVs, CD62P exhibited elevated levels (1.5- and 2-fold, $p<0.05$) already at RQ 0.9. Conclusively, phenotyping of SEC- and immuno-affinity captured ExerVs indicates contribution of platelets, leukocytes including lymphocytes as well as monocytes, and endothelial cells to the pool

of EVs released into the blood upon exercise. These seem to include CD9⁺, CD63⁺ and CD81⁺-subclasses with phenotypes which exhibit only minor differences.

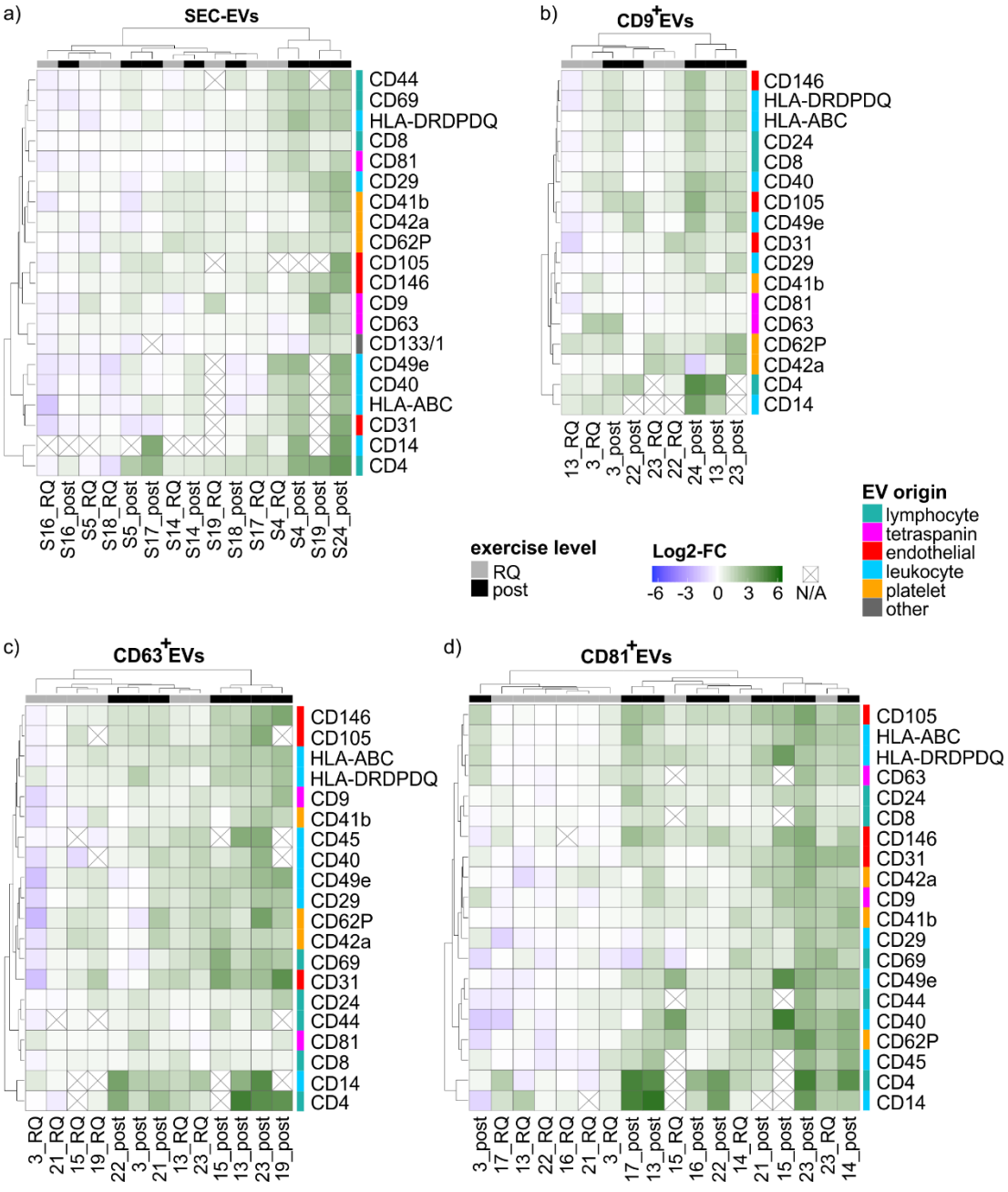

Figure 3.24: Individual changes of cell surface markers in ExerV subclasses. Heatmap visualization of individual MACSPlex marker increases in SEC-EVs (a) and immuno-affinity captured EV subclasses (b-d) including hierarchical clustering for markers as well as subjects. Log2-fold changes of MFI at RQ 0.9 and post in relation to pre exercise are presented.

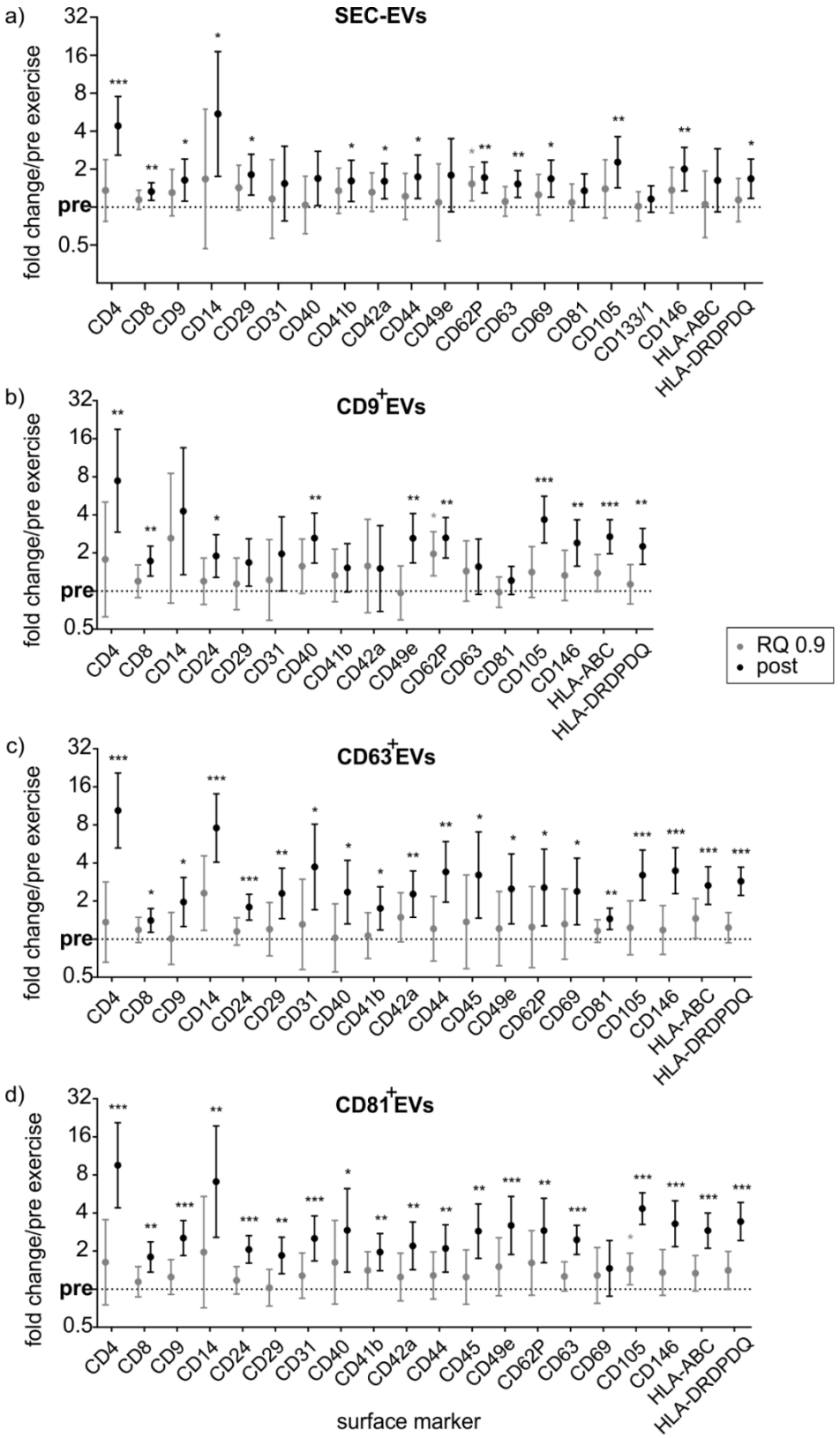

Figure 3.25: Origin and kinetics of ExerV subclasses. Mean cell surface marker elevations with 95%-CI at RQ 0.9 and post normalized to pre exercise in (a) SEC-EVs (n=9), (b) $CD9^+$EVs (n=5), (c) $CD63^+$EVs (n=7) and (d) $CD81^+$EVs (n=9). Bonferroni-corrected students t-test, *=p<0.05, **=p<0.01, ***=p<0.001.

4 Discussion

4.1 ExerVs are a mixture of EVs derived from multiple cell populations

4.1.1 Platelets, endothelial cells, and leukocytes contribute to the exercise-triggered release of extracellular vesicles into the circulation

Physical exercise induces broad physiological changes which are accompanied by the active release of EVs into the circulation (Frühbeis et al., 2015; Whitham et al., 2018). It is speculated that these ExerVs are involved in the adaptive mechanisms of exercise due to their possibility of acting as long-distant signaling mediators (Piccirillo, 2019; Safdar et al., 2018). This study intended to gain detailed knowledge on small EV release kinetics as well as their originating cell populations during acute exercise.

The phenotyping analysis of ExerVs provides profound insights into the composition of small EVs during physical exercise, revealing origin from endothelial cells, platelets and leukocytes including lymphocytes, monocytes and antigen-presenting cells. Two different multiplexed assays indicated the release of vesicles from multiple cell populations. EV Array technology analyzing EVs unpurified in blood plasma of exercising humans gave a first indication of endothelial and leukocyte origin (fig. 3.19). MACSPlex characterization of different ExerV subpopulations, defined by the method of isolation via size-exclusion-chromatography, CD9-, CD63- or CD81-immuno capture, resulted in a panel of marker proteins found to be significantly upregulated in each of the examined EV subpopulations (fig. 3.25). These can be assigned to endothelial cells ($CD31^+$, $CD105^+$, $CD146^+$), platelets ($CD41b^+$, $CD42a^+$, $CD62P^+$) and leukocytes, including lymphocytic cells ($CD4^+$, $CD8^+$) and antigen-presenting cells ($MHCII^+$). EVs generated in response to various exercise conditions were considered important players in organ cross-talk and long-term adaptive responses triggered by physical activity (Bei et al., 2017; Chaturvedi et al., 2015; Frühbeis et al., 2015; Lovett et al., 2018; Safdar et al., 2018; Whitham et al., 2018). During physical exercise the alteration of a variety of physiological processes can be observed, including enhanced

cardiovascular signaling, activated immune function and increased coagulation capacity (Pedersen et al., 2000; Vanhoutte et al., 2017; Womack et al., 2003). This is reflected by elevated levels of ROS, shear forces, catecholamines, cortisol as well as cytokines in the circulation immediately upon exercise. Conclusively, ExerV phenotyping analysis strongly supports the idea that ExerVs contribute to these signaling processes by functioning as mediators of endothelial signaling, coagulation processes and immune regulation.

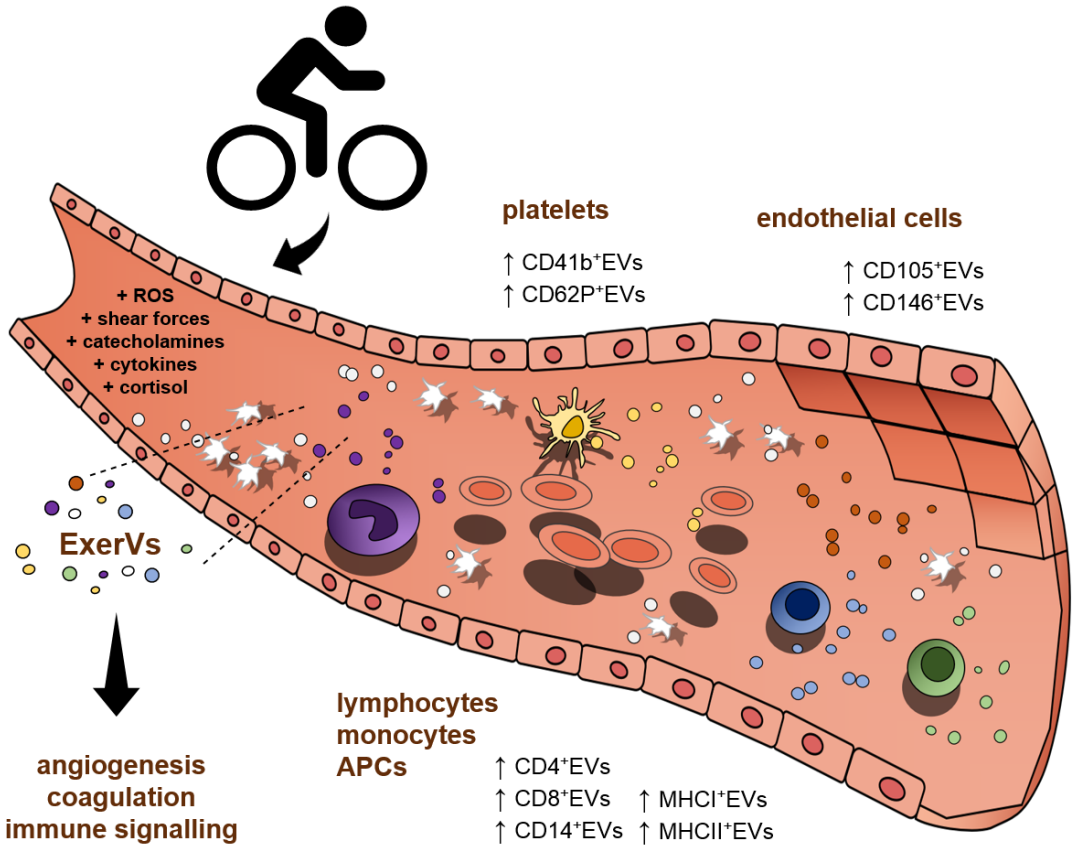

Figure 4.1: Origin and putative functions of ExerVs. During physical exercise, platelets, endothelial cells, and leukocyte subsets release extracellular vesicles into the blood stream. These may function in signaling processes like coagulation, angiogenesis and inflammation.

4.1.2 ExerV subclasses show highly similar release kinetics

Characterization of four different ExerV subpopulations revealed highly similar release kinetics and cellular sources of the ExerV subclasses. In WB and MACSPlex analysis ExerVs exhibited consistent marker elevations of more than twofold and comparable marker profiles in CD9⁺EVs, CD63⁺EVs,

CD81$^+$EVs and SEC-EVs (fig. 3.18, 3.20, 3.23, and 3.25). This might indicate that overall liberation of the different subpopulations into the circulation is triggered by the same release mechanisms. Alternatively, the three tetraspanins may be evenly distributed on all ExerVs. Interestingly, more detailed comparison of the phenotyping profiles of CD9$^+$EVs, CD63$^+$EVs, CD81$^+$EVs and SEC-EVs indicates minor divergences (fig. 3.25). While CD63$^+$EVs and CD81$^+$EVs exhibited strikingly similar cell surface marker profiles, CD9$^+$EVs and SEC-EVs displayed slight differences including a stronger increase in platelet-selectin (CD62P), which already becomes visible at RQ 0.9 during exercise. This might indicate a higher proportion of platelet-derived EVs in CD9$^+$ExerVs and SEC-ExerVs compared to CD63$^+$ExerVs and CD81$^+$ExerVs. This is also reflected by stronger CD41b signals in WB analysis of CD9$^+$EVs compared to CD63$^+$EVs and CD81$^+$EVs (fig. 3.17). More specific information on the composition of ExerVs may be provided utilizing the three tetraspanins independently instead of in the combination for EV-detection (APC-staining) in MACSPlex. Using MACSPlex assay, different research groups characterized the distribution of the tetraspanins in single cell populations like HEK-cells, MSCs, B-cells, NK cells and platelets (Koliha et al., 2016; Wiklander et al., 2018). However, phenotyping of EV subclasses in a heterogeneous mixture of EVs in the plasma of exercised subjects appears more complex. Isolation of more specific ExerV subpopulations e.g. by combining of SEC with IA-capture or by using e.g. CD105-antibodies coupled to magnetic beads and subsequent analysis in MACSPlex and WB may further shed light on ExerV composition. These findings highlight the multifaceted nature of EV mixtures in a complex sample material such as blood plasma and the potential of a detailed analysis of several populations of EVs in multiplexed assays.

4.1.3 ExerV release by other cellular populations?

While our ExerV phenotyping analysis strongly suggests a contribution of endothelial cells, platelets and leukocytes, other cells may also release EVs upon physical activity. Since muscle cells have a highly increased activity during exercise it is considered that they contribute to the pool of ExerVs (Guescini et al., 2015; Lovett et al., 2018; Whitham et al., 2018). A recent study

analyzed the proteomic content of EVs after exercise and proposed a model of myokine-containing EV release by muscle cells finally taken up in the liver (Whitham et al., 2018). However, the analyzed EVs were prepared by low-speed centrifugation and EV characterization is missing, which impairs the actual attribution of cargo to EVs. In our exercise setting, there was no evidence of a contribution of muscle cells to the ExerV pool. α-sarcoglycan, which was previously described to be released in EVs 1 h after exercise stimulation (Guescini et al., 2015), was not detectable in SEC-EVs or immuno-captured ExerVs (fig. 3.21). Likewise, no contribution of liver EVs to the pool of ExerVs could be detected. Though the contribution of other muscle or liver cell derived EV populations cannot be excluded, the rapid increase of EVs within 15 to 30 min during exercise may rather indicate a release from cells which are in direct contact to blood. In line with our ExerV phenotyping, Bryl-Gorecka et al. (2018) analyzed the proteomic content of ExerVs 1 h after completion of an exercise intervention and mainly found proteins associated with blood cells or endothelial cells (Bryl-Gorecka et al., 2018). Liberation of ExerVs by red blood cells and their precursors should be addressed in future studies given the high number of RBCs in blood and the stimulating effect of exercise on hematopoiesis (Hu et al., 2012). Furthermore, more detailed analysis of the ExerV subpopulations identified in MACSPlex analysis will further reveal contribution of more specific cellular sources to the pool of ExerVs. Interestingly, CD14, which is prominently expressed on monocytes/macrophages, is to a lower extend also expressed on neutrophils (Antal-Szalmas et al., 1997). Similarly, CD105 and CD146, which are mainly attributed to endothelial cells and EVs, are also found on mesenchymal stromal cells and EVs (Börger et al., 2016; Eirin et al., 2016; Lindoso et al., 2014). These considerations again highlight the complexity of EV mixtures in blood and the need for stringent and well-designed EV isolation and characterization strategies.

Taken together, antibody-based semi-quantitative analysis enabled the estimation of ExerV dynamics as well as originating cell populations. Further analysis addressing more specific ExerV subpopulations may further untangle the complex composition of EVs in the plasma of exercising humans to unravel their functions in multi-systemic signaling.

4.2 Putative functions of ExerVs

4.2.1 ExerV release by platelets indicates involvement in coagulation processes

Surface marker analysis of ExerVs revealed an incremental release of platelet-derived EVs into the blood during exercise, which is in line with the literature on platelet microparticles. In multiple studies, $CD41^+$, $CD42a^+$ and $CD62P^+$-platelet-EVs were demonstrated to increase during physical activity, starting at an early phase of exertion (Chaar et al., 2011; Frühbeis et al., 2015; Rakobowchuk et al., 2017; Schwarz et al., 2018; Sossdorf et al., 2011; Wilhelm et al., 2016). Likewise, WB and MACSPlex phenotyping of ExerVs implicated the liberation of $CD41b^+$-, $CD42a^+$-, and $CD62P^+$EVs from platelets during exercise (fig. 3.20 and 3.25). Furthermore, $CD62P^+$SEC-ExerVs and $CD62P^+CD9^+$-ExerVs exhibited a considerable increase already at submaximal workload. *In vitro* analyses demonstrated that elevated levels of shear stress and subsequent coagulative activity leads to the release of EVs by platelets (Miyazaki et al., 1996; Reininger et al., 2006). Furthermore, these PMPs exhibited pro-coagulant activity and enhanced thrombus formation. During exercise, pro-thrombic as well as fibrinolytic effects can be observed, and the fine-tuning of these counter-acting reactions are considered to be an adaptational response of regular physical exercise leading to improved blood hemostasis (el-Sayed, 1996; Womack et al., 2003). Thus, ExerV-release by platelets may be part of a sensitive signaling mechanism to maintain blood homeostasis. However, PMPs were also described to promote angiogenesis (Italiano et al., 2008; Kim et al., 2004), mediate pro-inflammatory signaling (Mause et al., 2005; Vajen et al., 2017) and affect hematopoiesis (Baj-Krzyworzeka et al., 2002). As reviewed by Boilard et al., EVs assigned to platelets may derive from activated platelets or megakaryocytes, can be phosphatidylserine positive or negative, and may contain mitochondria (Boilard et al., 2015). Further detailed characterization of platelet-derived ExerV subtypes or ExerV analysis in patients with coagulopathy or thrombophilia may provide deeper insights into the diverse functions of the multiple subclasses of platelet-ExerVs.

4.2.2 Endothelial cell-derived EV signaling upon exercise

Elevated levels of endothelial cell markers in several examined ExerV subpopulations implies a substantial release of small EVs from endothelial cells upon exercise. In MACSPlex analysis, the markers for endothelial cells (CD31, CD146 and CD105) were among the most upregulated markers after exhaustive cycling (fig. 3.25), indicating a robust secretion of endothelial EVs to the bloodstream during exercise. This finding is also supported by EV Array analysis (increasing levels of ICAM-I and tPA, fig. 3.19).

The effect of acute exercise on EV-release by endothelial cells was examined by several groups using flow cytometric analysis of endothelial microparticles (Lansford et al., 2016; Möbius-Winkler et al., 2009; Shill et al., 2018; Sossdorf et al., 2011). In contrast to our work, most of the studies found no or only marginal increases of EMPs immediately upon diverse exercise settings (including 4 h cycling and marathon running) but increased levels one day later. Only Lansford et al. found a doubling of activated $CD62E^+$EMPs after 30 min of moderate cycling exercise (Lansford et al., 2016). Most of the EMP analyses were focused on $CD31^+$ and AnxV-binding EMPs, considered as apoptotic EMPs (Wilhelm et al., 2018). These elevated levels of EMPs were related to harmful impact on e.g. vascular functions by pro-inflammatory and pro-coagulative signaling (Hromada et al., 2017). However, apoptotic processes take far longer than 15 to 30 minutes as analyzed in our exercise study. Accordingly, $CD31^+$EVs did not respond to exercise in the same extend as $CD105^+$ and $CD146^+$EVs in MACSPlex phenotyping analysis (fig. 3.25). This finding suggests an early active release of endothelial EVs triggered by different mechanisms than apoptosis, which might have a targeted function on recipient cells. For example, endothelial exosomes were demonstrated to promote tube formation and vessel sprouting in HUVECs (Sheldon et al., 2010) and might be associated with angiogenic signaling during exercise. Interestingly, Hergenreider et al. showed that in response to increased shear stress, HUVEC-EVs are capable of inducing an atheroprotective phenotype in smooth muscle cells by transferring miRNA species (Hergenreider et al., 2012). Conclusively, ExerV phenotyping indicates the immediate and active release of small endothelial EVs during a short bout of exhaustive exercise. In

contrast to apoptotic EMPs, these EVs might contribute to angiogenesis and the improvement of endothelial function under exercise conditions.

4.2.3 Immune signaling during exercise mediated by EVs?

An interesting finding from the surface marker analysis is the neat increase of EVs derived from leukocytes, including lymphocytes, monocytes and antigen presenting cells, during and immediately after exercise. EV Array as well as MACSPlex analysis detected several markers for T cells (CD4, CD8), monocytes (CD14), and AP cells (MHCII) on ExerVs (fig. 3.19 and 3.25). Increasing levels of cytokines and leukocytes in response to exercise reflect the induction of an inflammatory process during physical activity (Nielsen et al., 2016; Pedersen et al., 2000). However, the *in vivo* influence of exercise on immune cell release of EVs is rarely examined. Sossdorf et al. also found $CD14^+$ monocytic MPs elevated immediately and 45 min after 90 min of cycling exercise (80 % of IAT) (Sossdorf et al., 2011). Chaar et al. found MVs derived from neutrophils ($CD15^+$MP) elevated in response to three consecutive bouts of exercise (Chaar et al., 2011). The detection of immune-cell derived EVs under exercise conditions might indicate their contribution to immune signaling processes. EVs are considered important immune-modulatory vehicles which efficiently transfer antigens and immune-stimulatory signals (Robbins et al., 2014; Tkach et al., 2017). Likewise, muscle-derived EVs are believed to transport myokines (=cytokines released by muscle cells) to recipient tissues in response to exercise stimuli (Piccirillo, 2019; Whitham et al., 2018). Therefore, ExerVs may enable a directed transport of pro- or anti-inflammatory cargo to recipient cells of the circulatory system and the underlying tissues during and after exercise. Exercise is considered an anti-inflammatory stimulus in different diseases like rheumatic diseases or cancer (Benatti et al., 2015; Hojman, 2017). Analysis of the effects of ExerVs on target cells, e.g. *in vitro* on primary muscle cells, or *in vivo* in mice models of inflammatory diseases, may shed light on their contribution to beneficial immune adaptations. Furthermore, the assessment of ExerV release in patients suffering from inflammatory diseases, such as systemic lupus erythematosus, will further define their role in inflammatory signaling.

4.3 Limitations of the analysis of ExerVs

The isolation and characterization of ExerVs from blood plasma is struggled by EV heterogeneity, the co-isolation of non-EV components, and insufficient specificity of downstream analysis methods.

4.3.1 Estimation of ExerV concentration is hampered

Non-EV components in plasma and isolated EVs highly affected the total count of ExerVs measured with NTA or imaging flow cytometry. Though NTA identified the same EV-rich SEC-fractions as WB analysis (fig. 3.1 and fig. 3.2), and NTA of the pooled SEC-EVs (#4-6) revealed a typical size distribution for small EVs (fig. 3.3), the more than two-fold increase in EV numbers estimated semi-quantitatively by WB in this study (fig. 3.18, 3.20) or comparable EV elevations described in the literature (Frühbeis et al., 2015; Guescini et al., 2015; Whitham et al., 2018) were not measurable. In contrast to this, NTA suggested constant EV numbers in response to physical exercise (fig. 3.15 and 3.16). IF of BODIPY-stained EVs indicated a low increase in EV numbers during, but a decrease to baseline concentration immediately post exercise when analyzing EVs in plasma (fig. 3.14). Additionally, the intake of a high-fat meal had an enormous effect on particle numbers estimated by NTA which were elevated by an order of magnitude under postprandial conditions (Brahmer et al., 2019). Impaired WB analysis confirmed, that these elevated numbers were not due to EV increases in response to food-intake, but rather indicated an increased co-isolation of lipoprotein subclasses (chylomicrons). Similar findings were described by Sodar et al. who showed that flow cytometric analysis of MVs was highly confounded by food-intake (Sodar et al., 2016). Though Jamaly et al. did not observe similar effects of food intake on NTA of ultracentrifuged plasma EVs, they revealed that 66 % of the variation of EV particle numbers were dependent on VLDL concentration in the corresponding plasma samples (Jamaly et al., 2018). These findings indicate that EV enumeration using NTA and IF conducted under the presented conditions is highly susceptible to lipoprotein contamination of EV samples and both methods do not measure EVs without vesicle-specific labeling. However, IF analysis of single SEC fractions (fig. 3.16) demonstrates that also the choice

of membrane dye is of high importance for EV number calculation. Intriguingly, the highest numbers of EVs stained by BODIPY were determined in EV-poor/protein-high fractions estimated by WB (#7-10, fig. 3.2). Conclusively, the membrane dye seems to rather label lipoproteins or other non-EV plasma components than EVs. This was also recently demonstrated by de Rond et al. who compared five generic EV markers in flow cytometric analysis of isolated EVs and plasma-EVs (de Rond et al., 2018). Each of the tested markers failed to enable measurement of all EVs in the sample or additionally stained non-EV sample components. In further studies, an appropriate EV staining approach should be identified, which would enable correct ExerV enumeration. For example, SEC-EVs could be stained with an antibody for CD63 coupled to a fluorophore and measured in IF or fluorescent-NTA. Further isolation of EVs, e.g. involving antibodies for EV-associated marker proteins followed by detachment of the antibodies, could be used. This would also enable to measure EV subclasses in a given EV sample. Furthermore, multiple innovative EV isolation and characterization methods, which include flow field-flow fractionation (Sitar et al., 2015) and acoustic approaches (Lee et al., 2015; Rezeli et al., 2016), were recently developed. In addition, the invention of proper EV reference material has gained increasing attention (Lozano-Andres et al., 2019; Valkonen et al., 2017). These developments may provide the possibility to estimate actual ExerV concentrations in future experiments. Importantly, the calculation of EV numbers should be verified by (immuno-) EM imaging although it is time consuming and laborious (Thery et al., 2018; van der Pol et al., 2014). In conclusion, the estimation of ExerV numbers was impaired by non-EV plasma components during the conducted study, but several modifications of the downstream analysis strategy may enable calculation of ExerV numbers in future experiments. This will provide a profound basis to study the release kinetics of the various ExerV subclasses which might also function as minimal-invasive prognostic and diagnostic markers.

4.3.2 Multiplexed assays are confounded by a complex plasma composition

EV Array technology measuring unpurified EVs in plasma, similarly, was highly susceptible to be impaired by plasma components. Characterization of ExerV

kinetics needed modification of data evaluation (see chapter 2.5.6) to resolve ExerV changes in the background noise resulting from plasma. Adjusted evaluation allowed estimation of the kinetics of few markers but most of the markers were below detection threshold though detectable in WB and MACSPlex (e.g. CD9, CD63, CD81, and CD41, fig. 3.19). This finding indicates that non-EV components in plasma might block the epitopes for EV-capture on the microarray device. Immuno-capture based removal of lipoproteins or plasma proteins from the samples prior to measurement in EV Array analysis might improve EV Array characterization of ExerVs. However, Mork et al. demonstrated that separation of apolipoprotein B from plasma samples via anti-apolipoprotein B coated beads was accompanied by loss of 21 % of the EV signal in EV Array analysis (Mork et al., 2017). Further improvements in the sample preparation and analysis are needed to increase the sensitivity of EV Array technology. This may finally enable the resolution of the longitudinal changes of markers associated with ExerVs also by EV Array technology.

In the MACSPlex assay, the advantage of analyzing multiple cellular proteins in a heterogeneous pool of EVs is accompanied by possible over- or under-representation of some of the included markers. The data obtained from semi-quantitative analysis enabled estimation of the ExerV releasing cell populations (see chapter 3.4.3). However, antibody competition during EV-isolation, -capture and -detection in the MACSPlex analyzing process may lead to a bias in enrichment of signals for EV carrying epitopes for rather strong antibodies. Likewise, excess of EVs originating from a certain cell type (which carry one specific marker) may cover the effect of rather underrepresented EV species. Koliha et al. introduced the principle of MACSPlex technology and specified that the kit is designed to minimize antibody competition but cannot be excluded (Koliha et al., 2016). In addition, the linear range of the detection system may hamper exact estimation of ExerV dynamics. For example, high signal intensities were measured for e.g. CD29, CD42a and HLA-DRDPDQ irrespective of exercise status while CD4 and CD14 mostly were only detectable at the post exercise level (fig. 3.22). It is possible that fold changes of specific markers measured at the upper or lower limit of detection are divergent when measured in the appropriate EV concentration. Conclusively,

analyses should be performed in dilution series to obtain more detailed information about ExerV kinetics. This was also suggested by Wiklander et al. who evaluated the MACSPlex approach for different sample materials in more detail (Wiklander et al., 2018). Taken together, MACSPlex marker analysis constitutes an easy and quick tool to provide profound knowledge on the origin of ExerVs. However, precise assay design including EV isolation, choice of capture- and detection-antibody as well as utilization of different sample dilutions is obligatory.

4.3.3 Optimization of high-purity ExerV preparation is essential for further downstream characterization

To specifically address putative functions of ExerVs, the estimation of ExerV cargo is crucial. However, to apply more sensitive downstream analyses of ExerVs, like proteomic analysis or RNA-seq, the purification strategy needs to be further improved. Exemplified for one subject, LC-MS proteomic characterization of SEC-EVs revealed a high contamination of plasma proteins and lipoproteins impairing the detection of EV-specific proteomic content (fig. 3.4). Since RNA species can also be associated to co-isolated non-EV components e.g. HDL (Vickers et al., 2011), RNA-seq is expected to be impaired likewise (Jeppesen et al., 2019). With the aim to increase the purity of ExerV samples, a combined purification approach as well as modification of IA capture was conducted and evaluated. Density gradient centrifugation following SEC enabled the detection of CD81 protein which was not detectable in LC-MS of SEC samples before (fig. 3.10). Though, the purity of EVs was still poor. Technical reasons cannot be excluded (see chapter 3.1.3) and repetition of the isolation approach with improved IDG fraction collection may lead to higher-purity EVs. A comparable purification strategy was recently described by Karimi et al. who combined EV enrichment on a density cushion with SEC (Karimi et al., 2018). This approach led to a reduction of excessive lipoprotein co-isolation and enabled detailed proteomic as well as RNA analysis of the obtained vesicle fractions. Also, Jeppesen et al. could markedly increase purity of small EVs by combining density gradient centrifugation with UC or IA capture (Jeppesen et al., 2019). Still, these combined isolation approaches are highly laborious and increased sample input is needed. However, this may not

be feasible for routine EV analysis. Alternatively, the use of immuno-captured EVs can result in sufficiently pure EVs from reduced sample material, if isolation antibodies as well as magnetic beads can be removed from the samples. The modification of the elution protocol of $CD63^{+}$ExerVs resulted in higher concentrated EV samples and CD81 as well as Syntenin were detectable in LC-MS (fig. 3.8). However, this approach also did not lead to separation of high plasma protein and lipoprotein background impairing EV proteome analysis. Further optimization of the isolation approach, like further washing steps and variation of the EV lysis buffer, may increase the purity of EVs. Taken together, as already discussed (see chapter 4.3.1), ExerV recovery from plasma needs further improvements in quality and feasibility, which will enable proper evaluation of proteomic and RNA cargo in future studies.

4.3.4 The comparison of different ExerV studies is limited

The described challenges highlight the difficulty to compare ExerV study results, which comprise a collection of multiple different EV isolation methods and characterization strategies. In the present literature on small EVs or exosome-called EVs in exercise settings, low-speed centrifugation (Whitham et al., 2018), UC (Chaturvedi et al., 2015; Frühbeis et al., 2015; Guescini et al., 2015), commercial precipitation (Bei et al., 2017; Bertoldi et al., 2018; Oliveira et al., 2018), SEC (Brahmer et al., 2019; Lovett et al., 2018), as well as acoustic trapping (Bryl-Gorecka et al., 2018) were used to study EVs from human, mouse and rat plasma or serum. Importantly, these studies consistently found an increasing amount of EVs during or after acute or chronic exercise interventions. However, especially the analysis of proteomic and nucleic acid content is highly critical since high purity of ExerV populations is not provided in the indicated studies. Furthermore, biodistribution and functional analysis of isolated ExerVs may be highly influenced by co-isolated bioactive material. Encouragingly, the field of extracellular vesicle research is developing rapidly, and improved purification and analysis methods may enable comparable parallel analysis of ExerVs in the future.

5 Conclusion and future perspectives

The results of the present study strongly indicate a contribution of EV release by platelets, leukocytes and endothelial cells to a heterogenous pool of ExerVs, in a load-response related fashion. This finding provides a profound basis to create working hypotheses to study the putative functions of ExerVs in immediate signaling processes like coagulation, immune signaling and angiogenesis. Further steps to perform this research include the optimization of the technical workflows, identification of the triggers of ExerV formation and finally the elucidation of the functional properties of ExerVs.

First, to overcome the methodical challenges in ExerV characterization, improved EV isolation strategies are necessary, which reduce co-isolation of non-EV material and results in high-purity ExerVs are necessary. These will provide a more detailed analysis of the proteomic, metabolomic and nucleic acid content in defined ExerV subpopulations. Furthermore, standardized EV-isolation and –characterization techniques are required, which enable high-throughput analysis of ExerVs in controlled trials. At the minute, the combination of density gradient centrifugation and size exclusion chromatography is one of the most promising approaches to get pure sample material. This laborious and time consuming workflow is not feasible for high throughput examinations. Magnetic bead isolations are relevant isolation technique enabling a straight forward and time saving isolation procedure. Additionally, antibody based capturing allows the isolation of highly specific EV subclasses. Imaging flow cytometry, which allows the analysis of ExerVs on a single EV level could be a promising approach for counting, characterization and isolation of EV populations in the future. Methodical refinements of the listed and future techniques will allow deeper research on ExerV formation and functions.

Secondly, to further study the nature of ExerV release, variations in the exercise setting, analysis of recovery time points, as well as the inclusion of different subject cohorts will be versatile. Implementation of interval training bouts, endurance and resistance exercise settings as well as several weeks of exercise intervention will address time- and load-responsiveness of ExerV release. Furthermore, different subject cohorts may reveal additional

information on differences in ExerV release, which was already recorded in this study regarding low- and high-responders. Relevant study designs may include the comparison of trained versus untrained persons, young versus old persons, and healthy persons versus patients suffering from diseases such as the autoimmune disease systemic lupus erythematosus or cardiovascular diseases. Variations in the amount and composition of ExerV populations will shed light on the triggers and mechanisms of ExerV formation and release.

Thirdly, the functions of ExerVs or certain ExerV subclasses can be assessed. Comparison of proteomic and nucleic acid analyses of ExerVs with EVs obtained at rest and after a recovery time allows the identification of ExerV cargo. This may support and further define the contribution of ExerVs to the suggested signaling pathways angiogenesis, coagulation and immune regulation. Subsequently, the validation of the putative functions of ExerVs and their possible involvement in long-term adaptation processes to regular physical exercise can be addressed. Experimental approaches will include cell culture models of EV release as well as uptake by and effects on different target cells, which are involved in endothelial function, coagulation processes and immune regulation. Further steps include the identification of target cells and tissues in biodistribution assays. Subsequently, the analysis of the functional effects of administered ExerVs can be studied *in vivo* in animal exercise models, e.g. involving obese or elderly mice. Animal knock-out models which interfere with EV formation, release and/or trafficking in certain cellular populations, e.g. endothelial cells or the lymphoid lineage, are needed to validate the discovered physiological properties.

Finally, these analyses will uncover a possible contribution of ExerVs to the maintenance of whole-body homeostasis after exercise stimuli, which leads to long-term adaptations, and may provide possibilities for their use in prevention, diagnostics and treatment of diseases.

6 References

Ahmadizad, S., El-Sayed, M. S., & MacLaren, D. P. (2010). Effects of time of day and acute resistance exercise on platelet activation and function. *Clin Hemorheol Microcirc, 45*(2-4), 391-399.

Antal-Szalmas, P., Strijp, J. A., Weersink, A. J., Verhoef, J., & Van Kessel, K. P. (1997). Quantitation of surface CD14 on human monocytes and neutrophils. *J Leukoc Biol, 61*(6), 721-728.

Arraud, N., Gounou, C., Turpin, D., & Brisson, A. R. (2016). Fluorescence triggering: A general strategy for enumerating and phenotyping extracellular vesicles by flow cytometry. *Cytometry A, 89*(2), 184-195.

Arraud, N., Linares, R., Tan, S., Gounou, C., Pasquet, J. M., Mornet, S., & Brisson, A. R. (2014). Extracellular vesicles from blood plasma: determination of their morphology, size, phenotype and concentration. *J Thromb Haemost, 12*(5), 614-627.

Baek, R., & Jorgensen, M. M. (2017). Multiplexed Phenotyping of Small Extracellular Vesicles Using Protein Microarray (EV Array). *Methods Mol Biol, 1545*, 117-127.

Baietti, M. F., Zhang, Z., Mortier, E., Melchior, A., Degeest, G., Geeraerts, A., . . . David, G. (2012). Syndecan-syntenin-ALIX regulates the biogenesis of exosomes. *Nat Cell Biol, 14*(7), 677-685.

Baj-Krzyworzeka, M., Majka, M., Pratico, D., Ratajczak, J., Vilaire, G., Kijowski, J., . . . Ratajczak, M. Z. (2002). Platelet-derived microparticles stimulate proliferation, survival, adhesion, and chemotaxis of hematopoietic cells. *Exp Hematol, 30*(5), 450-459.

Balusu, S., Van Wonterghem, E., De Rycke, R., Raemdonck, K., Stremersch, S., Gevaert, K., . . . Vandenbroucke, R. E. (2016). Identification of a novel mechanism of blood-brain communication during peripheral inflammation via choroid plexus-derived extracellular vesicles. *Embo Molecular Medicine, 8*(10), 1162-1183.

Bei, Y., Xu, T., Lv, D., Yu, P., Xu, J., Che, L., . . . Xiao, J. (2017). Exercise-induced circulating extracellular vesicles protect against cardiac ischemia-reperfusion injury. *Basic Res Cardiol, 112*(4), 38.

Beiter, T., Fragasso, A., Hudemann, J., Niess, A. M., & Simon, P. (2011). Short-term treadmill running as a model for studying cell-free DNA kinetics in vivo. *Clin Chem, 57*(4), 633-636.

Benatti, F. B., & Pedersen, B. K. (2015). Exercise as an anti-inflammatory therapy for rheumatic diseases-myokine regulation. *Nat Rev Rheumatol, 11*(2), 86-97.

Berckmans, R. J., Nieuwland, R., Boing, A. N., Romijn, F. P., Hack, C. E., & Sturk, A. (2001). Cell-derived microparticles circulate in healthy humans and support low grade thrombin generation. *Thromb Haemost, 85*(4), 639-646.

Bertoldi, K., Cechinel, L. R., Schallenberger, B., Corssac, G. B., Davies, S., Guerreiro, I. C. K., . . . Siqueira, I. R. (2018). Circulating extracellular vesicles in the aging process: impact of aerobic exercise. *Mol Cell Biochem, 440*(1-2), 115-125.

Bianco, F., Perrotta, C., Novellino, L., Francolini, M., Riganti, L., Menna, E., . . . Verderio, C. (2009). Acid sphingomyelinase activity triggers microparticle release from glial cells. *EMBO J, 28*(8), 1043-1054.

Biro, E., Sturk-Maquelin, K. N., Vogel, G. M., Meuleman, D. G., Smit, M. J., Hack, C. E., . . . Nieuwland, R. (2003). Human cell-derived microparticles promote thrombus formation in vivo in a tissue factor-dependent manner. *J Thromb Haemost, 1*(12), 2561-2568.

Blumenthal, J. A., Babyak, M. A., Doraiswamy, P. M., Watkins, L., Hoffman, B. M., Barbour, K. A., . . . Sherwood, A. (2007). Exercise and pharmacotherapy in the treatment of major depressive disorder. *Psychosom Med, 69*(7), 587-596.

Boilard, E., Duchez, A. C., & Brisson, A. (2015). The diversity of platelet microparticles. *Curr Opin Hematol, 22*(5), 437-444.

Boing, A. N., van der Pol, E., Grootemaat, A. E., Coumans, F. A., Sturk, A., & Nieuwland, R. (2014). Single-step isolation of extracellular vesicles by size-exclusion chromatography. *J Extracell Vesicles, 3*.

Borg, G. A. (1982). Psychophysical bases of perceived exertion. *Med Sci Sports Exerc, 14*(5), 377-381.

Börger, V., Bremer, M., Görgens, A., & Giebel, B. (2016). Mesenchymal stem/stromal cell-derived extracellular vesicles as a new approach in stem cell therapy. *ISBT Science Series, 11*(S1), 228-234.

Brahmer, A., Neuberger, E., Esch-Heisser, L., Haller, N., Moeller Joergensen, M., Baek, R., . . . Krämer-Albers, E. (2019). Platelets, endothelial cells and leukocytes contribute to the exercise-triggered release of extracellular vesicles into the circulation. *Journal of Extracellular Vesicles*.

Breitbach, S., Sterzing, B., Magallanes, C., Tug, S., & Simon, P. (2014). Direct measurement of cell-free DNA from serially collected capillary plasma during incremental exercise. *J Appl Physiol (1985), 117*(2), 119-130.

Breitbach, S., Tug, S., Helmig, S., Zahn, D., Kubiak, T., Michal, M., . . . Simon, P. (2014). Direct quantification of cell-free, circulating DNA from unpurified plasma. *PLoS One, 9*(3), e87838.

Breitbach, S., Tug, S., & Simon, P. (2012). Circulating cell-free DNA: an up-coming molecular marker in exercise physiology. *Sports Med, 42*(7), 565-586.

Brill, A., Dashevsky, O., Rivo, J., Gozal, Y., & Varon, D. (2005). Platelet-derived microparticles induce angiogenesis and stimulate post-ischemic revascularization. *Cardiovasc Res, 67*(1), 30-38.

Bryl-Gorecka, P., Sathanoori, R., Al-Mashat, M., Olde, B., Jogi, J., Evander, M., . . . Erlinge, D. (2018). Effect of exercise on the plasma vesicular proteome: a methodological study comparing acoustic trapping and centrifugation. *Lab Chip, 18*(20), 3101-3111.

Buschow, S. I., Nolte-'t Hoen, E. N., van Niel, G., Pols, M. S., ten Broeke, T., Lauwen, M., . . . Stoorvogel, W. (2009). MHC II in dendritic cells is targeted to lysosomes or T cell-induced exosomes via distinct multivesicular body pathways. *Traffic, 10*(10), 1528-1542.

Chaar, V., Romana, M., Tripette, J., Broquere, C., Huisse, M. G., Hue, O., . . . Connes, P. (2011). Effect of strenuous physical exercise on circulating cell-derived microparticles. *Clin Hemorheol Microcirc, 47*(1), 15-25.

Charrin, S., Jouannet, S., Boucheix, C., & Rubinstein, E. (2014). Tetraspanins at a glance. *J Cell Sci, 127*(Pt 17), 3641-3648.

Chaturvedi, P., Kalani, A., Medina, I., Familtseva, A., & Tyagi, S. C. (2015). Cardiosome mediated regulation of MMP9 in diabetic heart: role of mir29b and mir455 in exercise. *J Cell Mol Med, 19*(9), 2153-2161.

Chen, C. C., Liu, L. N., Ma, F. X., Wong, C. W., Guo, X. N. E., Chacko, J. V., . . . Zhao, W. A. (2016). Elucidation of Exosome Migration Across the Blood-Brain Barrier Model In Vitro. *Cellular and Molecular Bioengineering, 9*(4), 509-529.

Colombo, M., Raposo, G., & Thery, C. (2014). Biogenesis, secretion, and intercellular interactions of exosomes and other extracellular vesicles. *Annu Rev Cell Dev Biol, 30*, 255-289.

Conde-Vancells, J., Rodriguez-Suarez, E., Embade, N., Gil, D., Matthiesen, R., Valle, M., . . . Falcon-Perez, J. M. (2008). Characterization and comprehensive proteome profiling of exosomes secreted by hepatocytes. *J Proteome Res, 7*(12), 5157-5166.

de Rond, L., van der Pol, E., Hau, C. M., Varga, Z., Sturk, A., van Leeuwen, T. G., . . . Coumans, F. A. W. (2018). Comparison of Generic Fluorescent Markers for Detection of Extracellular Vesicles by Flow Cytometry. *Clin Chem, 64*(4), 680-689.

Del Conde, I., Shrimpton, C. N., Thiagarajan, P., & Lopez, J. A. (2005). Tissue-factor-bearing microvesicles arise from lipid rafts and fuse with activated platelets to initiate coagulation. *Blood, 106*(5), 1604-1611.

Deregibus, M. C., Cantaluppi, V., Calogero, R., Lo Iacono, M., Tetta, C., Biancone, L., . . . Camussi, G. (2007). Endothelial progenitor cell derived microvesicles activate an angiogenic program in endothelial cells by a horizontal transfer of mRNA. *Blood, 110*(7), 2440-2448.

Dickhuth, H. H., Yin, L., Niess, A., Rocker, K., Mayer, F., Heitkamp, H. C., & Horstmann, T. (1999). Ventilatory, lactate-derived and catecholamine thresholds during incremental treadmill running: relationship and reproducibility. *Int J Sports Med, 20*(2), 122-127.

Distler, U., Kuharev, J., Navarro, P., Levin, Y., Schild, H., & Tenzer, S. (2014). Drift time-specific collision energies enable deep-coverage data-independent acquisition proteomics. *Nat Methods, 11*(2), 167-170.

Dragovic, R. A., Gardiner, C., Brooks, A. S., Tannetta, D. S., Ferguson, D. J., Hole, P., . . . Sargent, I. L. (2011). Sizing and phenotyping of cellular vesicles using Nanoparticle Tracking Analysis. *Nanomedicine, 7*(6), 780-788.

Duclos, M., & Tabarin, A. (2016). Exercise and the Hypothalamo-Pituitary-Adrenal Axis. *Front Horm Res, 47*, 12-26.

Eirin, A., Zhu, X. Y., Puranik, A. S., Woollard, J. R., Tang, H., Dasari, S., . . . Lerman, L. O. (2016). Comparative proteomic analysis of extracellular vesicles isolated from porcine adipose tissue-derived mesenchymal stem/stromal cells. *Sci Rep, 6*, 36120.

el-Sayed, M. S. (1996). Effects of exercise on blood coagulation, fibrinolysis and platelet aggregation. *Sports Med, 22*(5), 282-298.

Elmore, S. (2007). Apoptosis: a review of programmed cell death. *Toxicol Pathol, 35*(4), 495-516.

Erdbrugger, U., & Lannigan, J. (2016). Analytical challenges of extracellular vesicle detection: A comparison of different techniques. *Cytometry A, 89*(2), 123-134.

Erdbrugger, U., Rudy, C. K., Etter, M. E., Dryden, K. A., Yeager, M., Klibanov, A. L., & Lannigan, J. (2014). Imaging flow cytometry elucidates limitations of microparticle analysis by conventional flow cytometry. *Cytometry A, 85*(9), 756-770.

Fais, S. (2013). NK cell-released exosomes: Natural nanobullets against tumors. *Oncoimmunology, 2*(1), e22337.
Faude, O., Kindermann, W., & Meyer, T. (2009). Lactate threshold concepts: how valid are they? *Sports Med, 39*(6), 469-490.
Frühbeis, C., Helmig, S., Tug, S., Simon, P., & Kramer-Albers, E. M. (2015). Physical exercise induces rapid release of small extracellular vesicles into the circulation. *J Extracell Vesicles, 4*, 28239.
Gardiner, C., Di Vizio, D., Sahoo, S., Thery, C., Witwer, K. W., Wauben, M., & Hill, A. F. (2016). Techniques used for the isolation and characterization of extracellular vesicles: results of a worldwide survey. *J Extracell Vesicles, 5*, 32945.
Gardiner, C., Ferreira, Y. J., Dragovic, R. A., Redman, C. W., & Sargent, I. L. (2013). Extracellular vesicle sizing and enumeration by nanoparticle tracking analysis. *J Extracell Vesicles, 2*.
Goni, F. M., & Alonso, A. (2009). Effects of ceramide and other simple sphingolipids on membrane lateral structure. *Biochim Biophys Acta, 1788*(1), 169-177.
Görgens, A., Bremer, M., Ferrer-Tur, R., Murke, F., Tertel, T., Horn, P. A., . . . Giebel, B. (2019). Optimisation of imaging flow cytometry for the analysis of single extracellular vesicles by using fluorescence-tagged vesicles as biological reference material. *J Extracell Vesicles, 8*(1), 1587567.
Greening, D. W., Xu, R., Ji, H., Tauro, B. J., & Simpson, R. J. (2015). A protocol for exosome isolation and characterization: evaluation of ultracentrifugation, density-gradient separation, and immunoaffinity capture methods. *Methods Mol Biol, 1295*, 179-209.
Gu, Z., Eils, R., & Schlesner, M. (2016). Complex heatmaps reveal patterns and correlations in multidimensional genomic data. *Bioinformatics, 32*(18), 2847-2849.
Guescini, M., Canonico, B., Lucertini, F., Maggio, S., Annibalini, G., Barbieri, E., . . . Stocchi, V. (2015). Muscle Releases Alpha-Sarcoglycan Positive Extracellular Vesicles Carrying miRNAs in the Bloodstream. *PLoS One, 10*(5), e0125094.
Haller, N., Helmig, S., Taenny, P., Petry, J., Schmidt, S., & Simon, P. (2018). Circulating, cell-free DNA as a marker for exercise load in intermittent sports. *PLoS One, 13*(1), e0191915.
Haller, N., Lorenz, S., Pfirrmann, D., Koch, C., Lieb, K., Dettweiler, U., . . . Jung, P. (2018). Individualized Web-Based Exercise for the Treatment of Depression: Randomized Controlled Trial. *JMIR Ment Health, 5*(4), e10698.
Hanson, P. I., & Cashikar, A. (2012). Multivesicular body morphogenesis. *Annu Rev Cell Dev Biol, 28*, 337-362.
He, F., Li, J., Liu, Z., Chuang, C. C., Yang, W., & Zuo, L. (2016). Redox Mechanism of Reactive Oxygen Species in Exercise. *Front Physiol, 7*, 486.
Heijnen, H. F., Schiel, A. E., Fijnheer, R., Geuze, H. J., & Sixma, J. J. (1999). Activated platelets release two types of membrane vesicles: microvesicles by surface shedding and exosomes derived from exocytosis of multivesicular bodies and alpha-granules. *Blood, 94*(11), 3791-3799.

Hergenreider, E., Heydt, S., Treguer, K., Boettger, T., Horrevoets, A. J., Zeiher, A. M., . . . Dimmeler, S. (2012). Atheroprotective communication between endothelial cells and smooth muscle cells through miRNAs. *Nat Cell Biol, 14*(3), 249-256.

Hojman, P. (2017). Exercise protects from cancer through regulation of immune function and inflammation. *Biochem Soc Trans, 45*(4), 905-911.

Howley, E. T., Bassett, D. R., Jr., & Welch, H. G. (1995). Criteria for maximal oxygen uptake: review and commentary. *Med Sci Sports Exerc, 27*(9), 1292-1301.

Hromada, C., Muhleder, S., Grillari, J., Redl, H., & Holnthoner, W. (2017). Endothelial Extracellular Vesicles-Promises and Challenges. *Front Physiol, 8*, 275.

Hu, M., & Lin, W. (2012). Effects of exercise training on red blood cell production: implications for anemia. *Acta Haematol, 127*(3), 156-164.

Ismail, N., Wang, Y., Dakhlallah, D., Moldovan, L., Agarwal, K., Batte, K., . . . Marsh, C. B. (2013). Macrophage microvesicles induce macrophage differentiation and miR-223 transfer. *Blood, 121*(6), 984-995.

Issekutz, B., Jr., & Rodahl, K. (1961). Respiratory quotient during exercise. *J Appl Physiol, 16*, 606-610.

Italiano, J. E., Jr., Richardson, J. L., Patel-Hett, S., Battinelli, E., Zaslavsky, A., Short, S., . . . Klement, G. L. (2008). Angiogenesis is regulated by a novel mechanism: pro- and antiangiogenic proteins are organized into separate platelet alpha granules and differentially released. *Blood, 111*(3), 1227-1233.

Jahn, R., & Scheller, R. H. (2006). SNAREs--engines for membrane fusion. *Nat Rev Mol Cell Biol, 7*(9), 631-643.

Jamaly, S., Ramberg, C., Olsen, R., Latysheva, N., Webster, P., Sovershaev, T., . . . Hansen, J. B. (2018). Impact of preanalytical conditions on plasma concentration and size distribution of extracellular vesicles using Nanoparticle Tracking Analysis. *Sci Rep, 8*(1), 17216.

Janowska-Wieczorek, A., Wysoczynski, M., Kijowski, J., Marquez-Curtis, L., Machalinski, B., Ratajczak, J., & Ratajczak, M. Z. (2005). Microvesicles derived from activated platelets induce metastasis and angiogenesis in lung cancer. *Int J Cancer, 113*(5), 752-760.

Jeppesen, D. K., Fenix, A. M., Franklin, J. L., Higginbotham, J. N., Zhang, Q., Zimmerman, L. J., . . . Coffey, R. J. (2019). Reassessment of Exosome Composition. *Cell, 177*(2), 428-445 e418.

Johnstone, R. M., Adam, M., Hammond, J. R., Orr, L., & Turbide, C. (1987). Vesicle formation during reticulocyte maturation. Association of plasma membrane activities with released vesicles (exosomes). *J Biol Chem, 262*(19), 9412-9420.

Jorgensen, M., Baek, R., Pedersen, S., Sondergaard, E. K., Kristensen, S. R., & Varming, K. (2013). Extracellular Vesicle (EV) Array: microarray capturing of exosomes and other extracellular vesicles for multiplexed phenotyping. *J Extracell Vesicles, 2*.

Kalani, A., Kamat, P. K., Chaturvedi, P., Tyagi, S. C., & Tyagi, N. (2014). Curcumin-primed exosomes mitigate endothelial cell dysfunction during hyperhomocysteinemia. *Life Sci, 107*(1-2), 1-7.

Karimi, N., Cvjetkovic, A., Jang, S. C., Crescitelli, R., Hosseinpour Feizi, M. A., Nieuwland, R., . . . Lasser, C. (2018). Detailed analysis of the plasma

extracellular vesicle proteome after separation from lipoproteins. *Cell Mol Life Sci, 75*(15), 2873-2886.
Karpman, D., Stahl, A. L., & Arvidsson, I. (2017). Extracellular vesicles in renal disease. *Nat Rev Nephrol, 13*(9), 545-562.
Kim, H. K., Song, K. S., Chung, J. H., Lee, K. R., & Lee, S. N. (2004). Platelet microparticles induce angiogenesis in vitro. *Br J Haematol, 124*(3), 376-384.
Kjaer, M. (1998). Adrenal medulla and exercise training. *Eur J Appl Physiol Occup Physiol, 77*(3), 195-199.
Koliha, N., Wiencek, Y., Heider, U., Jungst, C., Kladt, N., Krauthauser, S., . . . Wild, S. (2016). A novel multiplex bead-based platform highlights the diversity of extracellular vesicles. *J Extracell Vesicles, 5*, 29975.
Kowal, J., Arras, G., Colombo, M., Jouve, M., Morath, J. P., Primdal-Bengtson, B., . . . Thery, C. (2016). Proteomic comparison defines novel markers to characterize heterogeneous populations of extracellular vesicle subtypes. *Proc Natl Acad Sci U S A, 113*(8), E968-977.
Lacroix, R., Plawinski, L., Robert, S., Doeuvre, L., Sabatier, F., Martinez de Lizarrondo, S., . . . Dignat-George, F. (2012). Leukocyte- and endothelial-derived microparticles: a circulating source for fibrinolysis. *Haematologica, 97*(12), 1864-1872.
Lannigan, J., & Erdbruegger, U. (2017). Imaging flow cytometry for the characterization of extracellular vesicles. *Methods, 112*, 55-67.
Lansford, K. A., Shill, D. D., Dicks, A. B., Marshburn, M. P., Southern, W. M., & Jenkins, N. T. (2016). Effect of acute exercise on circulating angiogenic cell and microparticle populations. *Exp Physiol, 101*(1), 155-167.
Lee, K., Shao, H., Weissleder, R., & Lee, H. (2015). Acoustic purification of extracellular microvesicles. *ACS Nano, 9*(3), 2321-2327.
Li, P., Kaslan, M., Lee, S. H., Yao, J., & Gao, Z. (2017). Progress in Exosome Isolation Techniques. *Theranostics, 7*(3), 789-804.
Linares, R., Tan, S., Gounou, C., Arraud, N., & Brisson, A. R. (2015). High-speed centrifugation induces aggregation of extracellular vesicles. *J Extracell Vesicles, 4*, 29509.
Lindoso, R. S., Collino, F., Bruno, S., Araujo, D. S., Sant'Anna, J. F., Tetta, C., . . . Camussi, G. (2014). Extracellular vesicles released from mesenchymal stromal cells modulate miRNA in renal tubular cells and inhibit ATP depletion injury. *Stem Cells Dev, 23*(15), 1809-1819.
Lobb, R. J., Becker, M., Wen, S. W., Wong, C. S., Wiegmans, A. P., Leimgruber, A., & Moller, A. (2015). Optimized exosome isolation protocol for cell culture supernatant and human plasma. *J Extracell Vesicles, 4*, 27031.
Lourenco, M. V., Frozza, R. L., de Freitas, G. B., Zhang, H., Kincheski, G. C., Ribeiro, F. C., . . . De Felice, F. G. (2019). Exercise-linked FNDC5/irisin rescues synaptic plasticity and memory defects in Alzheimer's models. *Nat Med, 25*(1), 165-175.
Lovett, J. A. C., Durcan, P. J., & Myburgh, K. H. (2018). Investigation of Circulating Extracellular Vesicle MicroRNA Following Two Consecutive Bouts of Muscle-Damaging Exercise. *Front Physiol, 9*, 1149.
Lozano-Andres, E., Libregts, S. F., Toribio, V., Royo, F., Morales, S., Lopez-Martin, S., . . . Yanez-Mo, M. (2019). Tetraspanin-decorated

extracellular vesicle-mimetics as a novel adaptable reference material. *J Extracell Vesicles, 8*(1), 1573052.

Lozzio, B. B., & Lozzio, C. B. (1979). Properties and usefulness of the original K-562 human myelogenous leukemia cell line. *Leuk Res, 3*(6), 363-370.

Lozzio, B. B., Lozzio, C. B., Bamberger, E. G., & Feliu, A. S. (1981). A Multipotential Leukemia Cell Line (K-562) of Human Origin. *Experimental Biology and Medicine, 166*(4), 546-550.

Lugini, L., Cecchetti, S., Huber, V., Luciani, F., Macchia, G., Spadaro, F., . . . Fais, S. (2012). Immune surveillance properties of human NK cell-derived exosomes. *J Immunol, 189*(6), 2833-2842.

Mader, A., & Heck, H. (1986). A theory of the metabolic origin of "anaerobic threshold". *Int J Sports Med, 7 Suppl 1*, 45-65.

Mathieu, M., Martin-Jaular, L., Lavieu, G., & Thery, C. (2019). Specificities of secretion and uptake of exosomes and other extracellular vesicles for cell-to-cell communication. *Nat Cell Biol, 21*(1), 9-17.

Mause, S. F., von Hundelshausen, P., Zernecke, A., Koenen, R. R., & Weber, C. (2005). Platelet microparticles: a transcellular delivery system for RANTES promoting monocyte recruitment on endothelium. *Arterioscler Thromb Vasc Biol, 25*(7), 1512-1518.

McConnell, R. E., Higginbotham, J. N., Shifrin, D. A., Jr., Tabb, D. L., Coffey, R. J., & Tyska, M. J. (2009). The enterocyte microvillus is a vesicle-generating organelle. *J Cell Biol, 185*(7), 1285-1298.

Melki, I., Tessandier, N., Zufferey, A., & Boilard, E. (2017). Platelet microvesicles in health and disease. *Platelets, 28*(3), 214-221.

Mesri, M., & Altieri, D. C. (1999). Leukocyte microparticles stimulate endothelial cell cytokine release and tissue factor induction in a JNK1 signaling pathway. *J Biol Chem, 274*(33), 23111-23118.

Miyazaki, Y., Nomura, S., Miyake, T., Kagawa, H., Kitada, C., Taniguchi, H., . . . Fukuhara, S. (1996). High shear stress can initiate both platelet aggregation and shedding of procoagulant containing microparticles. *Blood, 88*(9), 3456-3464.

Möbius-Winkler, S., Hilberg, T., Menzel, K., Golla, E., Burman, A., Schuler, G., & Adams, V. (2009). Time-dependent mobilization of circulating progenitor cells during strenuous exercise in healthy individuals. *J Appl Physiol (1985), 107*(6), 1943-1950.

Monguio-Tortajada, M., Galvez-Monton, C., Bayes-Genis, A., Roura, S., & Borras, F. E. (2019). Extracellular vesicle isolation methods: rising impact of size-exclusion chromatography. *Cell Mol Life Sci, 76*(12), 2369-2382.

Morales-Prieto, D. M., Stojiljkovic, M., Diezel, C., Streicher, P. E., Fraziska Roestel, F., Lindner, J., . . . Marz, M. (2018). Peripheral blood exosomes pass blood-brain-barrier and induce glial cell activation. *bioRXiv [Epub ahead of print]*.

Morelli, A. E., Larregina, A. T., Shufesky, W. J., Sullivan, M. L., Stolz, D. B., Papworth, G. D., . . . Thomson, A. W. (2004). Endocytosis, intracellular sorting, and processing of exosomes by dendritic cells. *Blood, 104*(10), 3257-3266.

Mork, M., Handberg, A., Pedersen, S., Jorgensen, M. M., Baek, R., Nielsen, M. K., & Kristensen, S. R. (2017). Prospects and limitations of antibody-mediated clearing of lipoproteins from blood plasma prior to

nanoparticle tracking analysis of extracellular vesicles. *J Extracell Vesicles, 6*(1), 1308779.
Mostefai, H. A., Andriantsitohaina, R., & Martinez, M. C. (2008). Plasma membrane microparticles in angiogenesis: role in ischemic diseases and in cancer. *Physiol Res, 57*(3), 311-320.
Nakai, W., Yoshida, T., Diez, D., Miyatake, Y., Nishibu, T., Imawaka, N., . . . Hanayama, R. (2016). A novel affinity-based method for the isolation of highly purified extracellular vesicles. *Sci Rep, 6*, 33935.
Nielsen, H. G., Oktedalen, O., Opstad, P. K., & Lyberg, T. (2016). Plasma Cytokine Profiles in Long-Term Strenuous Exercise. *J Sports Med (Hindawi Publ Corp), 2016*, 7186137.
Oliveira, G. P., Jr., Porto, W. F., Palu, C. C., Pereira, L. M., Petriz, B., Almeida, J. A., . . . Pereira, R. W. (2018). Effects of Acute Aerobic Exercise on Rats Serum Extracellular Vesicles Diameter, Concentration and Small RNAs Content. *Front Physiol, 9*, 532.
Onodi, Z., Pelyhe, C., Terezia Nagy, C., Brenner, G. B., Almasi, L., Kittel, A., . . . Giricz, Z. (2018). Isolation of High-Purity Extracellular Vesicles by the Combination of Iodixanol Density Gradient Ultracentrifugation and Bind-Elute Chromatography From Blood Plasma. *Front Physiol, 9*, 1479.
Paillard, T., Rolland, Y., & de Souto Barreto, P. (2015). Protective Effects of Physical Exercise in Alzheimer's Disease and Parkinson's Disease: A Narrative Review. *J Clin Neurol, 11*(3), 212-219.
Pedersen, B. K., & Febbraio, M. A. (2008). Muscle as an endocrine organ: focus on muscle-derived interleukin-6. *Physiol Rev, 88*(4), 1379-1406.
Pedersen, B. K., & Febbraio, M. A. (2012). Muscles, exercise and obesity: skeletal muscle as a secretory organ. *Nature Reviews Endocrinology, 8*(8), 457-465.
Pedersen, B. K., & Hoffman-Goetz, L. (2000). Exercise and the immune system: regulation, integration, and adaptation. *Physiol Rev, 80*(3), 1055-1081.
Petersen, A. M., & Pedersen, B. K. (2005). The anti-inflammatory effect of exercise. *J Appl Physiol (1985), 98*(4), 1154-1162.
Piccin, A., Murphy, W. G., & Smith, O. P. (2007). Circulating microparticles: pathophysiology and clinical implications. *Blood Rev, 21*(3), 157-171.
Piccirillo, R. (2019). Exercise-Induced Myokines With Therapeutic Potential for Muscle Wasting. *Front Physiol, 10*, 287.
Pitsavos, C., Panagiotakos, D., Weinem, M., & Stefanadis, C. (2006). Diet, exercise and the metabolic syndrome. *Rev Diabet Stud, 3*(3), 118-126.
Powers, S. K., Ji, L. L., Kavazis, A. N., & Jackson, M. J. (2011). Reactive oxygen species: impact on skeletal muscle. *Compr Physiol, 1*(2), 941-969.
Qu, M., Lin, Q., Huang, L., Fu, Y., Wang, L., He, S., . . . Sun, X. (2018). Dopamine-loaded blood exosomes targeted to brain for better treatment of Parkinson's disease. *Journal of Controlled Release, 287*, 156-166.
Qu, M. K., Lin, Q., Huang, L. Y., Fu, Y., Wang, L. Y., He, S. S., . . . Sun, X. (2018). Dopamine-loaded blood exosomes targeted to brain for better treatment of Parkinson's disease. *Journal of Controlled Release, 287*, 156-166.
Rakobowchuk, M., Ritter, O., Wilhelm, E. N., Isacco, L., Bouhaddi, M., Degano, B., . . . Mourot, L. (2017). Divergent endothelial function but similar platelet microvesicle responses following eccentric and concentric

cycling at a similar aerobic power output. *J Appl Physiol (1985), 122*(4), 1031-1039.

Rand, M. L., Wang, H., Bang, K. W., Packham, M. A., & Freedman, J. (2006). Rapid clearance of procoagulant platelet-derived microparticles from the circulation of rabbits. *J Thromb Haemost, 4*(7), 1621-1623.

Raposo, G., & Stoorvogel, W. (2013). Extracellular vesicles: exosomes, microvesicles, and friends. *J Cell Biol, 200*(4), 373-383.

Reininger, A. J., Heijnen, H. F., Schumann, H., Specht, H. M., Schramm, W., & Ruggeri, Z. M. (2006). Mechanism of platelet adhesion to von Willebrand factor and microparticle formation under high shear stress. *Blood, 107*(9), 3537-3545.

Rezeli, M., Gidlof, O., Evander, M., Bryl-Gorecka, P., Sathanoori, R., Gilje, P., . . . Laurell, T. (2016). Comparative Proteomic Analysis of Extracellular Vesicles Isolated by Acoustic Trapping or Differential Centrifugation. *Anal Chem, 88*(17), 8577-8586.

Ridder, K., Keller, S., Dams, M., Rupp, A. K., Schlaudraff, J., Del Turco, D., . . . Momma, S. (2014). Extracellular vesicle-mediated transfer of genetic information between the hematopoietic system and the brain in response to inflammation. *Journal of Neuroimmunology, 275*(1-2), 165-165.

Rizzo, V., McIntosh, D. P., Oh, P., & Schnitzer, J. E. (1998). In situ flow activates endothelial nitric oxide synthase in luminal caveolae of endothelium with rapid caveolin dissociation and calmodulin association. *J Biol Chem, 273*(52), 34724-34729.

Robbins, P. D., & Morelli, A. E. (2014). Regulation of immune responses by extracellular vesicles. *Nat Rev Immunol, 14*(3), 195-208.

Roecker, K., Striegel, H., & Dickhuth, H. H. (2003). Heart-rate recommendations: transfer between running and cycling exercise? *Int J Sports Med, 24*(3), 173-178.

Safdar, A., & Tarnopolsky, M. A. (2018). Exosomes as Mediators of the Systemic Adaptations to Endurance Exercise. *Cold Spring Harb Perspect Med, 8*(3).

Salomon, C., Ryan, J., Sobrevia, L., Kobayashi, M., Ashman, K., Mitchell, M., & Rice, G. E. (2013). Exosomal signaling during hypoxia mediates microvascular endothelial cell migration and vasculogenesis. *PLoS One, 8*(7), e68451.

Sapolsky, R. M., Romero, L. M., & Munck, A. U. (2000). How do glucocorticoids influence stress responses? Integrating permissive, suppressive, stimulatory, and preparative actions. *Endocr Rev, 21*(1), 55-89.

Schmidt, K. N., Gosselin, L. E., & Stanley, W. C. (1992). Endurance exercise training causes adrenal medullary hypertrophy in young and old Fischer 344 rats. *Horm Metab Res, 24*(11), 511-515.

Schwarz, V., Dusing, P., Liman, T., Werner, C., Herm, J., Bachelier, K., . . . Laufs, U. (2018). Marathon running increases circulating endothelial- and thrombocyte-derived microparticles. *Eur J Prev Cardiol, 25*(3), 317-324.

Sheldon, H., Heikamp, E., Turley, H., Dragovic, R., Thomas, P., Oon, C. E., . . . Harris, A. L. (2010). New mechanism for Notch signaling to endothelium at a distance by Delta-like 4 incorporation into exosomes. *Blood, 116*(13), 2385-2394.

Shet, A. S., Aras, O., Gupta, K., Hass, M. J., Rausch, D. J., Saba, N., . . . Hebbel, R. P. (2003). Sickle blood contains tissue factor-positive microparticles derived from endothelial cells and monocytes. *Blood, 102*(7), 2678-2683.

Shill, D. D., Lansford, K. A., Hempel, H. K., Call, J. A., Murrow, J. R., & Jenkins, N. T. (2018). Effect of exercise intensity on circulating microparticles in men and women. *Exp Physiol, 103*(5), 693-700.

Sielaff, M., Kuharev, J., Bohn, T., Hahlbrock, J., Bopp, T., Tenzer, S., & Distler, U. (2017). Evaluation of FASP, SP3, and iST Protocols for Proteomic Sample Preparation in the Low Microgram Range. *J Proteome Res, 16*(11), 4060-4072.

Simonsen, J. B. (2017). What Are We Looking At? Extracellular Vesicles, Lipoproteins, or Both? *Circ Res, 121*(8), 920-922.

Sitar, S., Kejzar, A., Pahovnik, D., Kogej, K., Tusek-Znidaric, M., Lenassi, M., & Zagar, E. (2015). Size characterization and quantification of exosomes by asymmetrical-flow field-flow fractionation. *Anal Chem, 87*(18), 9225-9233.

Skog, J., Wurdinger, T., van Rijn, S., Meijer, D. H., Gainche, L., Sena-Esteves, M., . . . Breakefield, X. O. (2008). Glioblastoma microvesicles transport RNA and proteins that promote tumour growth and provide diagnostic biomarkers. *Nat Cell Biol, 10*(12), 1470-1476.

Sodar, B. W., Kittel, A., Paloczi, K., Vukman, K. V., Osteikoetxea, X., Szabo-Taylor, K., . . . Buzas, E. I. (2016). Low-density lipoprotein mimics blood plasma-derived exosomes and microvesicles during isolation and detection. *Sci Rep, 6*, 24316.

Sossdorf, M., Otto, G. P., Claus, R. A., Gabriel, H. H., & Losche, W. (2011). Cell-derived microparticles promote coagulation after moderate exercise. *Med Sci Sports Exerc, 43*(7), 1169-1176.

Steensberg, A., Fischer, C. P., Keller, C., Moller, K., & Pedersen, B. K. (2003). IL-6 enhances plasma IL-1ra, IL-10, and cortisol in humans. *Am J Physiol Endocrinol Metab, 285*(2), E433-437.

Stegmann, H., Kindermann, W., & Schnabel, A. (1981). Lactate kinetics and individual anaerobic threshold. *Int J Sports Med, 2*(3), 160-165.

Stenmark, H. (2009). Rab GTPases as coordinators of vesicle traffic. *Nat Rev Mol Cell Biol, 10*(8), 513-525.

Steppich, B., Mattisek, C., Sobczyk, D., Kastrati, A., Schomig, A., & Ott, I. (2005). Tissue factor pathway inhibitor on circulating microparticles in acute myocardial infarction. *Thromb Haemost, 93*(1), 35-39.

Sun, M., Lanctot, K., Herrmann, N., & Gallagher, D. (2018). Exercise for Cognitive Symptoms in Depression: A Systematic Review of Interventional Studies. *Can J Psychiatry, 63*(2), 115-128.

Svedahl, K., & MacIntosh, B. R. (2003). Anaerobic threshold: the concept and methods of measurement. *Can J Appl Physiol, 28*(2), 299-323.

Takahashi, Y., Nishikawa, M., Shinotsuka, H., Matsui, Y., Ohara, S., Imai, T., & Takakura, Y. (2013). Visualization and in vivo tracking of the exosomes of murine melanoma B16-BL6 cells in mice after intravenous injection. *J Biotechnol, 165*(2), 77-84.

Tans, G., Rosing, J., Thomassen, M. C., Heeb, M. J., Zwaal, R. F., & Griffin, J. H. (1991). Comparison of anticoagulant and procoagulant activities of stimulated platelets and platelet-derived microparticles. *Blood, 77*(12), 2641-2648.

Taraboletti, G., D'Ascenzo, S., Borsotti, P., Giavazzi, R., Pavan, A., & Dolo, V. (2002). Shedding of the matrix metalloproteinases MMP-2, MMP-9, and MT1-MMP as membrane vesicle-associated components by endothelial cells. *Am J Pathol, 160*(2), 673-680.

Taylor, H. L., Buskirk, E., & Henschel, A. (1955). Maximal oxygen intake as an objective measure of cardio-respiratory performance. *J Appl Physiol, 8*(1), 73-80.

Thery, C., Ostrowski, M., & Segura, E. (2009). Membrane vesicles as conveyors of immune responses. *Nat Rev Immunol, 9*(8), 581-593.

Thery, C., Witwer, K. W., Aikawa, E., Alcaraz, M. J., Anderson, J. D., Andriantsitohaina, R., . . . Zuba-Surma, E. K. (2018). Minimal information for studies of extracellular vesicles 2018 (MISEV2018): a position statement of the International Society for Extracellular Vesicles and update of the MISEV2014 guidelines. *J Extracell Vesicles, 7*(1), 1535750.

Tkach, M., Kowal, J., Zucchetti, A. E., Enserink, L., Jouve, M., Lankar, D., . . . Thery, C. (2017). Qualitative differences in T-cell activation by dendritic cell-derived extracellular vesicle subtypes. *EMBO J, 36*(20), 3012-3028.

Trajkovic, K., Hsu, C., Chiantia, S., Rajendran, L., Wenzel, D., Wieland, F., . . . Simons, M. (2008). Ceramide triggers budding of exosome vesicles into multivesicular endosomes. *Science, 319*(5867), 1244-1247.

Tripisciano, C., Weiss, R., Eichhorn, T., Spittler, A., Heuser, T., Fischer, M. B., & Weber, V. (2017). Different Potential of Extracellular Vesicles to Support Thrombin Generation: Contributions of Phosphatidylserine, Tissue Factor, and Cellular Origin. *Sci Rep, 7*(1), 6522.

Tsatsoulis, A., & Fountoulakis, S. (2006). The protective role of exercise on stress system dysregulation and comorbidities. *Ann N Y Acad Sci, 1083*, 196-213.

Tsuchiya, S., Kobayashi, Y., Goto, Y., Okumura, H., Nakae, S., Konno, T., & Tada, K. (1982). Induction of maturation in cultured human monocytic leukemia cells by a phorbol diester. *Cancer Res, 42*(4), 1530-1536.

Tsuchiya, S., Yamabe, M., Yamaguchi, Y., Kobayashi, Y., Konno, T., & Tada, K. (1980). Establishment and characterization of a human acute monocytic leukemia cell line (THP-1). *Int J Cancer, 26*(2), 171-176.

Tug, S., Mehdorn, M., Helmig, S., Breitbach, S., Ehlert, T., & Simon, P. (2017). Exploring the Potential of Cell-Free-DNA Measurements After an Exhaustive Cycle-Ergometer Test as a Marker for Performance-Related Parameters. *Int J Sports Physiol Perform, 12*(5), 597-604.

Vajen, T., Benedikter, B. J., Heinzmann, A. C. A., Vasina, E. M., Henskens, Y., Parsons, M., . . . Koenen, R. R. (2017). Platelet extracellular vesicles induce a pro-inflammatory smooth muscle cell phenotype. *J Extracell Vesicles, 6*(1), 1322454.

Valkonen, S., van der Pol, E., Boing, A., Yuana, Y., Yliperttula, M., Nieuwland, R., . . . Siljander, P. R. (2017). Biological reference materials for extracellular vesicle studies. *European Journal of Pharmaceutical Sciences, 98*, 4-16.

van der Pol, E., Boing, A. N., Harrison, P., Sturk, A., & Nieuwland, R. (2012). Classification, functions, and clinical relevance of extracellular vesicles. *Pharmacol Rev, 64*(3), 676-705.

van der Pol, E., Coumans, F. A., Grootemaat, A. E., Gardiner, C., Sargent, I. L., Harrison, P., . . . Nieuwland, R. (2014). Particle size distribution of exosomes and microvesicles determined by transmission electron microscopy, flow cytometry, nanoparticle tracking analysis, and resistive pulse sensing. *J Thromb Haemost, 12*(7), 1182-1192.

Van Deun, J., Mestdagh, P., Agostinis, P., Akay, O., Anand, S., Anckaert, J., . . . Hendrix, A. (2017). EV-TRACK: transparent reporting and centralizing knowledge in extracellular vesicle research. *Nat Methods, 14*(3), 228-232.

Van Deun, J., Mestdagh, P., Sormunen, R., Cocquyt, V., Vermaelen, K., Vandesompele, J., . . . Hendrix, A. (2014). The impact of disparate isolation methods for extracellular vesicles on downstream RNA profiling. *J Extracell Vesicles, 3*.

van Niel, G., Charrin, S., Simoes, S., Romao, M., Rochin, L., Saftig, P., . . . Raposo, G. (2011). The tetraspanin CD63 regulates ESCRT-independent and -dependent endosomal sorting during melanogenesis. *Dev Cell, 21*(4), 708-721.

van Niel, G., D'Angelo, G., & Raposo, G. (2018). Shedding light on the cell biology of extracellular vesicles. *Nat Rev Mol Cell Biol, 19*(4), 213-228.

van Praag, H. (2008). Neurogenesis and exercise: past and future directions. *Neuromolecular Med, 10*(2), 128-140.

Vanhoutte, P. M., Shimokawa, H., Feletou, M., & Tang, E. H. (2017). Endothelial dysfunction and vascular disease - a 30th anniversary update. *Acta Physiol (Oxf), 219*(1), 22-96.

Vergauwen, G., Dhondt, B., Van Deun, J., De Smedt, E., Berx, G., Timmerman, E., . . . Hendrix, A. (2017). Confounding factors of ultrafiltration and protein analysis in extracellular vesicle research. *Sci Rep, 7*(1), 2704.

Vickers, K. C., Palmisano, B. T., Shoucri, B. M., Shamburek, R. D., & Remaley, A. T. (2011). MicroRNAs are transported in plasma and delivered to recipient cells by high-density lipoproteins. *Nat Cell Biol, 13*(4), 423-433.

Walsh, N. P., Gleeson, M., Shephard, R. J., Gleeson, M., Woods, J. A., Bishop, N. C., . . . Simon, P. (2011). Position statement. Part one: Immune function and exercise. *Exerc Immunol Rev, 17*, 6-63.

Warburton, D. E., Nicol, C. W., & Bredin, S. S. (2006). Health benefits of physical activity: the evidence. *CMAJ, 174*(6), 801-809.

Wasserman, K., Whipp, B. J., Koyl, S. N., & Beaver, W. L. (1973). Anaerobic threshold and respiratory gas exchange during exercise. *J Appl Physiol, 35*(2), 236-243.

Welton, J. L., Webber, J. P., Botos, L. A., Jones, M., & Clayton, A. (2015). Ready-made chromatography columns for extracellular vesicle isolation from plasma. *J Extracell Vesicles, 4*, 27269.

Whitham, M., Parker, B. L., Friedrichsen, M., Hingst, J. R., Hjorth, M., Hughes, W. E., . . . Febbraio, M. A. (2018). Extracellular Vesicles Provide a Means for Tissue Crosstalk during Exercise. *Cell Metab, 27*(1), 237-251 e234.

Wiklander, O. P. B., Bostancioglu, R. B., Welsh, J. A., Zickler, A. M., Murke, F., Corso, G., . . . Gorgens, A. (2018). Systematic Methodological Evaluation of a Multiplex Bead-Based Flow Cytometry Assay for

Detection of Extracellular Vesicle Surface Signatures. *Front Immunol, 9*, 1326.

Wilhelm, E. N., Gonzalez-Alonso, J., Parris, C., & Rakobowchuk, M. (2016). Exercise intensity modulates the appearance of circulating microvesicles with proangiogenic potential upon endothelial cells. *Am J Physiol Heart Circ Physiol, 311*(5), H1297-H1310.

Wilhelm, E. N., Mourot, L., & Rakobowchuk, M. (2018). Exercise-Derived Microvesicles: A Review of the Literature. *Sports Med, 48*(9), 2025-2039.

Willekens, F. L., Werre, J. M., Kruijt, J. K., Roerdinkholder-Stoelwinder, B., Groenen-Dopp, Y. A., van den Bos, A. G., . . . van Berkel, T. J. (2005). Liver Kupffer cells rapidly remove red blood cell-derived vesicles from the circulation by scavenger receptors. *Blood, 105*(5), 2141-2145.

Wolf, P. (1967). Nature and Significance of Platelet Products in Human Plasma. *Br J Haematol, 13*(3), 269-+.

Womack, C. J., Nagelkirk, P. R., & Coughlin, A. M. (2003). Exercise-induced changes in coagulation and fibrinolysis in healthy populations and patients with cardiovascular disease. *Sports Med, 33*(11), 795-807.

Woodman, C. R., Price, E. M., & Laughlin, M. H. (2005). Shear stress induces eNOS mRNA expression and improves endothelium-dependent dilation in senescent soleus muscle feed arteries. *J Appl Physiol (1985), 98*(3), 940-946.

Yanez-Mo, M., Siljander, P. R., Andreu, Z., Zavec, A. B., Borras, F. E., Buzas, E. I., . . . De Wever, O. (2015). Biological properties of extracellular vesicles and their physiological functions. *J Extracell Vesicles, 4*, 27066.

Yang, C., Mwaikambo, B. R., Zhu, T., Gagnon, C., Lafleur, J., Seshadri, S., . . . Hardy, P. (2008). Lymphocytic microparticles inhibit angiogenesis by stimulating oxidative stress and negatively regulating VEGF-induced pathways. *Am J Physiol Regul Integr Comp Physiol, 294*(2), R467-476.

Yang, T., Martin, P., Fogarty, B., Brown, A., Schurman, K., Phipps, R., . . . Bai, S. (2015). Exosome delivered anticancer drugs across the blood-brain barrier for brain cancer therapy in Danio rerio. *Pharm Res, 32*(6), 2003-2014.

Zierath, J. R., & Wallberg-Henriksson, H. (2015). Looking Ahead Perspective: Where Will the Future of Exercise Biology Take Us? *Cell Metab, 22*(1), 25-30.

Zouhal, H., Jacob, C., Delamarche, P., & Gratas-Delamarche, A. (2008). Catecholamines and the effects of exercise, training and gender. *Sports Med, 38*(5), 401-423.

7 Appendix

7.1 Supplementary data

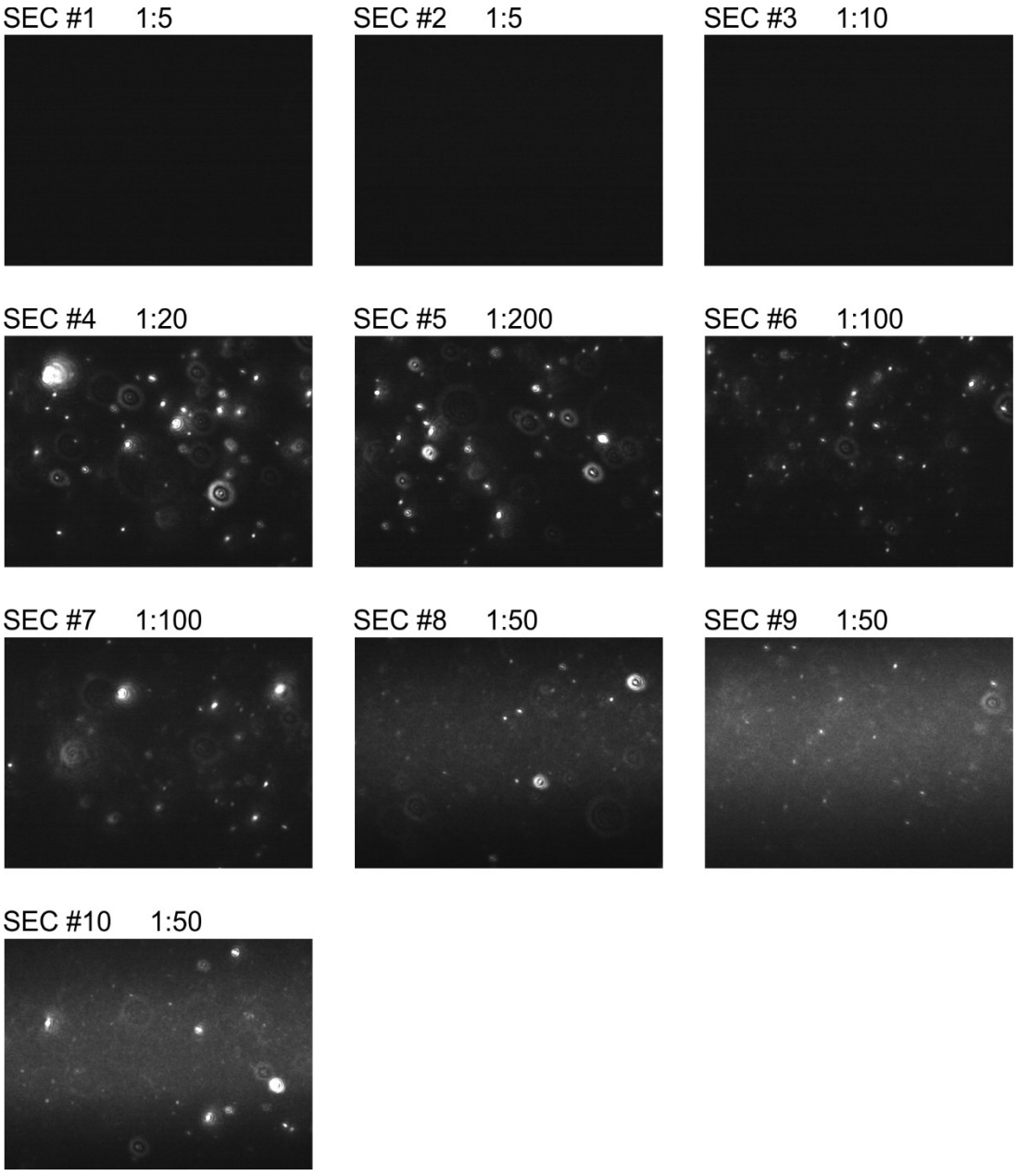

Figure S1: Nanoparticle tracking analysis of single SEC fractions. Screenshots taken from the videos of the NTA measurements of individual SEC fractions number (#)1 to 10 of separated plasma samples. Individual sample dilution is PBS is indicated.

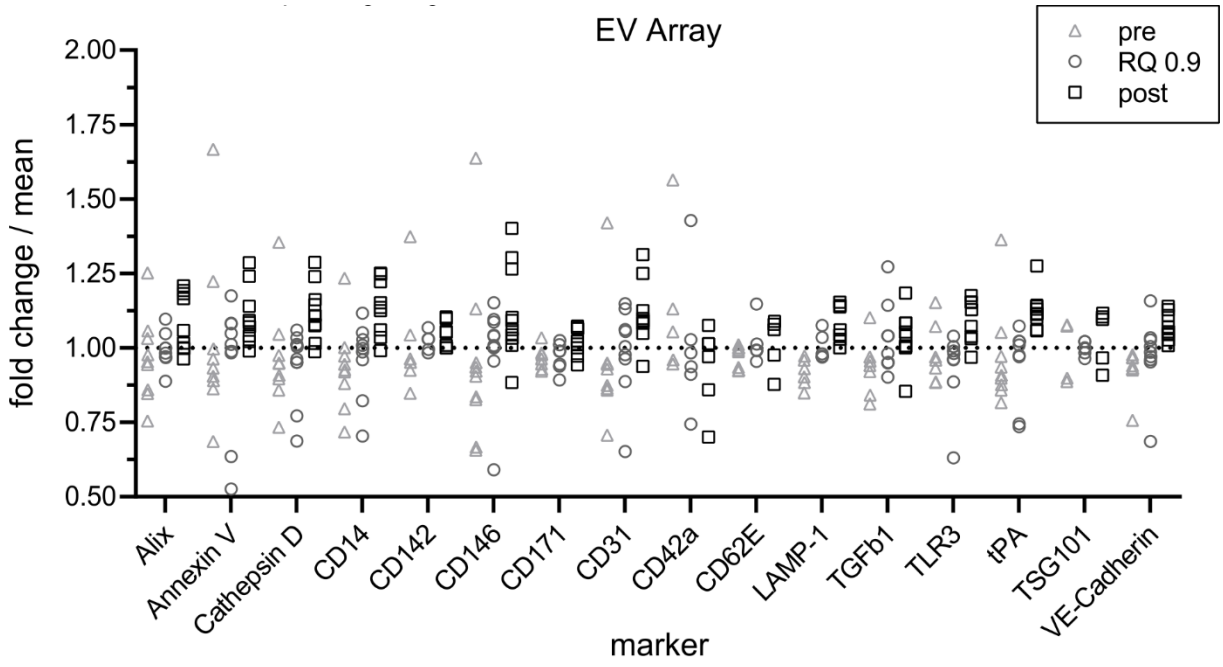

Figure S2: Individual data of EV Array marker profiles – values corresponding to fig. 3.19 a

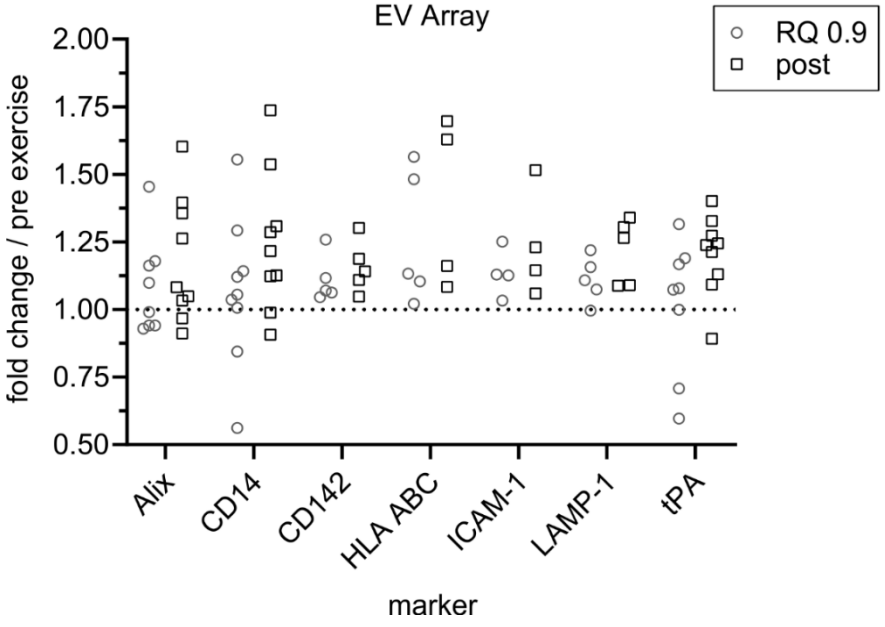

Figure S3: Individual data of significantly elevated markers in EV Array analysis – values corresponding to fig. 3.19 b

Table S1: Accumulation of EV data from multiple characterization approaches involving 21 subjects.

	unpurified EVs		CD9⁺EVs		CD63⁺EVs		CD81⁺EVs		SEC-EVs			
S*	*EV Array*	*IF*	*WB*	*MPlx*	*WB*	*MPlx*	*WB*	*MPlx*	*IF*	*NTA*	*WB*	*MPlx*
1	X	X							X			
2	X	X										
3	X		X	X	X	X	X	X				
4	X									X	X	X
5	X									X	X	X
6	X									X	X	
7	X									X	X	
8	X											
9	X									X	X	
10	X									X	X	
13			X	X	X	X	X	X				
14							X	X			X	X
15					X	X	X	X			X	X
16							X	X			X	X
17							X	X		X	X	X
18											X	X
19					X	X						X
21						X		X				
22			X	X	X	X	X	X				
23			X	X	X	X	X	X				
24				X								X
∑	10	2	4	5	6	7	8	9	1	7	11	9

IF Imaging flow cytometry, *MPlx* MACSPlex, *WB* western blotting, *NTA* nanoparticle tracking analysis; *The blood of S11, S12, and S20 was not used for the analysis of EVs in the scope of this thesis. Numbering is consistent to prevent misunderstanding.

Table S2: Statistical analysis of EV Array marker changes

marker	level	fold change	CI upper	CI lower	Bonferroni-Holm corrected post hoc p-value
Alix	post	1.17	1.30	1.04	0.02086
Alix	RQ 0.9	1.07	1.20	0.95	0.49669
CD14	post	1.22	1.44	1.04	0.03200
CD14	RQ 0.9	1.03	1.21	0.88	1.33387
CD142	post	1.15	1.24	1.07	0.00369
CD142	RQ 0.9	1.11	1.19	1.03	0.02222
HLA-ABC	post	1.35	1.65	1.10	0.01888
HLA-ABC	RQ 0.9	1.24	1.49	1.03	0.05271
ICAM-1	post	1.22	1.41	1.06	0.02678
ICAM-1	RQ 0.9	1.13	1.31	0.98	0.15612
LAMP-1	post	1.21	1.31	1.12	0.00052
LAMP-1	RQ 0.9	1.10	1.19	1.02	0.03614
tPA	post	1.19	1.37	1.03	0.03691
tPA	RQ 0.9	0.99	0.85	1.15	1.76157

CI confidence interval

Table S3: Statistical analysis of WB marker changes

marker	level	EV subclass	fold change	CI upper	CI lower	Bonferroni-Holm corrected post hoc p-value
CD9	post	CD63+EVs	1.88	2.75	1.28	0.01171
CD9	RQ 0.9	CD63+EVs	1.45	2.20	0.96	0.14503
CD9	post	CD81+EVs	1.79	2.15	1.49	0.00007
CD9	RQ 0.9	CD81+EVs	1.23	1.48	1.02	0.06189
CD9	post	SEC-EVs	2.56	3.92	1.68	0.00034
CD9	RQ 0.9	SEC-EVs	1.44	2.23	0.93	0.19283
CD41b	post	CD81+EVs	8.65	15.04	4.97	0.00001
CD41b	RQ 0.9	CD81+EVs	2.88	5.01	1.66	0.00331
CD41b	post	SEC-EVs	2.44	3.74	1.59	0.00058
CD41b	RQ 0.9	SEC-EVs	1.52	2.36	0.97	0.12737
CD63	post	CD81+EVs	1.93	2.74	1.36	0.00289
CD63	RQ 0.9	CD81+EVs	1.59	2.26	1.12	0.02643
CD63	post	SEC-EVs	1.91	2.53	1.44	0.00026
CD63	RQ 0.9	SEC-EVs	1.29	1.72	0.96	0.17247
CD81	post	SEC-EVs	2.15	3.18	1.45	0.00168
CD81	RQ 0.9	SEC-EVs	1.53	2.30	1.02	0.08305

CI confidence interval

Table S4: Statistical analysis of MACSPlex marker changes

marker	level	EV subclass	fold change	CI upper	CI lower	Bonferroni-Holm corrected post hoc p-value
CD4	post	SEC-EVs	4.40	7.52	2.58	0.00014
CD4	RQ 0.9	SEC-EVs	1.35	2.38	0.77	0.79570
CD4	post	CD9+EVs	7.45	19.01	2.92	0.00773
CD4	RQ 0.9	CD9+EVs	1.78	5.05	0.63	0.65701
CD4	post	CD81+EVs	9.56	20.76	4.40	0.00006
CD4	RQ 0.9	CD81+EVs	1.63	3.54	0.75	0.59156
CD4	post	CD63+EVs	10.40	20.57	5.26	0.00008
CD4	RQ 0.9	CD63+EVs	1.36	2.83	0.66	1.08704
CD8	post	CD9+EVs	1.72	2.27	1.31	0.00657
CD8	RQ 0.9	CD9+EVs	1.20	1.61	0.89	0.60064
CD8	post	SEC-EVs	1.33	1.56	1.13	0.00596
CD8	RQ 0.9	SEC-EVs	1.14	1.36	0.96	0.38817
CD8	post	CD81+EVs	1.80	2.36	1.36	0.00134
CD8	RQ 0.9	CD81+EVs	1.14	1.51	0.87	0.94466
CD8	post	CD63+EVs	1.41	1.75	1.13	0.01600
CD8	RQ 0.9	CD63+EVs	1.18	1.49	0.94	0.40177
CD9	post	SEC-EVs	1.64	2.41	1.11	0.04808
CD9	RQ 0.9	SEC-EVs	1.30	1.99	0.85	0.61414
CD9	post	CD81+EVs	2.53	3.48	1.84	0.00004
CD9	RQ 0.9	CD81+EVs	1.25	1.72	0.91	0.47621
CD9	post	CD63+EVs	1.97	3.07	1.26	0.02004
CD9	RQ 0.9	CD63+EVs	1.01	1.62	0.63	2.87174
CD14	post	CD63+EVs	7.57	14.13	4.06	0.00035
CD14	RQ 0.9	CD63+EVs	2.31	4.55	1.17	0.06732
CD14	post	CD81+EVs	7.08	19.50	2.57	0.00363
CD14	RQ 0.9	CD81+EVs	1.96	5.41	0.71	0.51793
CD14	post	SEC-EVs	5.47	17.09	1.75	0.03665
CD14	RQ 0.9	SEC-EVs	1.67	5.97	0.47	1.04739
CD24	post	CD81+EVs	2.06	2.65	1.60	0.00005
CD24	RQ 0.9	CD81+EVs	1.17	1.51	0.91	0.59153

CD24	post	CD63+EVs	1.79	2.26	1.42	0.00060
CD24	RQ 0.9	CD63+EVs	1.15	1.48	0.90	0.71901
CD24	post	CD9+EVs	1.89	2.79	1.28	0.01793
CD24	RQ 0.9	CD9+EVs	1.20	1.82	0.78	1.05016
CD29	post	CD81+EVs	1.85	2.58	1.32	0.00375
CD29	RQ 0.9	CD81+EVs	1.03	1.43	0.74	2.60916
CD29	post	CD63+EVs	2.30	3.63	1.45	0.00630
CD29	RQ 0.9	CD63+EVs	1.20	1.95	0.74	1.29742
CD29	post	SEC-EVs	1.81	2.62	1.24	0.01321
CD29	RQ 0.9	SEC-EVs	1.43	2.15	0.95	0.25664
CD31	post	CD81+EVs	2.52	3.80	1.67	0.00063
CD31	RQ 0.9	CD81+EVs	1.28	1.93	0.85	0.67087
CD31	post	CD63+EVs	3.73	8.11	1.71	0.01003
CD31	RQ 0.9	CD63+EVs	1.31	2.98	0.57	1.46190
CD40	post	CD63+EVs	2.35	4.20	1.32	0.02573
CD40	RQ 0.9	CD63+EVs	1.03	1.90	0.55	2.79085
CD40	post	CD81+EVs	2.92	6.24	1.36	0.02627
CD40	RQ 0.9	CD81+EVs	1.63	3.49	0.76	0.57468
CD40	post	CD9+EVs	2.62	4.14	1.66	0.00467
CD40	RQ 0.9	CD9+EVs	1.57	2.58	0.96	0.20667
CD41b	post	CD81+EVs	1.96	2.75	1.40	0.00194
CD41b	RQ 0.9	CD81+EVs	1.41	1.98	1.00	0.14183
CD41b	post	CD63+EVs	1.75	2.60	1.18	0.02829
CD41b	RQ 0.9	CD63+EVs	1.07	1.62	0.70	2.22711
CD41b	post	SEC-EVs	1.61	2.35	1.11	0.04967
CD41b	RQ 0.9	SEC-EVs	1.35	2.03	0.89	0.43423
CD42a	post	CD81+EVs	2.20	3.40	1.42	0.00428
CD42a	RQ 0.9	CD81+EVs	1.25	1.92	0.81	0.89606
CD42a	post	CD63+EVs	2.27	3.46	1.49	0.00389
CD42a	RQ 0.9	CD63+EVs	1.49	2.33	0.95	0.22821
CD42a	post	SEC-EVs	1.60	2.21	1.16	0.02123
CD42a	RQ 0.9	SEC-EVs	1.31	1.87	0.92	0.35623
CD44	post	CD81+EVs	2.10	3.23	1.36	0.00729
CD44	RQ 0.9	CD81+EVs	1.28	1.97	0.83	0.70822
CD44	post	SEC-EVs	1.74	2.59	1.17	0.03235
CD44	RQ 0.9	SEC-EVs	1.22	1.85	0.80	0.99274
CD44	post	CD63+EVs	3.40	5.90	1.96	0.00071
CD44	RQ 0.10	CD63+EVs	1.21	2.18	0.67	0.48582
CD44	post	CD9+EVs	10.46	85.53	1.28	0.03352
CD44	RQ 0.10	CD9+EVs	2.64	25.82	0.27	0.34803
CD45	post	CD81+EVs	2.88	4.72	1.75	0.00128
CD45	RQ 0.9	CD81+EVs	1.25	2.04	0.76	1.06361
CD45	post	CD63+EVs	3.21	7.04	1.47	0.02904
CD45	RQ 0.9	CD63+EVs	1.37	3.22	0.58	1.23898
CD49e	post	CD81+EVs	3.19	5.41	1.88	0.00080
CD49e	RQ 0.9	CD81+EVs	1.50	2.55	0.89	0.36460
CD49e	post	CD9+EVs	2.61	4.10	1.66	0.00449
CD49e	RQ 0.9	CD9+EVs	0.97	0.59	1.58	2.62917
CD49e	post	CD63+EVs	2.50	4.72	1.32	0.02740
CD49e	RQ 0.9	CD63+EVs	1.21	2.38	0.62	1.63533
CD62P	post	CD9+EVs	2.64	3.81	1.82	0.00130
CD62P	RQ 0.9	CD9+EVs	1.97	2.94	1.32	0.01515
CD62P	post	SEC-EVs	1.71	2.27	1.29	0.00339
CD62P	RQ 0.9	SEC-EVs	1.53	2.09	1.12	0.03339
CD62P	post	CD81+EVs	2.91	5.24	1.62	0.00426
CD62P	RQ 0.9	CD81+EVs	1.61	2.90	0.90	0.31323
CD62P	post	CD63+EVs	2.56	5.14	1.27	0.03874
CD62P	RQ 0.9	CD63+EVs	1.25	2.61	0.60	1.58205
CD63	post	CD81+EVs	2.45	3.20	1.88	0.00001

CD63	RQ 0.9	CD81+EVs	1.26	1.64	0.97	0.24630
CD63	post	SEC-EVs	1.52	1.95	1.19	0.00770
CD63	RQ 0.9	SEC-EVs	1.11	1.45	0.84	1.30058
CD69	post	CD63+EVs	2.38	4.37	1.30	0.02748
CD69	RQ 0.9	CD63+EVs	1.31	2.50	0.69	1.10546
CD69	post	SEC-EVs	1.68	2.35	1.20	0.01602
CD69	RQ 0.9	SEC-EVs	1.25	1.82	0.86	0.64237
CD81	post	CD63+EVs	1.45	1.76	1.19	0.00450
CD81	RQ 0.9	CD63+EVs	1.16	1.43	0.94	0.42393
CD105	post	CD81+EVs	4.33	5.77	3.25	0.00000
CD105	RQ 0.9	CD81+EVs	1.44	1.92	1.08	0.04613
CD105	post	CD9+EVs	3.67	5.61	2.40	0.00052
CD105	RQ 0.9	CD9+EVs	1.41	2.24	0.89	0.36254
CD105	post	CD63+EVs	3.20	5.07	2.03	0.00082
CD105	RQ 0.9	CD63+EVs	1.23	2.01	0.75	1.10742
CD105	post	SEC-EVs	2.27	3.62	1.42	0.00903
CD105	RQ 0.9	SEC-EVs	1.39	2.37	0.82	0.58232
CD146	post	CD81+EVs	3.29	4.99	2.17	0.00005
CD146	RQ 0.9	CD81+EVs	1.35	2.05	0.89	0.42985
CD146	post	CD63+EVs	3.48	5.29	2.29	0.00012
CD146	RQ 0.9	CD63+EVs	1.18	1.84	0.76	1.28799
CD146	post	CD9+EVs	2.40	3.65	1.57	0.00530
CD146	RQ 0.9	CD9+EVs	1.33	2.10	0.84	0.55934
CD146	post	SEC-EVs	2.00	2.97	1.34	0.00693
CD146	RQ 0.9	SEC-EVs	1.36	2.07	0.90	0.39927
HLA-ABC	post	CD81+EVs	2.90	4.00	2.10	0.00001
HLA-ABC	RQ 0.9	CD81+EVs	1.34	1.84	0.97	0.22208
HLA-ABC	post	CD63+EVs	2.65	3.74	1.88	0.00018
HLA-ABC	RQ 0.9	CD63+EVs	1.46	2.10	1.01	0.13129
HLA-ABC	post	CD9+EVs	2.69	3.66	1.97	0.00039
HLA-ABC	RQ 0.9	CD9+EVs	1.39	1.94	0.99	0.16857
HLA-DRDPDQ	post	CD81+EVs	3.42	4.84	2.42	0.00000
HLA-DRDPDQ	RQ 0.9	CD81+EVs	1.41	1.99	1.00	0.15654
HLA-DRDPDQ	post	CD63+EVs	2.87	3.71	2.21	0.00001
HLA-DRDPDQ	RQ 0.9	CD63+EVs	1.23	1.62	0.94	0.36426
HLA-DRDPDQ	post	CD9+EVs	2.25	3.13	1.62	0.00191
HLA-DRDPDQ	RQ 0.9	CD9+EVs	1.13	1.62	0.79	1.32814
HLA-DRDPDQ	post	SEC-EVs	1.68	2.41	1.17	0.02369
HLA-DRDPDQ	RQ 0.9	SEC-EVs	1.14	1.69	0.77	1.48009

CI confidence interval

7.2 Publications

Brahmer A, Neuberger E, Esch-Heisser L, Haller N, Moeller Joergensen M, Baek R, Möbius W, Simon P, Krämer-Albers EM. Platelets, endothelial cells, and leukocytes contribute to the exercise-triggered release of Extracellular Vesicles into the circulation. Journal of Extracellular Vesicles. 2019. Volume 8.

Neuberger E, **Brahmer A**, Moser D, Le Guiner C, Moullier P, Snyder RO, Simon P. Preparation of synthetic reference material as a standard for nested qPCR based transgene detection. Accepted for publication in Gene Therapy & Molecular Biology.

Ehlert T, Tug S, **Brahmer A**, Neef V, Heid F, Werner C, Jansen-Winkeln B, Kneist W, Lang H, Gockel I, Simon P. Establishing PNB-qPCR for quantifying minimal ctDNA concentrations during tumour resection. Sci Rep. 2017 Aug 21;7(1):8876. doi: 10.1038/s41598-017-09137-w. PubMed PMID: 28827745; PubMed Central PMCID: PMC5566323.

Bicker A, **Brahmer AM**, Meller S, Kristiansen G, Gorr TA, Hankeln T. The Distinct Gene Regulatory Network of Myoglobin in Prostate and Breast Cancer. PLoS One. 2015 Nov 11;10(11):e0142662. doi: 10.1371/journal.pone.0142662. eCollection 2015. PubMed PMID: 26559958; PubMed Central PMCID: PMC4641586.

7.3 Presentations and Posters

Neuberger E, **Brahmer A**, Boztepe B, Krämer-Albers EM, Simon P. Association Of Circulating Cell-free Dna Released During Physical Exercise With Extracellular Vesicles. American College of Sports Medicine (ACSM) Annual Meeting. Orlande, Florida, USA. May 28 - Jun 01, 2019. Poster presentation.

Simon P, **Brahmer A**, Esch-Heisser L, Neuberger E, Krämer-Albers EM. Origin of extracellular vesicles released during exercise. American College of Sports Medicine (ACSM) Annual Meeting, 2019, Orlando, Florida, USA.

Fiedler J, **Brahmer A,** Neuberger E, Boztepe B, Simon P. Molecular changes impacted by the diving reflex. 11th Baltic sport science conference. Tartu, Estonia, 2018.

Brahmer A, Esch-Heisser L, Simon P, Krämer-Albers EM. Origin of extracellular vesicles released during exhaustive exercise. Annual Meeting of The International Society for Extracellular Vesicles, 2018, Barcelona, Spain. Oral presentation and poster presentation.

Brahmer A, Neuberger E, Simon P, Krämer-Albers EM. Characterization of extracellular vesicles released during exhaustive exercise. 4th International Symposium on Resilience Research. Poster presentation.

Brahmer A. Extracellular Vesicles in the plasma of exercising humans. 1st Annual Meeting of The German Society for Extracellular Vesicles, Frankfurt, Germany. Oral presentation.

Brahmer A, Esch-Heisser L, Krämer-Albers EM and Simon P. Impact of high-fat diet prior to physical exercise on the analysis of cell-free DNA and extracellular vesicles. 10th International Symposium on Circulating Nucleic Acids in Plasma and Serum, 2017, Montpellier, France. Poster presentation.

Neuberger EW, Frühauf H, Boeschen M, Oltmanns F, **Brahmer A**, Simon P. Inflammatory response of monocytic THP1 cell line on NET DNA. 10th international symposium on circulating nucleic acids in plasma and serum (CNAPS), 2017, Corum, Montpellier.

Albus M, **Brahmer A**, Tug S, Helmig S, Zahn D, Kubiak T, Simon P. Cell-free DNA levels in healthy subjects. 9th International Symposium on Circulating Nucleic Acids in Plasma and Serum, 2015, Berlin, Germany. Poster presentation, as representative for first author.

Neuberger E, Mooses M, Durussel J, Wang J, Lees M, Mooses K, **Brahmer A**, Wang G, Pitsiladis Y, Simon P. Small RNA sequencing of red blood cell specific miRNAs reveals expression changes after 6 weeks of recombinant EPO (rEPO) administration in healthy recreational athletes. American Journal of Hematology, 2015